Department of Precision and Microsystems Engineering

Actuation System Design for a 3 DoF Contactless Wafer Stage

X.Huang

Report no : MSD 2016.016
Coach : H.P. Vuong MSc.
Professor : Dr.Ir. R.A.J. van Ostayen
Specialisation : Mechatronic System Design
Type of report : Thesis
Date : 13 April, 2016

Actuation System Design for a 3 DoF Contactless Wafer Stage

by

Xinsheng Huang

in partial fulfillment of the requirements for the degree of

Master of Science

at the Delft University of Technology,
to be defended publicly on Wednesday April 13, 2016 at 14:00.

Student number:	1520814	
Department:	Precision and Microsystems Engineering	
Supervisor:	Dr. Ir. R.A.J. van Ostayen	
	H.P. Vuong MSc.	
Thesis committee:	Dr. Ir. R.A.J. van Ostayen	TU Delft
	H.P. Vuong MSc.	TU Delft
	Dr. S.H. HosseinNia	TU Delft
	Dr. Ir. D.H. Plettenburg (BMechE)	TU Delft

TU Delft Delft University of Technology

Preface

It was an amazing adventure in the field of mechatronics in the last year. I never regret being a student of mechanical engineering especially as an MSD student. It was a lot of fun putting my hands on the cutting edge technology and exploring for new findings, of course including some peaks that show up in our measurements due to the naughty fellow students who like jumping when we are doing measurements. Now we know the eigenfrequency of our MSD lab!

I've learned a lot during this MSc project. A lot of knowledge from different field is involved in this project, from mechatronics to fluid dynamics, from pneumatics to piezo, from dSpace to Matlab, reading a lot of books and articles was fun, I even built a little air bearing at home to show my family what kind of amazing technology I am working with, the air-can powered air bearing didn't last for more than 2 minutes though.

Acknowledgment

Hereby I would like to express my appreciation to all the people who contributed to this project.

I would like to thank Ron van Ostayen. He is my supervisor and an expert in air bearing and mechatronics, associate professor in PME. Thank you for your advice and the coaching during the project, thank you for pointing me to the right direction when I'm in doubt.

Phuc Vuong, also my supervisor, PHD in MSD group, the cool guy who created the Flowerbed contactless wafer stage. Thank you for all your support and help, it's my pleasure to work with you together in the lab.

Hassan HosseinNia, assistant professor in PME, an expert in control engineering. Thank you for the advice and support for designing the controller.

René Delfos, assistant professor in Fluid Dynamics department. Thank you for your advice in fluid dynamics for my model.

Rob Luttjeboer, lab coordinator of the MSD group. Thank you for your support in all my lab equipments.

Hans Drop, the "Boss" of the employer workshop, now retired. Thank you for your support in the workshop, my beautiful metal components shines for you.

Gerard van Vliet, coordinator of the student workshop. Thank you for your advice and help of laser cutting.

Jos van Driel, coordinator of the Meetshop. Thank you for your help in the measuring equipments.

Jan Neve, MSc coordinator in PME. Thank you for sorting out the trouble in my study programme so that I can focus in the research project.

Floris Klein Horsman, Martijn van Beek, Ruud Hoogeboom, Bart Joziasse, Haris Habib, Oscar van de Ven, Johan Vogel, Ruijun Deng, Yangyang Wang, Joost Kortleve, Arjan Scheerhoorn. My fellow students and PhDs. Thanks for this amazing time.

Furthermore, I would like to thank my family for their endless support and love.

Xinsheng Huang
Delft, March 2016

Contents

1

Introduction

Smart devices, a milestone of technology, becomes an important part in people's life, either it's a smartphone or a health tracker, even a water boiler can be smart. Such devices become smart because they have semiconductor computer chips integrated inside. These chips can perform computation and carry out automatic tasks without direct control from the user. Computer chips are made from silicon wafer in the production line, these silicon wafers are made with very high precision and they are very fragile and sensitive to any damage, even a slight scratch on the surface will destroy the nanometer scale structure on the silicon wafer, which leads to malfunctioning of the chip, making it useless.

The handling/transportation of the wafers are mostly based on mechanical support, with the wafer sitting on top of a solid component, by moving the solid component the wafer is moved to another place. These kinds of handling techniques have solid-to-solid contact on the surface of the silicon wafer, if there is some strong vibration or disturbance occurred it may damage the surface of the wafer due to the relative motion between the handling surface and the wafer surface. Another issue is the possibility of wafer surface contamination. If the handling surface is contaminated, touching the wafer will transfer the contamination to the wafer. These kinds of drawbacks of the solid contact is well known, therefore the manufacturing instruments are generally isolated to provide a safe, stable and clean environment.

There is another wafer handling technique called contactless wafer handling. The general idea of contactless wafer handling is to interact with the silicon wafer without solid contact. A very common method for contactless wafer handling is the implementation of air bearing.

Air bearing is basically a thin film of pressurized air which can support a load, as shown in Figure 1.1. It's the same working principle of how a puck on an air hockey table can be floating. The pressurized air carries the weight of the puck, prevents it from touching the table, so that there is no friction between the puck and the table, and the puck can fly at a very high speed and there is very little energy loss during the movement. Contactless wafer stage with air bearing is therefore a very attractive new type of wafer handling method. [1]

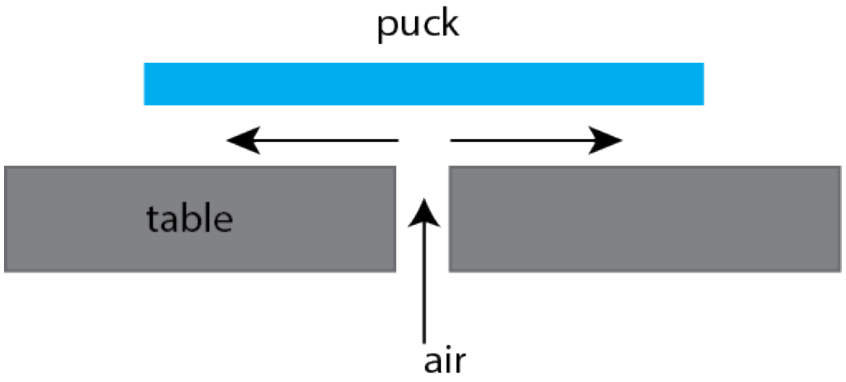

Figure 1.1: Schematic of a puck floating on top of the air hockey table. Pressurized air flows under the puck, supporting its weight

More advanced technology is being studied in the field of air bearing, and there are prototypes created to investigate different ways to drive the wafer when it's floating. It is very beneficial to combine the air bearing with driving technique integrated so that the wafer can move to the desired position while floating. In the Mechatronic System Design (MSD) group of the Precision and Microsystem Engineering (PME) department at TU Delft, a x-y-θ 3 DoF contactless wafer stage called the "Flowerbed" was successfully developed by H.P.Vuong in a PhD research project. Figure 1.2 is a photo of the experimental setup of the Flowerbed. There are hexagonal nozzles with a small hole in the middle, these nozzles can tilt to all directions. Wafer is floating on top of these nozzles and move to any horizontal direction by tilting the nozzles. Figure 1.3 is a schematic of the working principle of the nozzles. There are two plates connected to the nozzles, the top plate is fixed in position, while the control plate can move horizontally, so that the nozzles can tilt to the desired direction.

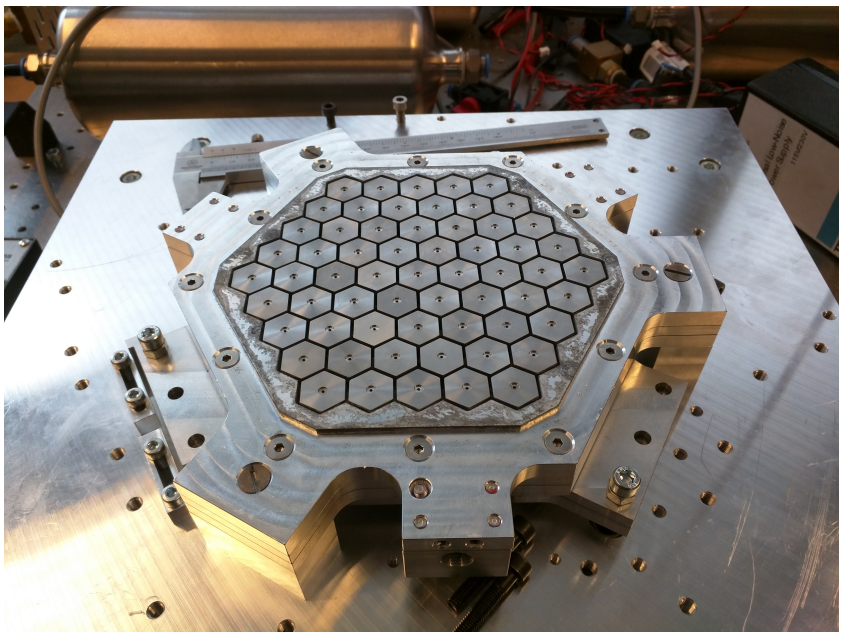

Figure 1.2: Picture of the Flowerbed, the tilting orientation of all the nozzles can be controlled altogether by positioning the control plate at the desired place and orientation, so that the wafer can be driven in x and y direction, as well as rotation

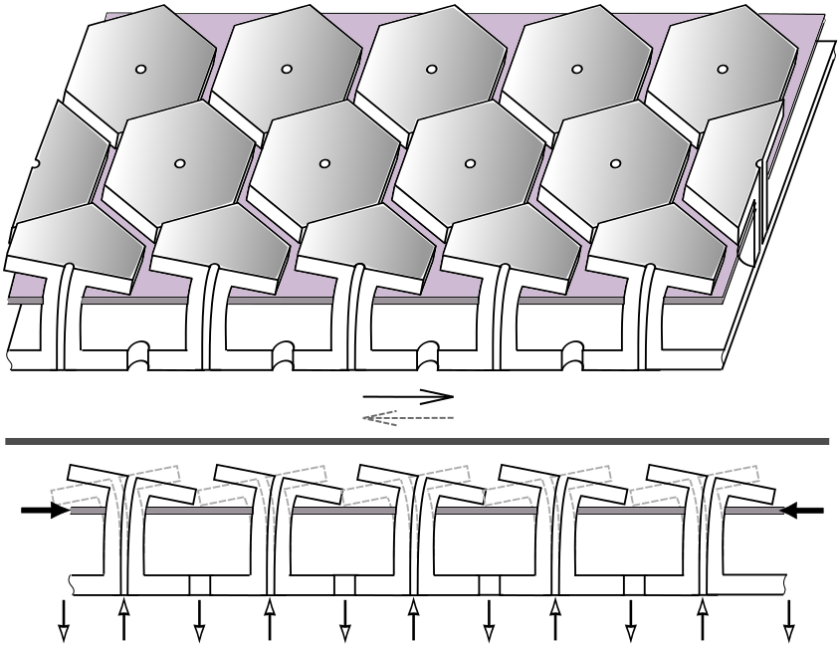

Figure 1.3: Schematic of the nozzles. The nozzles are controlled by two horizontal plates. The top plate in purple color is fixed in position, the bottom control plate in white color can move horizontally, in this way the nozzles can be tilted in any direction. Figure created by H.P.Vuong

This tilting nozzles design makes it easy to drive all the nozzles together with only one component, which is the moving control plate, but all these nozzles will contribute their stiffness and end up with a high equivalent stiffness of the moving plate in the x-y-θ direction. The high stiffness is very special for such kind of wafer stage, and normal actuation solution is not very suitable for the Flowerbed. This brings up the specification of the Flowerbed regarding the actuation system.

1.1. Specification

The Flowerbed has a symmetrical hexagonal nozzle array, which contains 61 nozzles, as shown in Figure 1.4. Each nozzle has a hexagonal shape, with a circumradius of 8mm and an inradius (apothem) of 7mm. The air gap between each nozzle is 1mm. The whole nozzle array forms a hexagonal shape with a circumradius of 75mm and an inradius (apothem) of 65mm. The bottom plate (control plate) shown in Figure 1.5 has a hexagonal shape with three connecting joints, these three connecting joints form a triangle with inradius (apothem) of 88mm. This control plate will be connected to the actuation system.

The most important specification of the Flowerbed regarding to this research project is the equivalent stiffness and the maximum displacement/rotation of the moving plate in x-y-θ direction. The translational displacement is limited in a circle with a diameter of 40µm as shown in Figure 1.6, the Flowerbed can move freely inside this workspace. The maximum rotation is limited to ±0.7mrad, which equals to 0.04°. The translation stiffness in the x-y direction is 1.53×10^5N/m, the rotational stiffness is 3.59Nm/rad, and is achievable in any position inside the workspace. The required bandwidth of the Flowerbed is 150Hz.

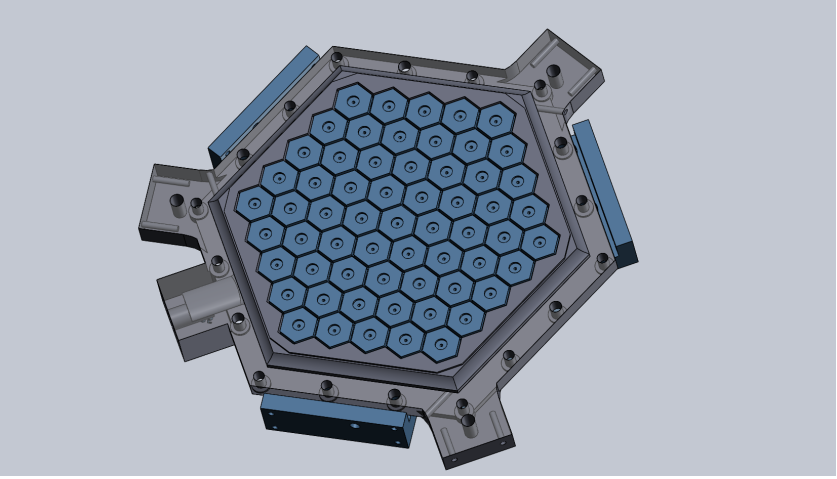

Figure 1.4: CAD Model of the Flowerbed created by H.P. Vuong, showing the hexagonal array of the nozzles, indicated in blue color

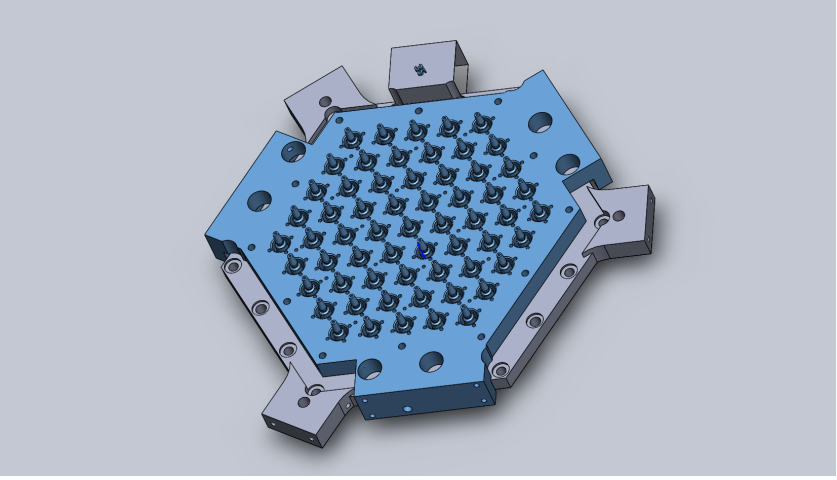

Figure 1.5: CAD Model of the Flowerbed created by H.P. Vuong, bottom view, showing the control plate of the assembly, indicated in blue color

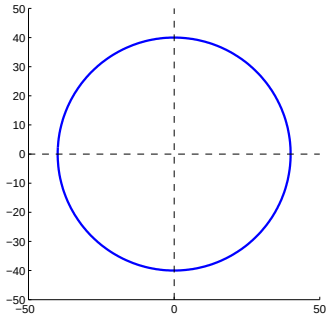

Figure 1.6: Workspace of the control plate of Flowerbed is a circle with a diameter of 40µm from the center point. The control plate can move freely inside this 40µm with 3 DoF, it can achieve the rotation of ±0.7mrad at any position inside the workspace

1.2. Requirements

The requirement for the actuation is set by the specification of the Flowerbed:

- The actuation system should be able to provide 3 degrees of freedom (x-y-θ) control to the Flowerbed.
- The actuation system should be able to reach the displacement limit of the Flowerbed, which is ±40μm translational and ±0.7mrad rotational.
- The actuator of the system should be able to generate a maximum force of 140N.
- The actuator of the system should be able to reach a bandwidth of 150Hz.
- The actuation system should be as cost effective as possible.

From these requirements, the objective of this research project can be defined.

1.3. Objective

The objective of this thesis is to design an actuation system for this high stiffness 3 DoF contactless wafer stage. To be specific, design a suitable type of actuation configuration for the Flowerbed, and design the actuator from scratch to meet the requirement if necessary.

1.4. Research Approach

With the objective determined, the research approach in this project is as follows:

- Study different types of actuators, determine which types could be suitable for the Flowerbed.
- Study different types of actuation configurations, determine which types could be suitable for the Flowerbed.
- Determine a combination of the actuator and configuration
- Design the configuration fo the Flowerbed
- Establish a model for the chosen type of actuator.
- Verify the model with test setup.
- Design an actuator according to the requirement of the Flowerbed using the established model and finally produce a prototype.

1.5. Thesis overview

The following contents of this thesis will be arranged as:

- Chapter 2 is a review of the literature where the state-of-the-art actuation technology regarding 3 DoF wafer stage will be discussed.
- Chapter 3 is the discuss regarding different types of actuators, in this chapter some actuators of different types will be chosen and tested for the performance, in order to study their advantage/weakness.

- Chapter 4 is about the design of the actuation configuration, it contains the study of how the actuators should be arranged. In the end of Chapter 4 a combination of actuator/configuration will be chosen for the Flowerbed.
- Chapter 5 contains the modeling of the pneumatic actuator, as well as the validation of the model.
- Chapter 6 is about a compact design of a piezoelectric valve, which is going to be implemented in the final prototype.
- Chapter 7 is the discuss of the final prototype, including the parameter, manufacturing, controller design, and the performance.
- Chapter 8 summarize the knowledge developed in this research, finalize it into a design toolbox and a design method.
- Chapter 9 and 10 are the conclusion and recommendation of this research project.

2

Literature Review

With the experimental setup of the Flowerbed and the research objective discussed in Chapter 1, a literature review is done to support the research of this thesis. The Flowerbed is a special contactless wafer positioning system because of its high stiffness, and this high stiffness causes some difficulties in designing an actuation system. Many of the already established and proven designs may not have their optimal performance when applied on the Flowerbed because they are mostly based on a wafer stage with very low or even zero stiffness. In this chapter, some already established actuation configuration relevant to the Flowerbed will be discussed in Section 2.1. In Section 2.2, relevant actuators will be reviewed.

2.1. Actuation system review

The experimental setup of Flowerbed needs to be actuated in 3DoF (degrees of freedom) x-y-θ and it has a high stiffness for the actuation. Relevant actuation solutions are reviewed to investigate the feasibility.

2.1.1. 3 DoF piezoelectric dual stage

In 1999, Chang et al. have developed a 3 DoF ultra-precision x-y-θ micro positioner using piezo technology. [2][3] Figure 2.1 shows the schematic of the micro positioner. It uses two stacked stage to achieve 3 DoF positioning.

The base is an x-y stage shown in Figure 2.1a, it implements four piezoelectric actuators marked as No.21x and No.21y. Each of these four piezoelectric actuators is connected to an amplification beam marked as 2,4,6,7. These amplification beams are rigid beams with compliant joints connected between the frame and the center stage. The position of the piezoelectric actuator is chosen such that the displacement of the actuator will be amplified into a larger displacement of the stage due to the principle of leverage. The second stage is a θ stage, as shown in Figure 2.1b, with two piezoelectric actuators included, which are marked with No.21_R. It has the same working principle as the x-y stage, with the amplification beam marked as No.8,9.

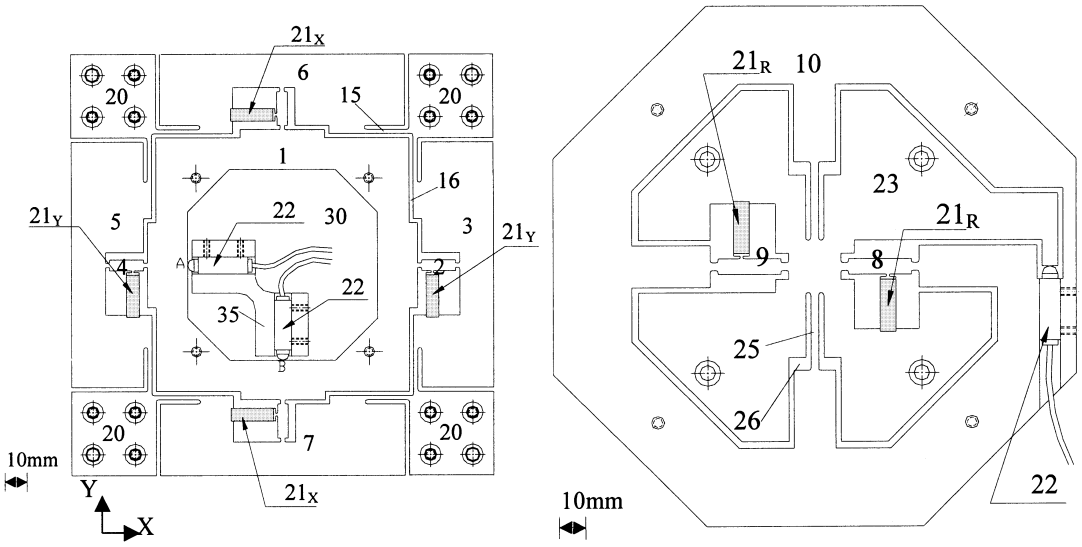

(a) (b)

Figure 2.1: Schematic of a dual stage 3 DoF micro positioner, with a) the translation x-y stage and b) rotation θ stage. [2][3] Components marked with No.21 are the piezo actuators, where No.22 indicates the position sensor for measuring the displacement.

2.1.2. 4 DoF electromagnetic precision stage

In 2012, Ahn et al. have successfully developed a 4 DoF precision stage using voice coil motors (VCM) and flexure guides [4]. It's also a stacked dual stage but the base has only z direction, the top stage will be discussed in this section.

The x-y-θ top stage has a square shape, with four voice coil motors located symmetrically, as shown in Figure 2.2a. Motor 1 and 2 deliver the force in x direction, while motor 3 and 4 deliver the force in y direction. The force in rotation is realized by combining the force from all four actuators to create a torque. The stage has a very large displacement of 2.28mm in x and y direction, and a rotational displacement of 44.0mrad. The force constant of the voice coil motors is 5.22N A^{-1}.

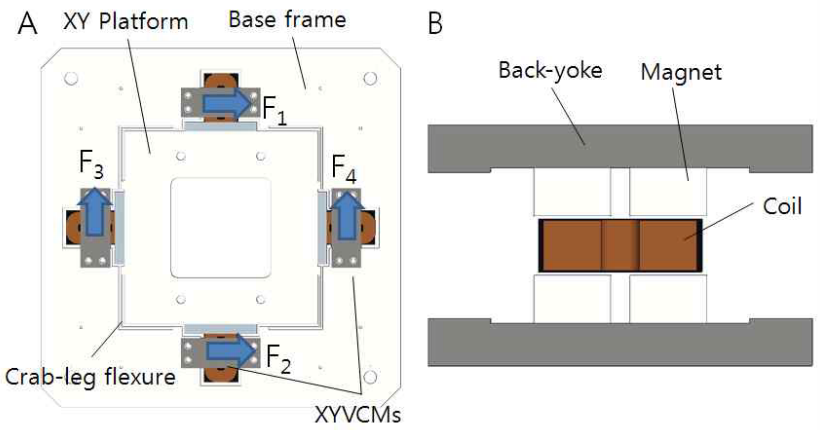

(a) Schematic of a 4 DoF electromagnetic precision stage.[4] This schematic shows only the x-y stage which utilize 4 voice coils to achieve translational displacement.

2.1.3. 3 DoF flexure-based parallel mechanism

In 2010, Tian et al. have developed a parallel mechanism for micro/nano positioning, using the concept of a 3-RRR parallel manipulator. [5]

Figure 2.3 shows the schematic of the parallel mechanism. The design of the mechanism is based on a monolithic flexure-based 3-revolute-revolute-revolute (3-RRR) parallel mechanism. 3-RRR means that the connection between the moving end-effector in the center to the outside world is realized by a serial chain of three revolute joints and there are three serial chains. Three actuators are correlated, they have to cooperate so that the end effector in the middle can achieve x-y-θ displacement. Each actuator is located between A and B joints as shown in Figure 2.3b, the position of the actuator determines the amplification of the displacement. The maximum displacement of the end effector in the middle is limited by the stiffness of the joints shown in Figure 2.3b because of the limited maximum stroke of the piezo actuator.

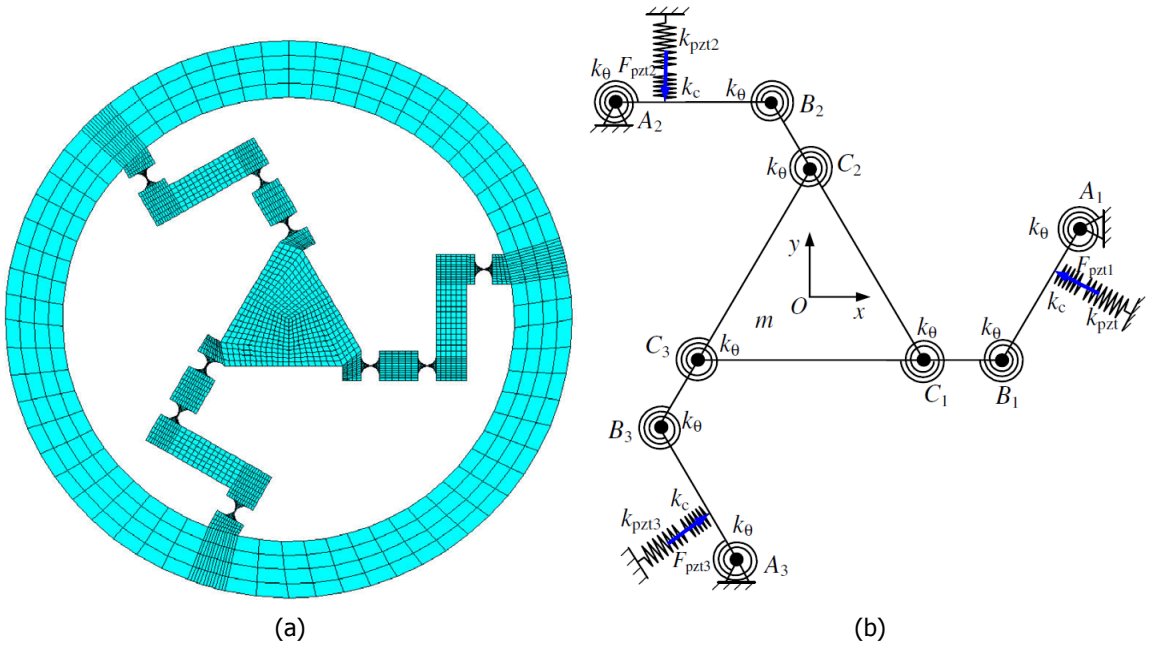

Figure 2.3: Schematic and a FEM layout of the 3 DoF flexure based parallel mechanism developed by Tian et al.. [5] The concept of 3-RRR parallel manipulator is implemented so that it's able to actuate the stage with only 3 actuators, and the mechanical amplification design is integrated for using the small piezo actuators.

2.1.4. 3 DoF planar parallel manipulator

In 1999, Robert L. Williams II and Atul R.Joshi have developed a 3 DoF planar parallel manipulator using pneumatic cylinders with the concept of 3-RPR parallel manipulator. [6]

Figure 2.4 shows the schematic of the planar 3 DoF parallel manipulator. The 3-RPR parallel manipulator means that the connection between the end effector and the external world is a serial chain of revolute-prismatic-revolute joints, and there are three such chains, as shown in Figure 2.4a. The pneumatic cylinders used in the prismatic joints of their experimental setup has very large displacement, hence the end effector has a very large workspace. The end effector and the joints in this parallel manipulator have zero translational stiffness, the displacement of the end effector is only limited by the maximum stroke of the pneumatic cylinders.

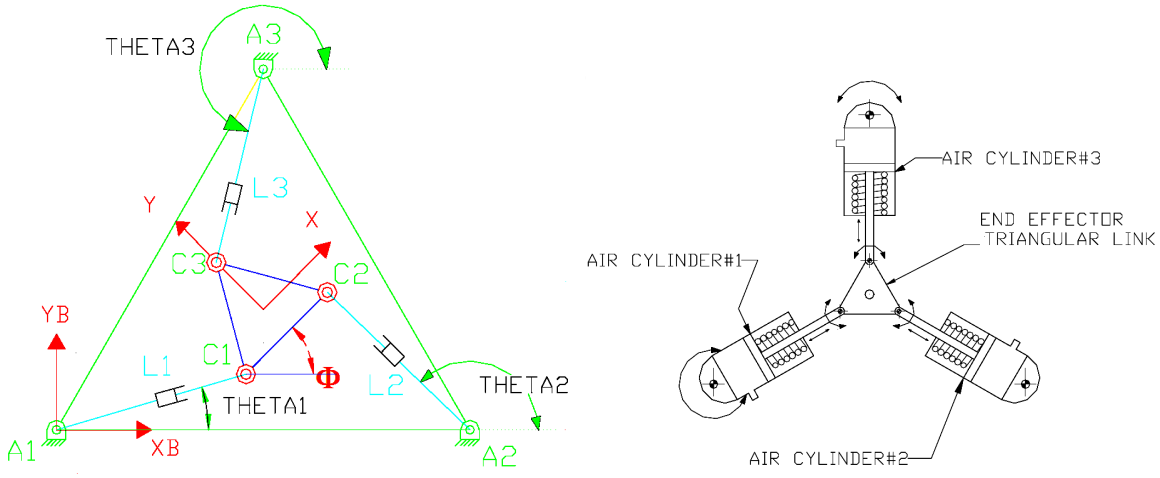

(a) (b)

Figure 2.4: Schematic and configuration layout of the 3 DoF 3-RPR parallel manipulator developed by Williams II et al.. [6] It utilize 3 pneumatic actuators cooperating to control the position and orientation of the end effector in the middle, by changing their length L1, L2 and L3

2.2. Actuators

Actuators are very important components of an actuation system. Choosing the right actuators and matching the performance with the actuation configuration will greatly increase the performance of the system, therefore knowing the characteristic of the actuators is essential. In this section, some actuators relevant to the Flowerbed project will be reviewed.

2.2.1. Piezoelectric actuator

Piezo actuators are a commonly used type of actuator, which provides fast actuation and provides precision positioning.

Piezoelectric effect is the generation of a mechanical strain in response to a voltage [7]. It is present in certain materials, these materials don't have a center of symmetry, as shown in Figure 2.5a. When stress is applied to the material, the positive and negative charges shift and the center of gravity of these charges do not coincide anymore, resulting a potential difference (voltage). The piezoelectric actuator makes use of the reverse piezoelectric effect, when the material is applied with a voltage, it will induce strain and change its shape.

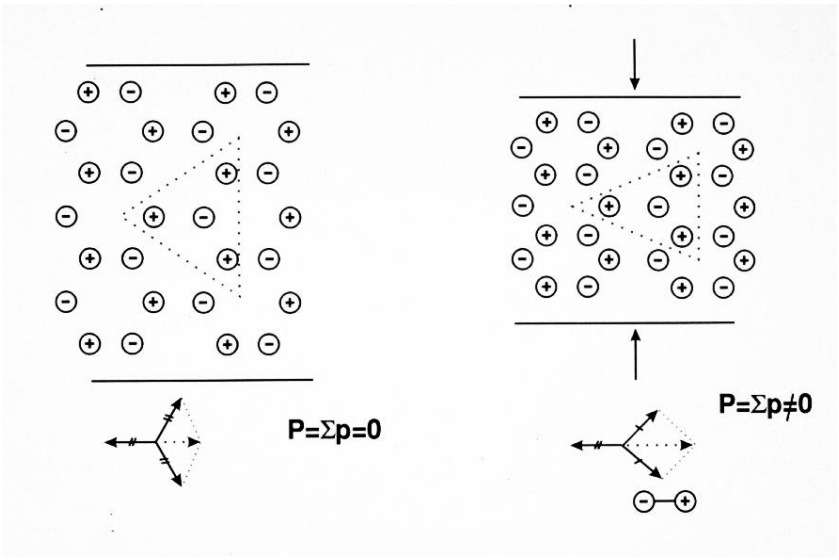

(a) Non-centrosymmetric crystal structure under stress, the piezoelectric material will induce a potential difference under stress [7]

One of the commonly used piezo actuator types is linear stack piezo, as shown in Figure 2.6. A stack piezo actuator consists layers of piezoelectric material, by stacking these piezoelectric layers it will gain more displacement under same voltage. As the more stacks the actuator has, the larger the stroke it has, and the weaker it can be, a very important specification of the piezo actuator should be mentioned: the blocking force. The blocking force is the maximum force generated by the actuator, and this force is measured with the actuator locked in position. This means that if a piezo actuator is loaded with high stiffness, it may not be able to achieve any displacement due to the limit of the blocking force [8]. One advantage of the piezo stack actuators is that it has a very fast dynamic performance up to several kHz. This makes piezo actuators very suitable for high bandwidth position control, and they are often used in micro mechanisms. One big disadvantage of the piezo actuators is that it has very limited of stroke, in most case limited to only tens of μm. The limited stroke of the piezo requires special design for the displacement amplification if it needs to drive devices with larger displacement.

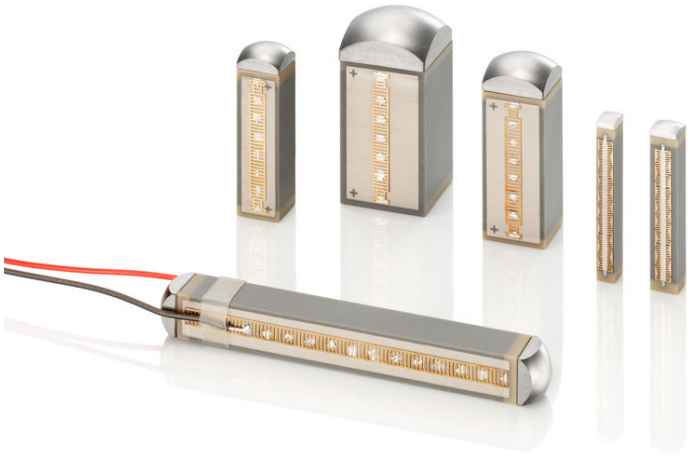

Figure 2.6: Picture of the stack piezo actuators from PI

2.2.2. Pneumatic actuator

Pneumatics has long since played an important role as a technology in the performance of mechanical work [9]. Pneumatic actuator is a type of actuator which utilizes compressed air to provide various force/stroke and is simple in construction with relatively low cost, it's suitable for a very wide range of applications. There are many types of pneumatic actuators. In this section a single-acting cylinder will be reviewed.

Figure 2.7 shows the schematic of a single-acting pneumatic cylinder. The cylinder has one connection which can be switched to air supply or exhaust. When the connection is switched to air supply, the pressure inside the chamber of the cylinder will start to build up. The pressure generates a force on the cylinder and pushes it outwards. Once the connection is switched to exhaust, the pressurized air will start to flow out and the pressure will decrease, the cylinder will then be pushed back to its original position by the preloading spring.

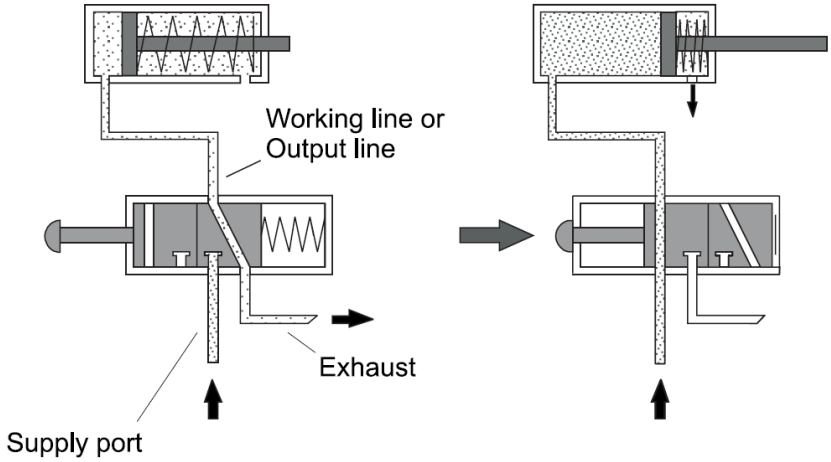

Figure 2.7: Schematic of a single-acting cylinder [9]. The pressure inside the cylinder will build up if the connection is switched to air supply

One important advantage of pneumatic actuator is that compressed air is available from existing pipelines inside many facilities, it can be utilized directly for the pneumatic actuator. Also, the cost can be relatively low but it depends on the supply pressure. One drawback of this actuation technology is that the pressure builds up inside the cylinder cost time. The time it needs is dependent on the air flow rate, which corresponds to the resistance inside the components. Compared to piezo actuator, a pneumatic actuator is slower but stronger and cheaper.

2.2.3. Voice coil actuator

Voice coil actuator is a direct drive, limited motion device that uses a permanent magnet field and a coil winding to produce a force proportional to the current applied to the coil [10].

Figure 2.8 shows the schematic of a voice coil actuator. A copper coil is attached on the coil holder, and the coil holder is placed in the air gap of the iron. There is a permanent magnet embedded in the soft iron and the magnetic field of the magnet goes through the air gap and the copper coil. When there is current flowing through the coil, the Lorentz force will apply on the coil, and push it outwards or inwards along the air gap, depending on the direction of the electric current.

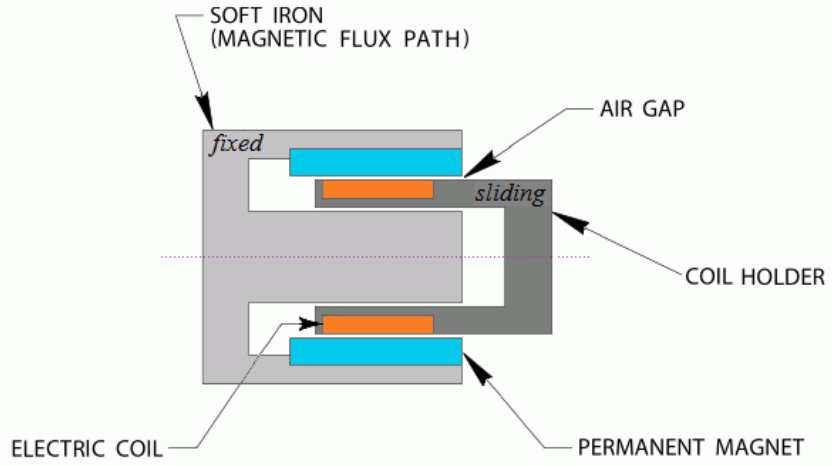

Figure 2.8: Schematic of a voice coil motor. The permanent magnet in the iron generates a magnetic field through the air gap and the copper coil, a force will apply on the copper coil if there is current flowing through, pushing the coil outwards or inwards along the air gap. Figure taken from http://ariwatch.com

The construction of the voice coil actuator is very simple and reliable. There is no contact between the coil and iron, and there is no backlash on the actuator. The force can be controlled by the current flow in the copper coil and it's a relatively linear relation. Voice coil actuator is very suitable for high precision and high-frequency actuation, but the energy consumption of the voice coil can be very high because of the heat loss caused by the current in the copper coil, and the size of a voice coil actuator can be very large if a large force is needed.

2.3. Discussion

This chapter reviews the literature related to the actuation configuration for the flowerbed, as well as the actuators. These relevant solutions will be discussed and further investigated in the following chapters. In the next chapter, some actuators will be studied and tested, in order to study their advantage/weakness.

3

Actuators

In the previous chapter, literature of different types of actuator relevant to this research project was reviewed. The stiffness of the Flowerbed is relatively high and is an important factor in the design because the bending stiffness of all the nozzles contribute to the translational stiffness in the moving plate. This high stiffness requires that the actuator must have enough force to drive the moving plate, at the same time provide enough bandwidth for the control system.

In this chapter, three different actuators of two types are tested and the advantages/disadvantages of them will be discussed, the dynamic performance of the actuator will be measured. The test will reveal the characteristic of the actuators and will provide valuable data for the next chapter, which is designing the actuation configuration.

3.1. Types of actuators chosen

Flowerbed is a contactless wafer stage which implements compressed air. Using the already available resource, in this case, compressed air as a part of the power system, is very beneficial for actuation system because it eliminates the need for external power source like a current amplifier for Lorentz actuator etc., therefore pneumatic actuator is desirable in this research. On the other hand, piezo actuators, famous for their dynamic performance, is also a good candidate.

There are other different types of actuators, for example, the voice coil motor reviewed in the previous chapter, but in this case a voice coil motor with a maximum force of 140N will be to huge to fit in the Flowerbed, and it will be extremely power hungry and very hot due to the high current needed to deliver the force. Therefore, considering the cost and size, only the pneumatic actuators and piezo actuators will be discussed in this chapter.

Pneumatic actuator is a widely used type of actuator. It uses compressed air to provide pressure and generate force, to be specific, relatively large force. Due to the characteristic of compressed air, a pneumatic actuator is generally not very fast, as air needs to flow in and flow out in order to build up the pressure or reduce it, but at the cost of the speed, it can build up to a very high pressure, hence very high force for the chosen application. If the actuator is specially designed for specific application, it can also be fast if properly designed. A pneumatic actuator relies on several external components to ensure proper functioning: restriction and a controllable valve. It should be mentioned that these components will add space to the actuator, for example, the commonly used solenoid valves, the faster the valve, the larger they could be. The total space needed for the pneumatic actuator should be considered during the design.

Piezo actuator is another type of actuator which is widely used for precision actuation. The piezo material can change its shape under voltage. It can expand, retract, or shear depending on the material crystal construction. Generally, the expanding piezo is more commonly seen, in the form of ”stack

piezo" linear actuators. Piezo actuators have a stroke from a couple of micrometers up to hundreds of micrometers, and it has a very fast response with a bandwidth of up to certain kHz. Furthermore, piezo actuators are very small compared to other types of actuators. This makes it also very suitable for projects that are sensitive to the size of the components.

There are many pneumatic actuators available in the market, most of them are designed for large force actuation or long stroke, which doesn't require fast response in micrometer scale. Even though some are designed for fast actuation, they may still be too slow for such small stroke because of their large size. Meanwhile, piezo actuators are fast, but generally they have a very small stroke of just a certain µm, the ones with large stroke is extremely expensive and is hard to acquire.

Therefore, in the following section, some pneumatic and piezo actuators will be chosen to carry out a performance test.

3.2. Actuators performance test

In this section, a lab test is carried out to investigate some easily acquired actuators. The dynamic performance of these actuators will be tested to reveal how fast they can be and how they can be implemented for the Flowerbed application.

The pneumatic actuators tested are Festo Fluidic Muscle, Festo Clamping Modules EV, and PI PICMA stack piezo, as shown in Figure 3.1.

(a) Festo Fluidic Muscle (b) Festo Clamping Modules EV (c) PI PICMA Stack Piezo

Figure 3.1: Stock Actuators for testing

The input of the system is the signal coming out from dSpace, range from 0V to 10V. Frequency response test is driven under PRBS (Pseudorandom binary sequence) signal generator, which generates random inputs with different frequencies into the actuator. The output will be recorded in dSpace with a sampling frequency of 1×10^4Hz, and with the help of MATLAB SysID toolbox, the frequency response of the actuators can be obtained. Figure 3.2a shows the schematic of the test setup. The supply pressure for the pneumatic actuators is 4bar, and the maximum driving voltage for the stack piezo actuator is 100V.

3.2.1. Festo Pneumatic Fluidic Muscle

Festo Fluidic Muscle is a pneumatic tensile actuator which mimics natural muscular movement [11]. It consists of a contraction formed by a pressurized rubber hose, sheathed in high-strength fibers. When internal pressure is applied, the hose expands in its peripheral direction, creating a tensile force and a contraction motion in the muscle's longitudinal direction. The Fluidic Muscle can be therefore used as a linear single-acting actuator, which behaves like a spring with a changing external force, as shown in Figure 3.3.

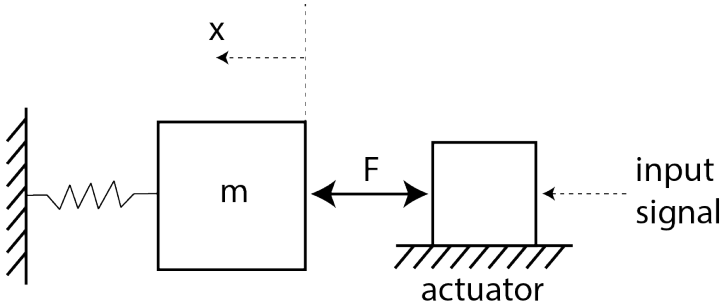

(a) Schematic of the performance test of the actuators

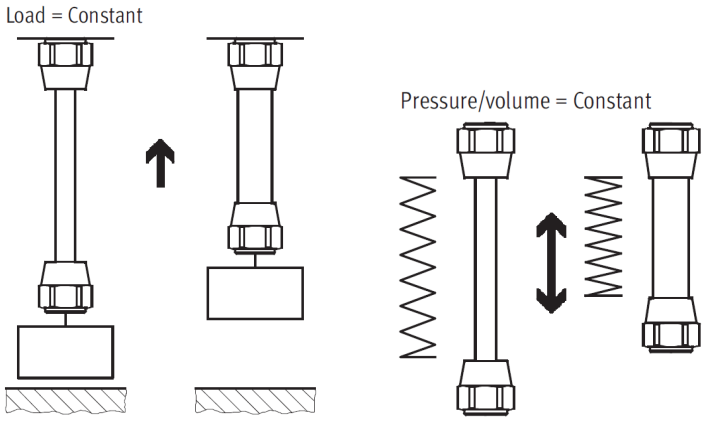

Figure 3.3: Schematic of the Festo Fluidic Muscle, it behaves like a spring with a changing external force, so it can be used as a force actuator or a preloaded spring depending on the situation

The specific Fluidic Muscle used in the test is MAS-10-N100-AA-MCFK. Its specification is:

- Max. lifting force 630N
- Max. permissible contraction 25mm
- Max. operating pressure 8bar

The Fluidic Muscle can deliver a force of 630N, and a stroke of 25mm. They are both much higher than the requirement of the Flowerbed. Figure 3.4 shows the actual test setup for the pneumatic muscle. The actuators are coupled with an aluminium spring as preload, and the output is the displacement of the spring, measured by a capacitive sensor.

The frequency response of the Fluidic Muscle is shown in Figure 3.5. The behavior of a pure force on a preloaded spring is showning some weakness when the frequency response is taken into consideration. The rubber hose is very soft and unfortunately, the stiffness is dependent on the actuation frequency. The result of the weakness is that the eigenfrequency of the Fluidic Muscle is very low at only about 100Hz, and the magnitude of the response in low frequency is increasing with increased frequency. Furthermore, the internal volume of the Fluidic Muscle is large, and the large volume leads to a long time needed to build up the internal pressure. Increasing the supply pressure from 4 bar to 5 bar can improve the performance, but not by much. It's very difficult to achieve a bandwidth above 50Hz in this case, the Fluidic Muscle is not a suitable actuator for the Flowerbed application.

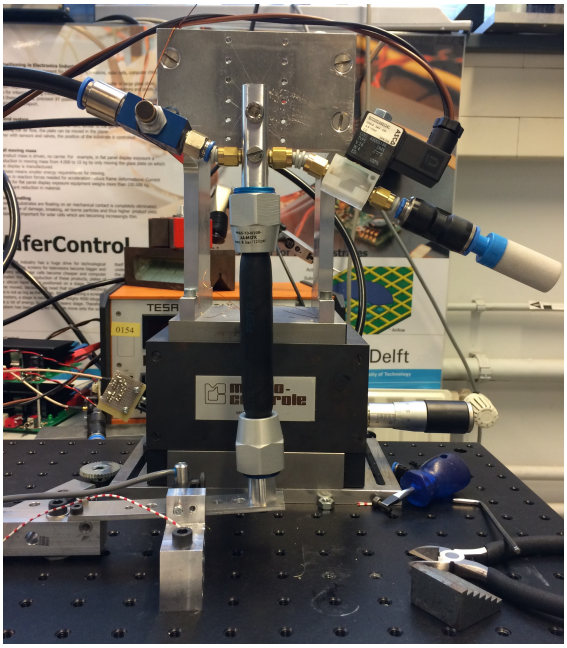

(a) Test setup for the pneumatic muscle

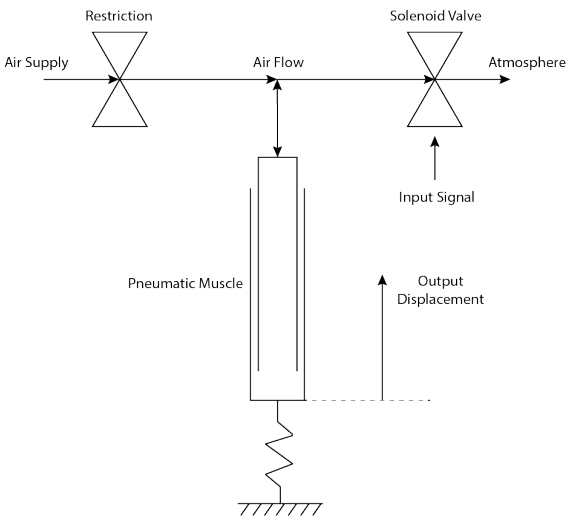

(b) Schematic of the test setup for the pneumatic muscle

Figure 3.4

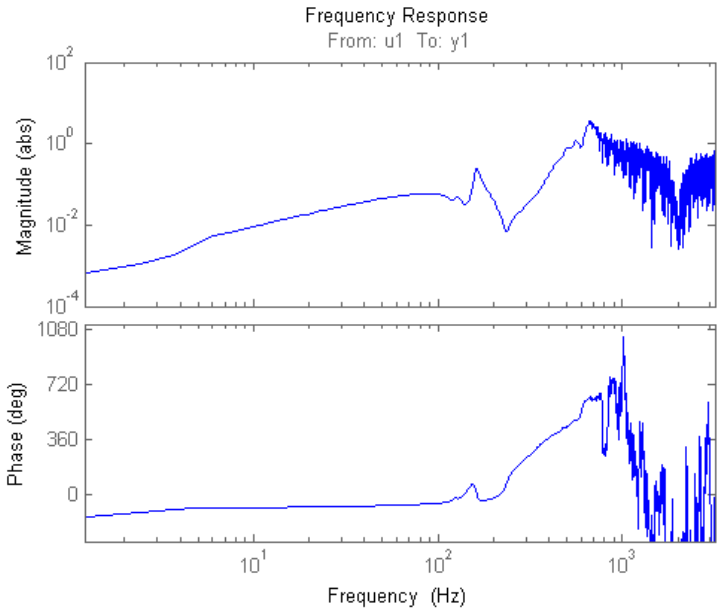

Figure 3.5: Frequency Response of the Fluidic Muscle

3.2.2. Festo Pneumatic Clamping Module

The Festo Clamping Module EV is a pneumatic linear single acting actuator which implements a rubber membrane/diaphragm to constrain the movement. Figure 3.6 shows the cross section of the Clamping Module [12]. It consists of a pressure chamber with a moving membrane, in the center of the rubber membrane is a thick rubber clamping block which provides an even force on the clamping

surface. When the internal pressure is applied, the membrane expands and pushes out in its normal direction, and hence provide the clamping force.

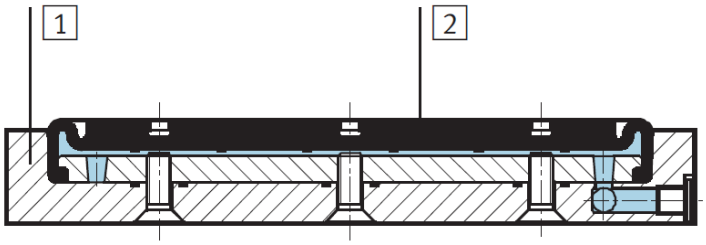

Figure 3.6: Cross section of the Clamping Module. No.1 is the aluminium housing, No.2 is the moving rubber membrane. When pressure is applied, the rubber membrane will move along its normal direction, in this case it will move upwards

The specific Clamping Module EV used in this test is EV-15/40-4. Its specification is:

- Max. pushing force 369N
- Max. permissible stroke 4mm
- Max. working pressure 2-6bar

The Clamping Module EV can deliver a force of 369N which is more than twice needed for the Flowerbed. Judging from the cross section, it has much less internal volume than the Fluidic Muscle, which is a big advantage, because the time needed to build up the internal pressure would be significant less. The test setup of the Clamping Module EV is exactly the same as that for the Fluidic Muscle shown in Figure 3.4.

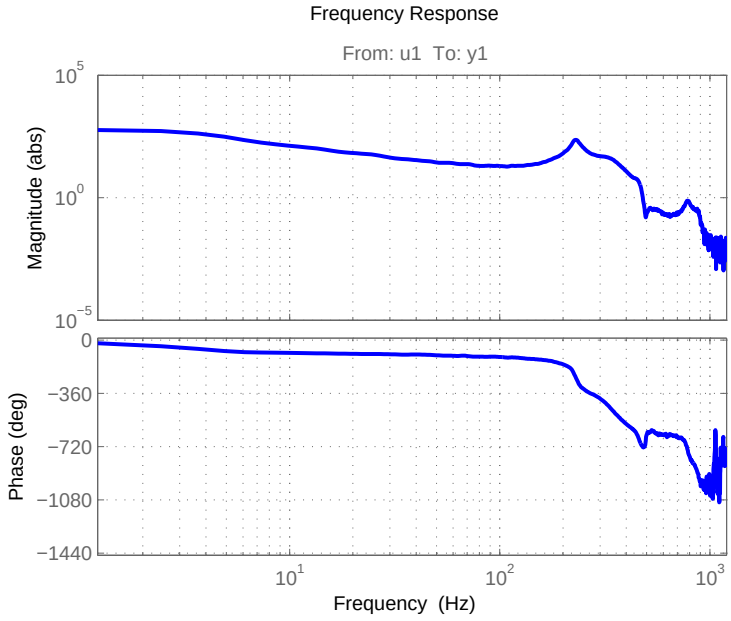

Figure 3.7: Frequency Response of the Clamp Module

The frequency response of the Clamping Module EV is shown in Figure 3.7, it shows a much better frequency response than the Fluidic Muscle thanks to the relatively small internal volume design and small rubber membrane. Smaller air space inside the actuator gives it a faster response, and the

rubber membrane design provides a flatter response in low frequency. Still the rubber membrane and the rubber clamping block show some weakness in dynamic performance. The soft rubber and the clamping block has very low stiffness, and this leads to a first eigenfrequency of around 220Hz, with the phase goes beyond -360°. The expected bandwidth of the Clamping Module EV is lower than 100Hz

3.2.3. Stack piezo actuator

The stack piezo actuator is a stack of many linear piezoelectric material in layers. Each layer of piezoelectric material is a small piezo actuator, and by stacking them together, one can achieve a combined piezoelectric actuator with larger stroke. Unlike the pneumatic actuators which are force actuators, the stack piezo actuator is a position actuator with a certain stiffness. The difference is how this stiffness will affect the actuation system, the discussion of the stiffness will be included in the next chapter.

The specific piezo actuator used in this test is the PI PICMA Stack Multilayer Piezo Actuator P-885.51. Its specification is:

- Max. displacement 18µm
- Stiffness 50N/µm
- Blocking force 900N
- Resonant frequency 70kHz

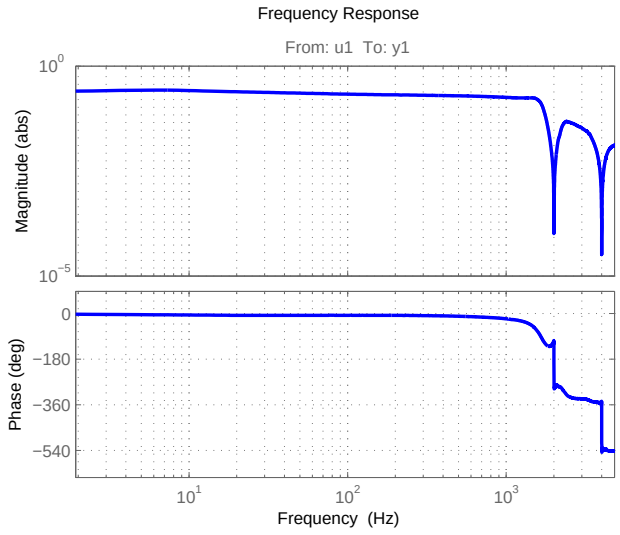

Figure 3.8: Frequency Response of PICMA Piezo

The frequency response of the piezo actuator is shown in Figure 3.8. The PICMA piezo actuator has by far the best frequency response in the test. Nearly constant response magnitude and no phase lag up to about 1000Hz. One can expect 1000Hz as the bandwidth of this piezo actuator.

It's an excellent actuator for extremely high-speed application because of the high bandwidth, however, the small stroke, 18µm in this case is the weakness of such piezo actuator, it needs displacement amplification mechanism to meet the requirement of the Flowerbed. There are some high-end piezo actuators with large stroke to overcome this weakness, for example, the PICA Power Piezo Actuators from PI, which has a specific model with 180µm stroke, but the cost is too much (more than 1700 euro

without electronic components at the time of writing), therefore, it's not practical to implement those extremely expensive high-end piezo actuators in this application.

3.3. Discussion

In this chapter, the specification and performance of two pneumatic actuators and one piezo stack actuator were discussed. The data of these actuators is compared to the requirements of the Flowerbed and concluded with their advantages and weakness.

Festo Pneumatic Fluidic Muscle is a very powerful actuator, it can deliver very large pulling force, but the large internal volume and the inconsistent stiffness with low first eigenfrequency makes it not suitable for fast actuation.

Festo Pneumatic Clamping Module EV, on the other hand, has a significantly faster performance. The reason is that it has much less internal volume due to the implementation of a membrane, and the rubber membrane with rubber clamping block have higher first eigenfrequency than the Fluidic Muscle. The Clamping Module is not designed for fast actuation and indeed it's still not fast enough for the Flowerbed. However the test in this chapter shows the possibility of implementing a fast pneumatic actuator for the Flowerbed.

PI Stack Piezo actuator is an extremely fast actuator which has a bandwidth 6 times higher than required, however, its stroke is very limited. The stroke of the specific piezo actuator tested is only 18µm, if this actuator is going to be implemented in the Flowerbed, it needs a displacement magnification mechanism. There are extremely expensive high-end stack piezo actuators which meets the requirement of the Flowerbed, but they will not be considered due to the high cost.

The linear membrane pneumatic actuator, as well as the linear stack piezo actuator, are both suitable for the Flowerbed, but their need to be tailored for the Flowerbed, and their different weakness required different design in the mechanism.

In the next chapter, the design of the actuation configuration will be discussed, where the advantage/weakness of both types of actuators will be taken into account, and one combination of actuator/configuration will be chosen for the Flowerbed.

4

Actuation Configuration

In the previous chapter, several actuators were tested and the advantage/weakness was discussed. Pneumatic actuator tends to be relatively slow but has a large force, and it's possible to improve the performance with proper design, but the size of the pneumatic actuator must be taken into account due to the required external components. Piezo actuators are extremely fast but they have very small stroke, which is in need of displacement amplification mechanisms to meet the requirement of the Flowerbed, and the stiffness of the piezo actuator could also affect the total displacement if it's applied to a very stiff load, in this case, the Flowerbed.

In this chapter, the configuration of the actuators will be discussed. Three configurations will be examined and two of them will be modeled according to the advantage/weakness of the actuators, and finally one combination of actuator/configuration will be chosen for the Flowerbed.

Recalling the working principle of the nozzles, 61 nozzles are arranged in a hexagonal array. The control plate has 3 degrees of freedom planar movement, with a translational movement of ±40μm in x and y direction and a small ±0.7mrad rotation, it needs at least 3 actuators for the actuation to achieve the 3 DoF movement. More actuators can provide more force and redundancy, which could be beneficial depending on the situation but not necessarily so.

The 3DoF x-y-θ stage developed by Chang et al. reviewed in Chapter 2 is a very robust design. The piezo actuator combined with displacement amplification beam shown in Figure 4.1 makes it possible to achieve large displacement of the stage using piezo actuators with small displacement. In their original design, the x-y-θ actuation is realized by two-stage structure, where the top stage shown in Figure 4.1 only controls displacement in x-y direction. The paired actuators move always in the same direction, for example, the two 21x actuators will both expand at the same time to ensure they only actuate the x+ displacement. This configuration can be modified into x-y-θ actuation by implementing differential control. For example, if the top 21x and left 21y actuator expand, while the bottom 21x and right 21y actuator contract, they will drive the stage into a clockwise θ rotation.

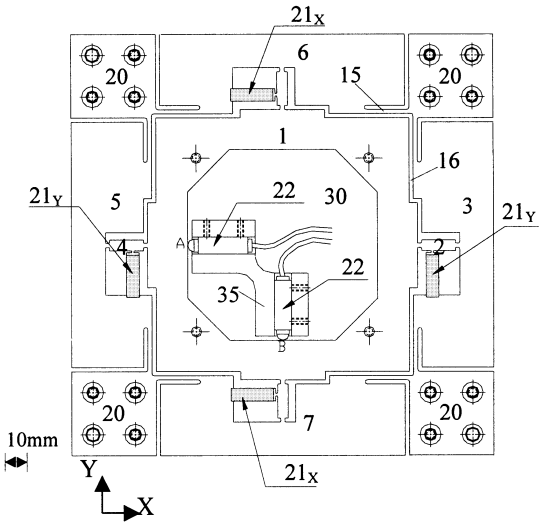

Figure 4.1: The x-y top stage design of Chang et al. [5] In fact this design can be further refined with differential control of the actuators to further achieve x-y-θ actuation

Using four actuators to control x-y-θ displacement is a very common concept, and is in fact widely used in many precision positioning applications. However, implementing this concept in the Flowerbed application would be difficult. The reason is that the control plate of the Flowerbed has a hexagonal shape with only three connections arranged axisymmetrically, as shown in Figure 4.2. If the above-mentioned configuration is implemented in the Flowerbed, it needs an extra mechanism to change the shape of hexagon into a square in order to connect four actuators. This extra mechanism will add weight to the system and increase the complexity, therefore, this configuration is not desired. The best solution of the configuration should adapt to the hexagonal shape of the control plate of the Flowerbed.

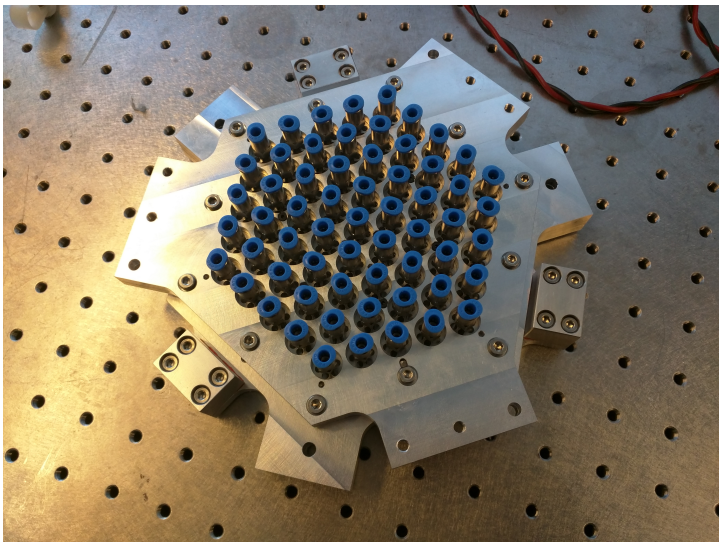

Figure 4.2: The control plate of the Flowerbed. It has hexagonal shape with three connection, arranged axisymmetrically.

In fact, the hexagonal shape of the control plate is very suitable for implementing a special kind of concept called ”planar parallel manipulator” actuation system. Parallel manipulator is defined as a closed-loop kinematic chain mechanism, its end-effector is linked to the base by several independent kinematic chains. Generally, a parallel manipulator has good performances in accuracy, rigidity, and it’s able to carry large loads [13].

Using the parallel manipulator concept, the Flowerbed can achieve the 3 DoF planar movement with only 3 actuators, and at the same time reduce moving components, making the system simple and reliable, reducing the cost. In the following sections of this chapter, two different configurations of the parallel manipulator concept will be discussed regarding the complexity and capability with the actuators discussed in the previous chapter, one combination of actuator/configuration will be chosen for this Flowerbed application. The complete modeling of the parallel manipulator can be found in Appendix A.

4.1. Parallel manipulator, type 3-RPR

A 3-RPR parallel manipulator is a type of parallel robot that implements linear actuators, as shown in Figure 4.3. The linear actuators change the length of the links L_i, by the cooperation of the actuators, the links change their length according to a transformation matrix so that the end-effector with the moving coordinate H will move to a desired position in the base coordinate B, which is also called the world coordinate.

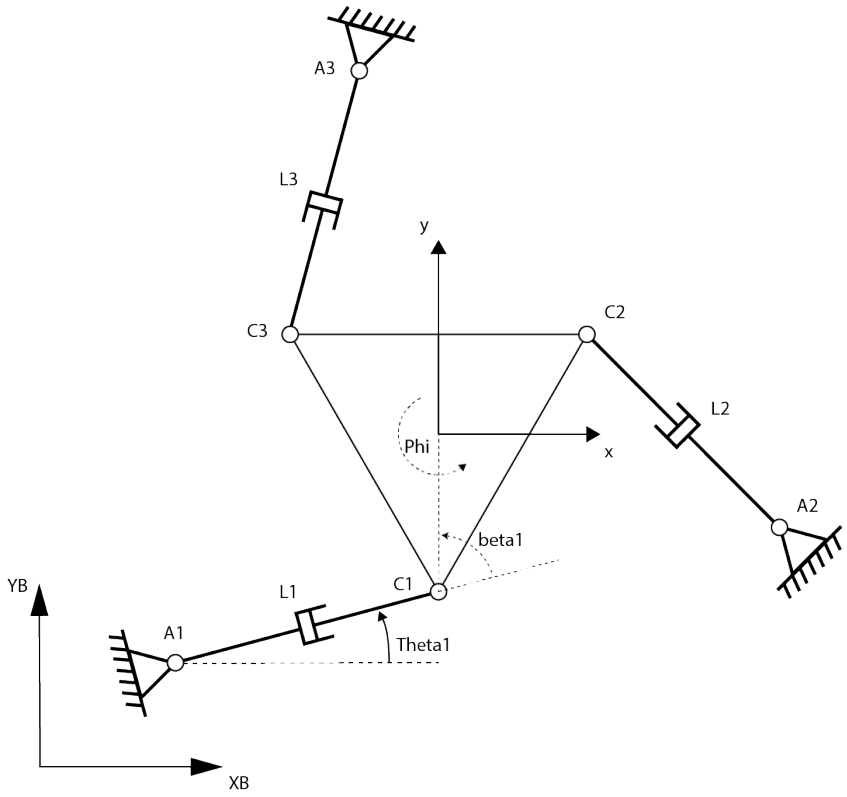

Figure 4.3: Schematic of a 3-RPR parallel manipulator

4.1.1. Kinematics modelling

Based on the geometric and the displacement between the links, the closed loop constraint equation of the 3-RPR parallel manipulator can be written as Eq.4.4. ${}^{B}\mathbf{C}_i$ is the position of the joints C_i in the base coordinate, while ${}^{H}\mathbf{C}_i$ is the position in the moving coordinate. ${}^{B}\mathbf{A}_i$ is the position of the joints A_i in the base coordinate. L_i is the length of the links A_iB_i. ${}^{B}\mathbf{P}_H$ is the position of the end-effector in the base coordinate, ${}^{B}_{H}\mathbf{R}$ is the transformation matrix from the moving coordinate to the base coordinate. i=1,2,3. [6]

$$ {}^{B}\mathbf{C}_i = {}^{B}\mathbf{P}_H + {}^{B}_{H}\mathbf{R}\,{}^{H}\mathbf{C}_i = {}^{B}\mathbf{A}_i + L_i e^{i\theta_i} \tag{4.1} $$

where: $ {}^{B}\mathbf{P}_H = \begin{Bmatrix} x \\ y \end{Bmatrix}$ and $ {}^{B}_{H}\mathbf{R} = \begin{bmatrix} cos\phi & -sin\phi \\ sin\phi & cos\phi \end{bmatrix}$

The relation between the linear velocity of the actuators $\dot{L} = [\dot{L}_1\ \dot{L}_2\ \dot{L}_3]^T$ and the velocity of the end-effector $X = [\dot{x}\ \dot{y}\ \dot{\phi}]^T$ of the 3-RPR configuration can be derived as

$$ \dot{L} = \mathbf{M}\dot{X} \tag{4.2} $$

where **M** is the inverse Jacobian matrix of the 3-RPR parallel manipulator.

For very small displacement, Eq.4.2 can be linearized as

$$ \Delta L = \mathbf{M}\Delta X \tag{4.3} $$

The linearized equation Eq.4.3 translate the displacement of the end-effector to the displacement of the linear actuators.

Figure 4.4 shows one 3-RPR configuration with $\theta_i = 0$ from the model. The model demonstrates a circular movement of the model in Figure 4.5. The end-effector is placed at (40µm,0) and starts to draw a circle counter clockwise around (0,0) with a radius of 40µm, with the position of the actuators shown in the right part of the graph, the horizontal axis on the right side is the angle of the circle in degrees. The graph shows how the actuators cooperate when the end-effector draws a circle with its maximum displacement.

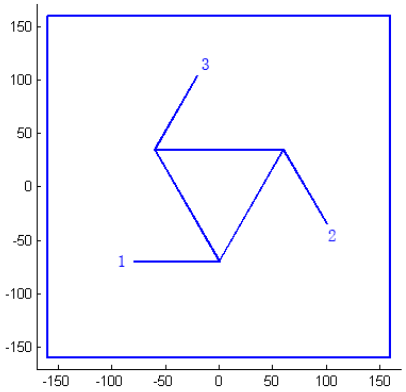

Figure 4.4: One possible 3-RPR configuration with θ_i=0

Furthermore, the maximum rotation of the flowerbed is ±0.7µrad, this leads to a displacement of 0.049µm of the actuator. The flowerbed should be able to do maximum rotation while it's at the limit of the workspace. The actuator should be able to move 80.049µm, but 0.049µm falls into the tolerance of the manufacturing, the required stroke of the actuator stays at 80µm. The 3-RPR configuration has no problem in rotating the Flowerbed while at its maximum translational displacement.

4.1.2. Advantage/disadvantage of 3-RPR configuration

One of the advantages of the 3-RPR configuration is that it's simple and straightforward. All three actuators apply force to create linear displacement, they can cooperate with each other and control the displacement of the Flowerbed. There is no displacement amplification mechanism, therefore,

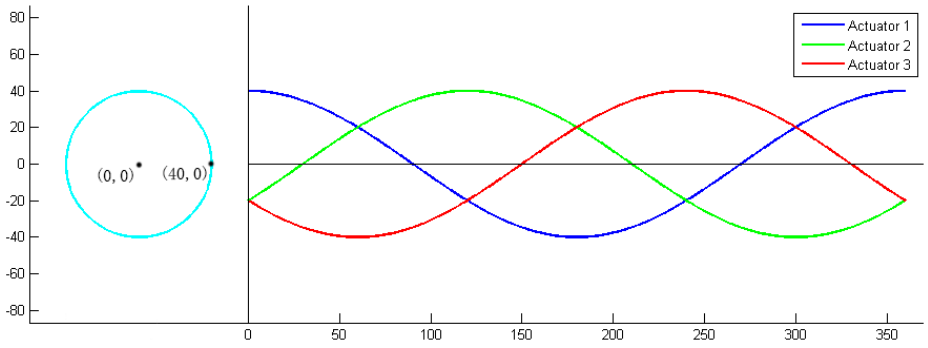

Figure 4.5: Demonstration of the circular movement of the 3-RPR parallel manipulator. This demo shows the cooperation of the actuators when the end-effector draws a circle with a radius of 40µm

the actuator must have 80µm total displacement in order to achieve the ±40µm displacement of the Flowerbed. Piezo actuator, in this case, will not be suitable due to the small displacement of the piezo.

Compliant joints are chosen for this configuration, as shown in Figure 4.6. The working line of the force of the actuators is in fact in line with the links and joints. This will ensure that the compliant joint will experience less deformation other than bending. Compliant joints are very suitable for such precision actuation system.

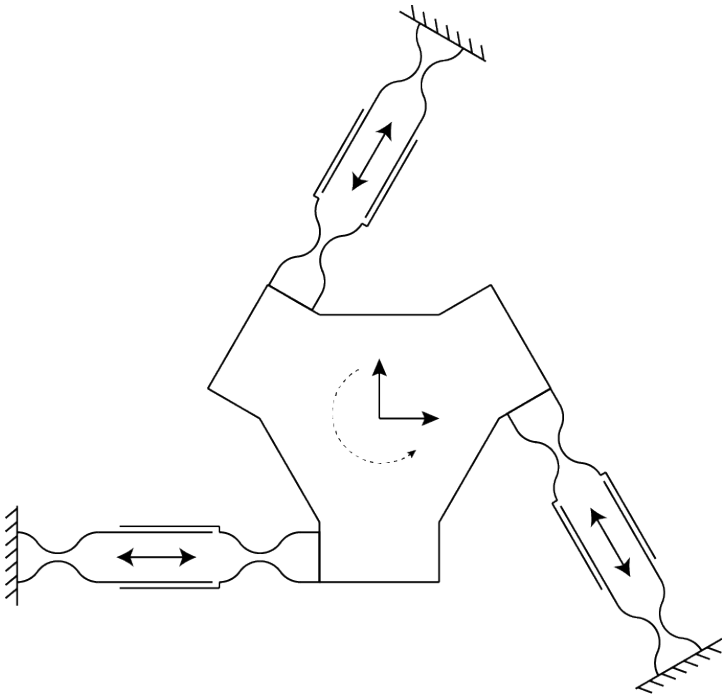

Figure 4.6: Schematic of the joints of a 3-RPR parallel manipulator. The compliant joints are placed at a position so that the force of the actuators is along the center line of the joints, reducing the deformation other than bending of the ideal compliant joints

4.2. Parallel manipulator, type 3-RRR

A 3-RRR parallel manipulator is a type of planar robot with only revolute joints in each chain, as shown in Figure 4.7a. Six links determine the position of the platform together by controlling the angle

of the joints A1, A2 and A3. Generally, the actuator of this type is a rotational actuator located at the joints A1, A2 and A3, however, a rotational actuator with very small stroke is hard to find, and linear actuators with small strokes is easily available, therefore the configuration of 3-RRR is slightly modified, as shown in Figure 4.7b. Changing the actuator to linear has some advantage in this application, it opens the ability to use actuators with a different stroke. By connecting the linear actuator at a different position on the link, one can change the amplification of the displacement, hence adapting the configuration to different parameters.

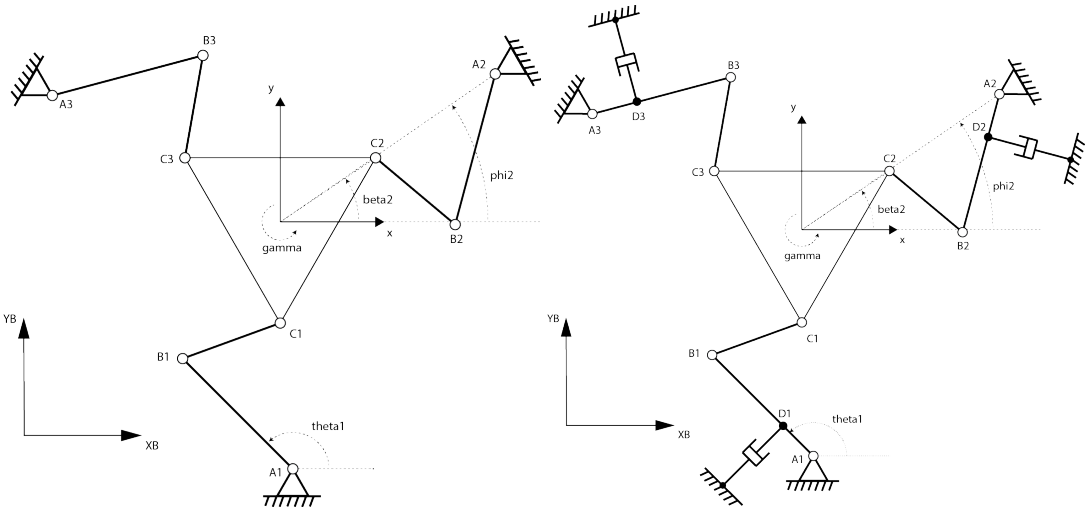

(a) Schematic of a common 3-RRR parallel manipulator,9 revolute joints, the actuation is done by rotational actuators located at joints A1, A2 and A3

(b) Schematic of a modified 3-RRR parallel manipulator, it has only passive revolute joints, the actuation is done by an external linear actuator, the position of the linear actuator will determine the amplification of the displacement, very suitable for small stroke actuators

Figure 4.7

4.2.1. Kinematics modelling

Based on the geometric and the displacement between the links, the closed loop constraint equation of the 3-RRR parallel manipulator can be written as Eq. 4.4, with $\mathbf{r} = (x, y)^T$ is the position of the center of the flowerbed, $\mathbf{u}_i$ and $\mathbf{w}_i$ are the unit vectors of the links B_iC_i and A_iB_i, respectively; $\mathbf{a}_i$ and $\mathbf{b}_i$ is the position of the joints A_i and C_i in the world coordinate. $\mathbf{R}$ is the rotation matrix of the end effector. l_1 is the length of the links A_iB_i and l_2 is the length of the links B_iC_i.[5]

$$\mathbf{r} + \mathbf{R}\mathbf{b}_i - \mathbf{a}_i - l_1\mathbf{u}_i = l_2\mathbf{w}_i \tag{4.4}$$

where: $\mathbf{R} = \begin{bmatrix} cos\gamma & -sin\gamma \\ sin\gamma & cos\gamma \end{bmatrix}$ and $\mathbf{r} = \begin{Bmatrix} x \\ y \end{Bmatrix}$

The initial position of the joint angles can be therefore determined by the position and orientation of the end-effector, with the lengths of the links given as known parameters. There are two possible positions for each chain, as can be imagined, they are symmetric. In this research only the possible position shown in Figure 4.7a will be investigated.

The relation between the angular velocity $\dot{\mathbf{x}} = [\theta_1\ \theta_2\ \theta_3]_T$ of the joints A_i and the displacement of the platform $\mathbf{p} = [x\ y\ \gamma]^T$ can be derived:

$$\dot{\mathbf{x}} = \mathbf{J}\dot{\mathbf{p}} \tag{4.5}$$

where J is the Jacobian of the model.

For very small displacement, the above equation can be linearized as

$$\Delta \mathbf{x} = \mathbf{J} \Delta \mathbf{p} \tag{4.6}$$

The linearized relation in Eq.4.6 translate the displacement of the end-effector to the rotation of the joints. Further if the linear actuator is implemented as previously shown in Figure 4.7b, the rotation of the joints can be further translated into the linear displacement of the actuators:

$$\Delta \mathbf{q} = l_a \Delta \mathbf{x} \tag{4.7}$$

where l_a is the length between the connecting point of the actuator and the joint $A_i D_i$.

The kinematic equation 4.6 can be therefore rewritten as

$$\Delta \mathbf{q} = \mathbf{J}_a \Delta \mathbf{p} \tag{4.8}$$

where $\mathbf{q} = [s_1 \ s_2 \ s_3]^T$ is the displacement of the linear actuators, $\mathbf{J}_a$ is the new Jacobian for the modified 3-RRR configuration with the linear actuators.

4.2.2. Stiffness of the 3-RRR configuration

The small strokes of the linear actuators result in very high requirements on the joints, especially when using position actuators like piezo. Generally, a 3-RRR manipulator has rotational joints made of roller bearings for large displacement, however in the Flowerbed application, such bearing doesn't have the accuracy for micrometer movement because of the backlash and the clearance in the bearing. Instead, all the joints will be compliant.

The ideal compliant joint has no stiffness in the rotational direction but in reality there is always some stiffness. This stiffness of the compliant joint can not be neglected because it will affect the µm displacement of the Flowerbed due to the increase of the total stiffness of the manipulator. Piezo actuator is used in this configuration, and the piezo actuator is position actuator. The stiffness of the manipulator will cause a high load on the piezo, reducing the effective stroke.

Furthermore, due to the implementation of the linear actuators, these actuators will apply a force perpendicular to the link, cause a shear stress on the compliant joints. The compliant joints must be strong enough to reduce the deformation in the shear direction, but it will increase the stiffness in the rotation direction as well. Figure 4.8 shows the schematic of the manipulator with the stiffness in the joints. This difficulty can be solved by designing a better position of the joints, aligning the force to the longitudinal direction of the compliant joints, but still it will increase the complexity of the design.

The equation of the equilibrium of the system is

$$\mathbf{K} \Delta \mathbf{P} = \mathbf{J}_a^T \mathbf{F} \tag{4.9}$$

where $\mathbf{K} = k_\theta \Sigma_{i=1}^{3} \mathbf{J}_i^T \mathbf{J}_i + k_a \mathbf{J}_a^T \mathbf{J}_a$ is the equivalent stiffness of the system regarding to the linear actuators and $\mathbf{F} = [F_1 \ F_2 \ F_3]^T$ is the force of the actuators.

4.2.3. Limited displacement under stiffness

This modified 3-RRR configuration is specifically designed for actuators with very little stroke, for example, the stack piezo actuators. The piezo actuators are position actuators with a certain stiffness, the actual displacement of the actuator is affected by the stiffness of the external system, in this case, it's the Flowerbed in 3-RRR configuration. Once the stiffness is too high, the piezo actuator will not be able to extend its length anymore, hence, the stiffness of the 3-RRR configuration is very important.

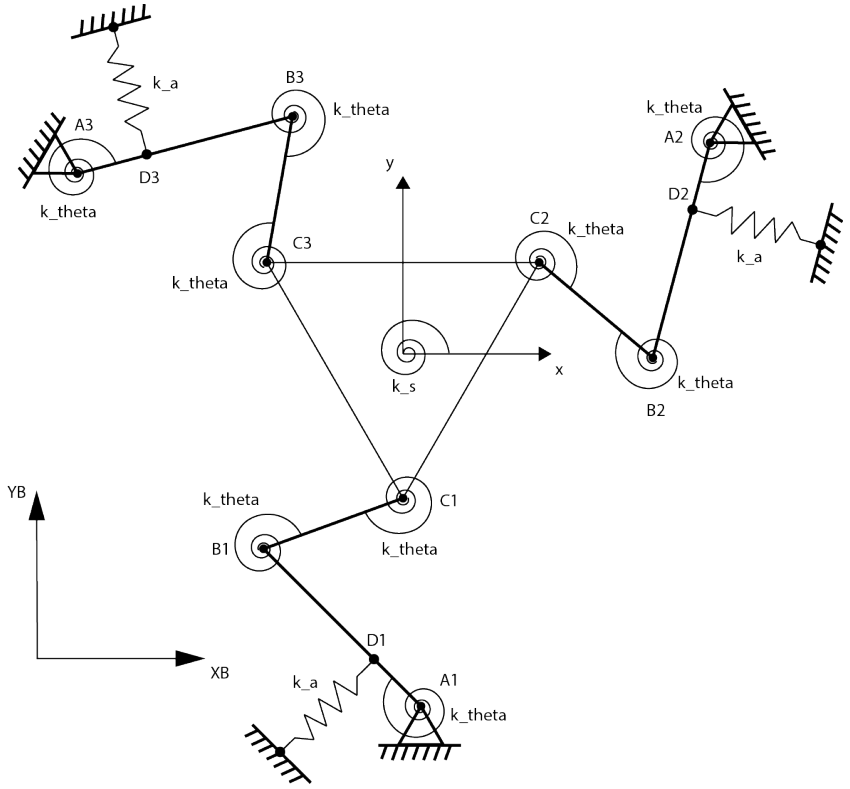

Figure 4.8: Schematic of a 3-RRR parallel manipulator with compliant joints, the joints have stiffness, as well as the actuators, they will contribute to the total stiffness of the system

To illustrate this problem, a Matlab model is made using the previously established model. Figure 4.9 shows the 3-RRR configuration of the model, together with the available space of the Flowerbed. The links can not be too long because of the constraint of the available space of 320x320mm, there still need to be space to mount the links and the actuators.

In this model, the actuators only have a maximum stroke of 16µm. They will be located at a position between A_i to B_i in order to find an optimum position for maximum displacement of the end-effector. The position coordinate is normalized, with 0 equals a position at joint A_i and 1 equals a position at joint B_i. In the first simulation, the actuators will move according to the transformation matrix so that the Flowerbed will move to the y direction, in this case, the input of the simulation is $[-16\ 8\ 8]$ µm. The stiffness of the joints will be changed to investigate its effect on the maximal displacement of the end-effector. The rotational stiffness of the joints can be approximated by: [5]

$$k_\theta = \frac{2Ebt^{5/2}}{9\pi R^{1/2}} \tag{4.10}$$

where E is the elastic modulus of the material, b is the width of the flexure hinge, t is the minimum thickness of the flexure hinge, and R is the radius of the flexure hinge. In in Tian's research the rotational stiffness is 7.6Nmm/rad, in this model the rotational stiffness is chosen as 1Nmm/rad to demonstrate the effect of the reduced displacement with a weaker piezo actuator.

Figure 4.10 shows the result of the simulation. In Figure 4.10a the joints have no stiffness, the stiffness comes from the end-effector and the actuators. When the actuators are positioned at 0.1 of the total length of link A_iB_i, the end-effector has the maximum displacement of 97.9µm. If the stiffness of the joints becomes 1Nmm/rad, the displacement will be significantly reduced to 24.5µm as shown in Figure 4.10b. It should be noticed that the stiffness of the joints not only affects the maximum displacement of the end-effector, it also changes the optimal position of the actuator. The

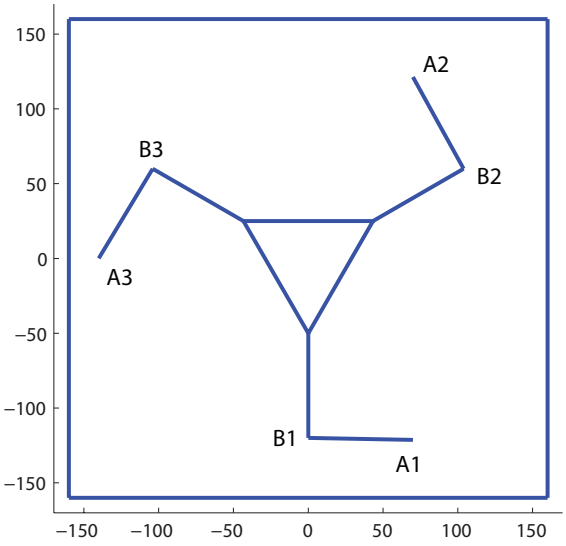

Figure 4.9: Simulation of the 3-RRR configuration, it shows one possible position and lengths of the links

result suggests that the stiffness of the joints, as well as the end effector, is extremely important, as they can significantly reduce the displacement of the system, therefore in the end, it requires a very stiff actuator, or a large stroke actuator just to compensate for the reduction of the displacement caused by the stiffness of the system.

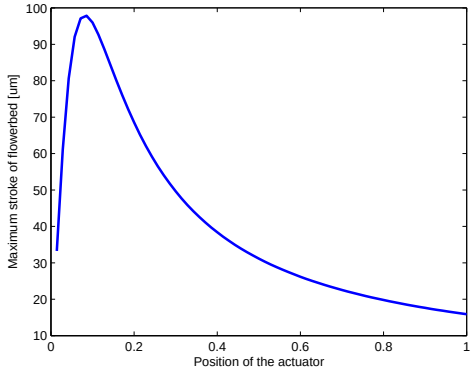

(a) No stiffness in the joints. The max displacement of the end-effector is 97.9µm, with the actuator located at 0.1 of the total length in A_iB_i

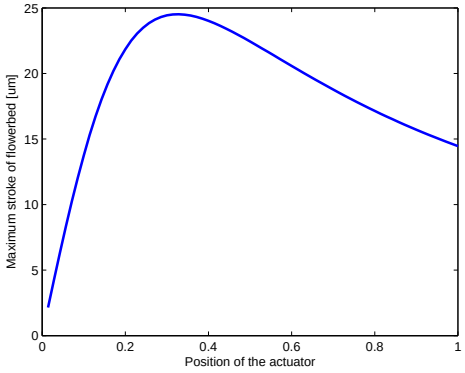

(b) Increased stiffness in the joints. The max displacement of the end-effector is significantly reduced to 24.5µm, and the optimal position of the actuator is changed to 0.33 of the total length in A_iB_i

Figure 4.10: First simulation of the 3-RRR configuration, increased stiffness lead to significant change of maximum displacement of the end-effector

Furthermore, the compliant joints for some complex 3-RRR configuration can suffer from force with different directions, as shown in Figure 4.11. When the compliant beam has only a normal force applied, the joint will mostly see a bending moment applied to it and the joint will act as a rotational bearing. However when there is another force acting on the beam, the joint may undergo some shear stress or tensile stress and start to bend/stretch in an undesired way. Such undesired deformation will reduce the bending angle of the joint, in some worse case, it will change the kinematics matrix and the

Jacobian matrix of the parallel manipulator, causing the end-effector to shift its displacement or even fail.

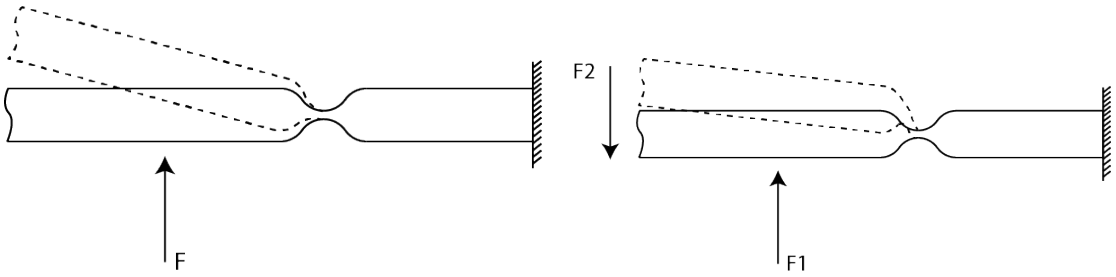

(a) Pure bending of the compliant joints when only normal force is applied, the joint only exercises a bending moment, it works as a pure rotational bearing

(b) When other forces apply on the link, the joint will exercise not only a bending moment, but some shearing force or even suffers from tensile stress, the deformation becomes not longer pure bending, but together with some shearing and stretching. This will change the characteristic of the joint and affect the displacement of the end-effector

Figure 4.11

4.2.4. Advantage/disadvantage for the modified 3-RRR configuration

The modified 3-RRR configuration has a major advantage of amplifying the displacement by choosing a suitable location of the linear actuator. This leverage effect makes it possible to implement some strong actuators with a small stroke, but the stiffness of the joints can weaken this advantage and become a weakness. Furthermore, in practice, the compliant joints not only has deformation in the rotational direction but also in the shear direction. This deformation is not simulated in the model, but should also be considered in further research. The complexity of the 3-RRR configuration increases the difficulty of manufacturing and the six links may have inneglectable weight which can reduce the dynamic performance of the parallel manipulator.

4.3. Discussion

Parallel manipulators have their advantage of relatively strong and fast performance with all the actuators cooperating and the accuracy is relatively high when using the compliant joints. Such concepts are very popular in the field of robotics and are widely used for precise actuation. In this chapter the 3-RRR and 3-RPR planar parallel manipulators are discussed, models for both concepts are made and demonstrated for the most critical aspects regarding their advantages and disadvantages.

The 3-RRR configuration provides a possibility to amplify the stroke of the actuator, it's a possible and feasible design for a strong actuator with small stroke like linear stack piezo actuator. However, the joint stiffness may affect the effectiveness of the displacement amplification design, causing the maximum displacement to reduce. Furthermore, the design is relatively complex, it will increase the difficulty during manufacturing.

The 3-RPR configuration is simple and straightforward. There is no displacement amplification, therefore, it must be combined with actuators which have large stroke, for example, the pneumatic actuators. The construction is very reliable and it has fewer components.

Judging from the results in this chapter, The 3-RPR configuration appears to be a better solution when combined with pneumatic actuators. This combination is chosen for the Flowerbed.

With the combination chosen, it brings up a question about whether it is possible to make such a pneumatic actuator, that can meet the requirement of the Flowerbed, under the 3-RPR configuration:

- The actuator should have a stroke of 80μm.
- The actuator should be able to generate a maximum force of 140N.
- The actuator should be able to reach a bandwidth of 150Hz.
- The actuator should be as cost effective as possible.
- The actuator should be compact so that it can fit into the Flowerbed system.

In the following chapters, this question will be answered. It starts with a study of the pneumatic actuator with working principle and modeling in the next chapter. Models will be established and verified. Because the Flowerbed has some special requirements for the actuator, the following part of this research is to explore the limit of the special designed pneumatic actuator, to explore whether it is possible to make a pneumatic actuator which can meet the special requirement of the Flowerbed, especially the bandwidth of the actuator.

5

Modelling of a Pneumatic Actuator

In the previous chapters, the pneumatic actuator was introduced and finally chosen for the Flowerbed together with the 3-RPR parallel manipulator configuration, which utilizes three pneumatic actuators to control the planar movement of the control plate of the Flowerbed.

Pneumatic actuator, which utilizes compressed air as power source, is a relatively low cost, high power actuator. They are commonly used as long stroke and high force applications, but they're not commonly seen for high speed, small stroke applications, even the Festo Clamping Module EV has a stroke of 3mm. In fact, there is currently no pneumatic actuators available for the Flowerbed application. Previous test in this research showed some possibility of fast actuation by trading stroke for speed. It brings up a question about whether it is possible to make such a pneumatic actuator, that can meet the requirement of the Flowerbed, under the 3-RPR configuration:

- The actuator should have a stroke of 80μm.
- The actuator should be able to generate a maximum force of 140N.
- The actuator should be able to reach a bandwidth of 150Hz.
- The actuator should be as cost effective as possible.
- The actuator should be compact so that it can fit into the Flowerbed system.

A stroke of 80μm is very small for a pneumatic actuator, and the 150Hz bandwidth is a challenge for this research. In order to meet the requirements, the pneumatic actuators must be studied before a prototype can be made. In this chapter, a model of the pneumatic actuator will be established and this model will be verified with test setups and simulation from another researcher. This model will be the first step before the design takes place.

5.1. Working principle of a pneumatic actuator

A pneumatic actuator is driven by a pressure regulator. Compressed air could be available by a compressor in a small application while in the production line it's mostly supplied via pipeline, distributed over the facility. The compressor brings the air from ambient pressure P_a up to supply pressure P_s and feeds it to the inlet of the pressure regulator. Air flows through the air channel into the pressure chamber, then through the solenoid orifice valve and finally out to the ambient atmosphere.

The solenoid orifice valve inside the pressure regulator is controlling the air flow through the pressure chamber. By changing the air flow rate, the pressure P_a inside the pressure chamber can be regulated. By closing the valve, pressure P_a will build up, this will generate a force to the normal

surface of the moving disk, cause the membrane to deform and push the load, which is a spring steel in this case. It should be noted that the orifice after the pump is to limit the maximum air flow rate of the whole system, adjust air flow rate control effectiveness of the valve.

The schematic of the actuator is shown in Figure 5.1 and 5.2. In fact, this configuration is not the only option for the pneumatic actuator. The Orifice restriction at the inlet can also be a valve, hence two valves controlling the air flow at the same time. This is called differential valve control, but in this research, the single valve configuration is used. More information about this configuration can be found in Appendix D.

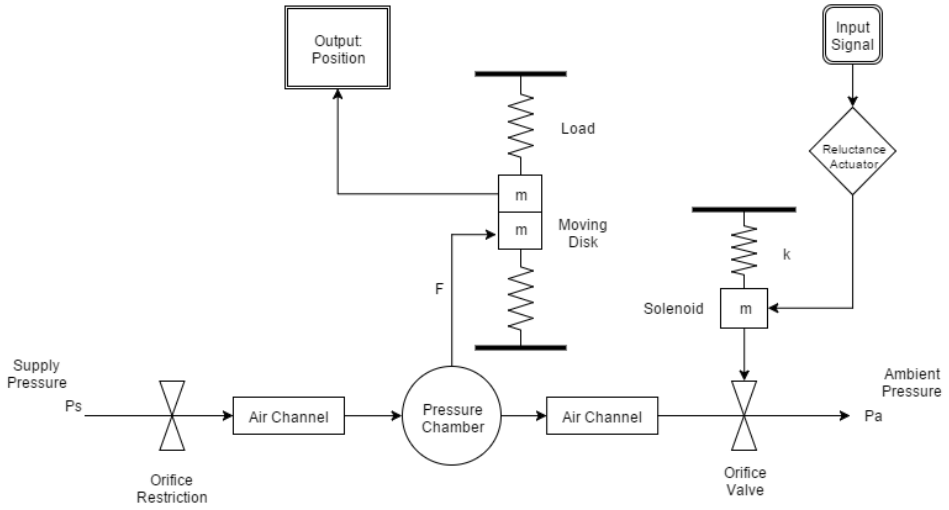

Figure 5.1: Schematic of the pneumatic actuator with load

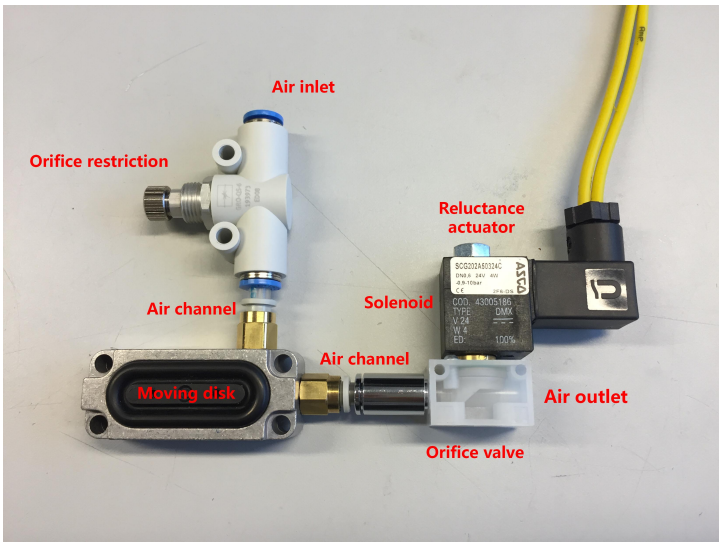

Figure 5.2: Photo of an actual pneumatic actuator without load

5.2. Subsystems of a pneumatic actuator

A complete pneumatic actuator consists several internal components, and these components form different subsystems. A separate study for each subsystem should be carried out and models for each must be made before the complete model for a pneumatic actuator can be established.

Generally a pneumatic actuator, together with the load, have one air dynamic subsystem, one valve subsystem and some mass-spring subsystems, as shown in Figure 5.1. They all have their own characteristic and they coupled together to determine the performance of the actuator.

5.2.1. Air dynamic subsystem

The air dynamic subsystem consists of the air channel, pressure chamber and both orifices as shown in Figure 5.3. The most important parameters in this subsystem are the pressure of the source P_s, the resistance of the orifices R and the volume inside the pressure regulator. These parameters determine the pressure inside and also how fast the pressure can change.

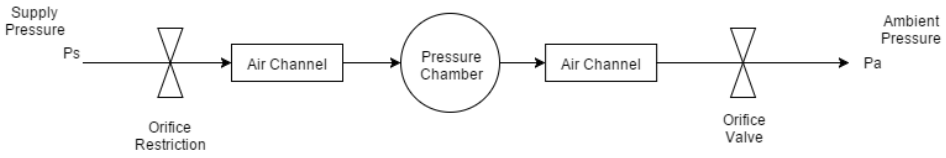

Figure 5.3: Schematic of the air dynamic subsystem

5.2.2. Solenoid valve subsystem

The outlet orifice is generally a valve driven by external components, solenoid actuator for example. Solenoid-orifice valve is very commonly used for controlling the flow rate in a fluid system for its relatively low price and simple construction.

The solenoid actuator is generally a magnetic reluctance actuator preloaded by a spring, as shown in Figure 5.4a and 5.4b. The reluctance actuator controls the distance between the solenoid core and the orifice hole so that it can control the air flow inside the valve. The photos of the reluctance actuator, solenoid and the orifice is shown in Figure 5.5a and 5.5b. It has a basic mass-spring system characteristic but sometimes a low pass characteristic exists in the control signal, as can be found in the ASCO solenoid valves.

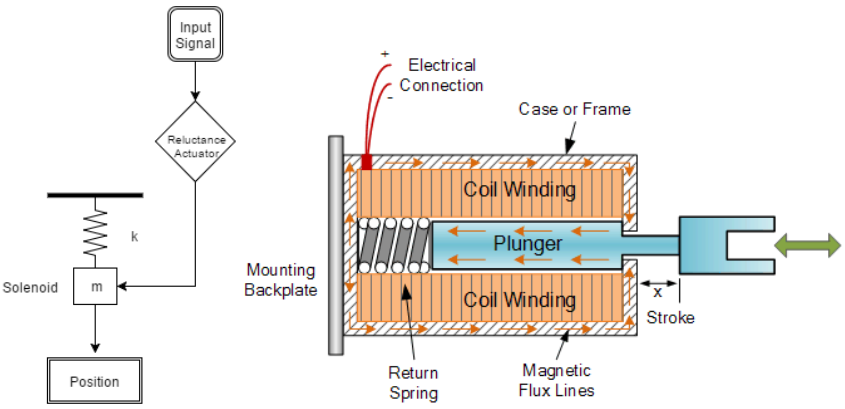

(a) Schematic of the valve subsystem

(b) Cross section of a general solenoid actuator. Figure taken from http://www.electronics-tutorials.ws

Figure 5.4

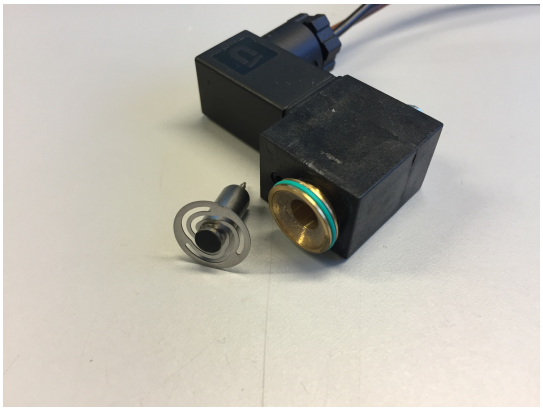

(a) Photo of the solenoid core and the reluctance actuator. The reluctance actuator applies a force to pull the solenoid core towards the housing

(b) Photo of the solenoid core and the orifice. The distance between core and the orifice determines the air flow. This distance is controlled by the reluctance actuator

Figure 5.5

5.2.3. Mass-spring load subsystem

The moving disk is driven by the pressure inside the pressure chamber and it is a pure mass-spring system. As shown in Figure 5.6, the moving part of the actuator is connected to a spring and is moving up and down under the change of the pressure inside the pressure chamber.

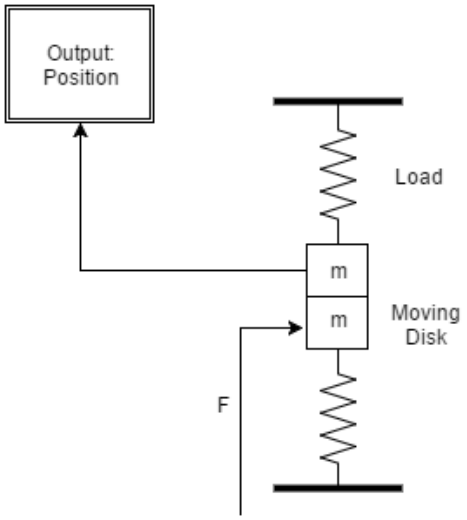

Figure 5.6: Schematic of the load

However, this subsystem is not a simple single mass-spring system. In this research, the load is going to be modelled as two mass-spring systems in serial.

5.2.4. Pressure regulator subsystem

Figure 5.7 shows the schematic of a pressure regulator, the core component of a pneumatic actuator. A pressure regulator consists the two subsystems of air dynamics and the valve dynamics. The function of the pressure regulator is to control the pressure inside the chamber. The force of the pneumatic actuator is generated by the pressure, and because the stroke of the pneumatic actuator in this project is so small, the pressure regulator is the most important system in this project.

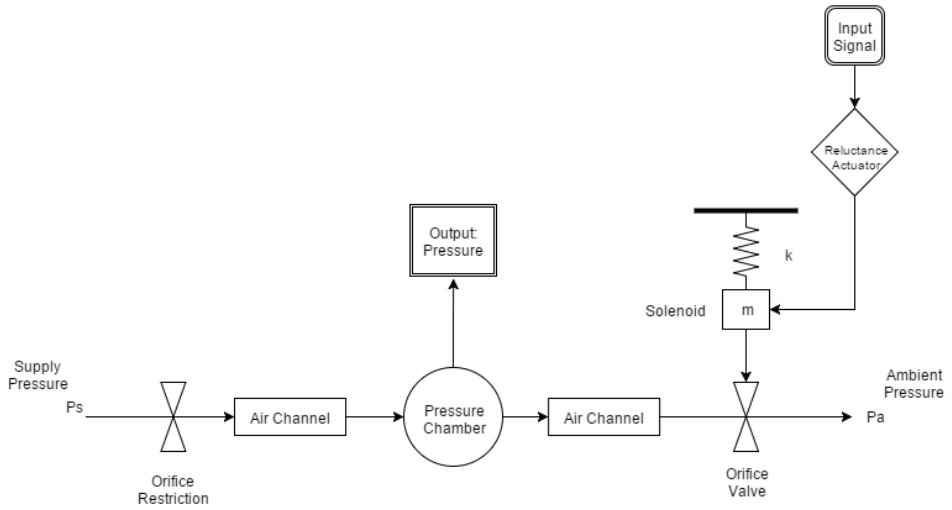

Figure 5.7: Schematic of the pressure pegulator

5.3. Modelling of the pneumatic actuator

In order to design a suitable pneumatic actuator from scratch for the Flowerbed project, it is very useful to fully understand the performance that comes out by different parameters, and provide a direct guideline of designing such an actuator from a given performance requirement. One can design or modify an actuator to their requirements if there is a tool to predict the performance, hence this tool should be able to describe the characteristic of a pneumtaic actuator, and it starts with modelling.

5.3.1. Modelling air dynamics

The Model of the pressure regulator is based on fluid dynamics on a lumped model with compressible air. The air dynamic system is described by an equivalent circuit, as shown in Figure 5.8a. Each component can be expressed as equivalent electrical components, they are voltage source, resistors, and capacitor in this case, and they form an RC circuit. This circuit can be further simplified by neglecting the resistors from the air channel due to the very small resistance compared to the orifice. The simplified circuit is shown in Figure 5.8b.

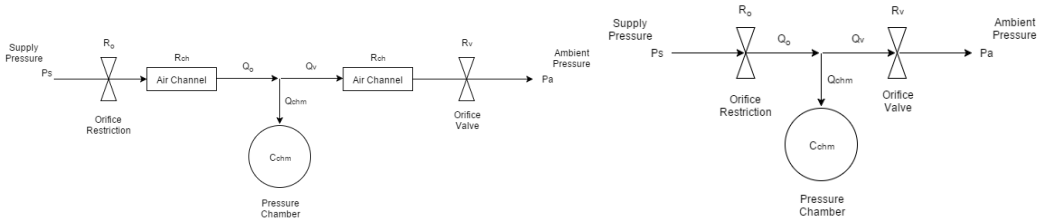

(a) Fluid dynamic model of the pressure regulator (b) simplified fluid dynamic model

Figure 5.8

In this model, the parameters of the subsystem are given as:

P_s	4bar	Supply pressure
P_a	1bar	Ambient pressure
$R_{orifice}$	7.50×10^9Pa s/m^3	Inlet orifice resistance
R_{valve}	7.24×10^9Pa s/m^3	Valve resistance
$V_{chamber}$	1.92×10^{-7}m^3	Internal volume (total) of the actuator

Based on the simplified lumped model, a one-dimensional fluid dynamic differential equation (ODE) can be set up by mass conservation: [14]

$$\dot{m}_o = \dot{m}_{chm} + \dot{m}_v \tag{5.1}$$

$$\rho_o Q_o = \rho_{chm} Q_{chm} + \rho_v Q_v \tag{5.2}$$

Substitute the linearized resistance into Eq.5.2:

$$\rho_o \frac{P_s - P_{chm}}{R_o} = \rho_{chm} C_{chm} \dot{P}_{chm} + \rho_v Q_v \tag{5.3}$$

Using Laplace transformation to transform into Laplace domain:

$$\frac{\rho_o P_s}{R_o} - \frac{\rho_o}{R_o} P_{chm} = s\rho_{chm} C_{chm} P_{chm} + \rho_v Q_v \tag{5.4}$$

The transfer function of the model becomes

$$P(s) = \frac{P_{chm}}{Q_v} = \frac{\rho_o P_s - R_o \rho_v Q_v}{Q_v (s\rho_{chm} R_o C_{chm} + \rho_o)} \tag{5.5}$$

The transfer function shows that the air dynamic system is first order, the pole of the system is

$$s = -\frac{\rho_o}{\rho_{chm}} \cdot \frac{1}{R_o C_{chm}} \tag{5.6}$$

In this model a proportional valve is chosen, which means that the input signal and the flow rate of the valve is proportional, under the working range of the valve. The input of the transfer function is the flow rate, and the output is the pressure inside the pressure chamber. This transfer function is valid only when a proportional valve is used, because the valve is controlled by the input signal and there is a constant gain between the input signal and the flow rate. This constant gain between the input signal and the flow rate is a design parameter, which should be obtained from the datasheet or from measurements.

In order to neglect this unknown gain, the transfer function will be normalized, which means that the transfer function will be multiplied with the reciprocal of P(0) so that the magnitude of the transfer function becomes 1 when the frequency is zero. The new transfer function becomes:

$$G_{air}(s) = \frac{P(s)}{P(0)} \tag{5.7}$$

The purpose of the normalization is to neglect the unknown gain inside the valve and focus on the phase change and the slope of the bode plot of the frequency response, which is the most important aspects of the air dynamic model.

The frequency response of the model is shown in Figure 5.9. The input is the flow rate of the valve, the output is the pressure inside the pressure chamber. As is mentioned above, the transfer function is of first order, with the pole determined by the R_o and C_{chm}. The pole of the model is located at a frequency of 5.99Hz. The complete modelling can be found in Appendix B.

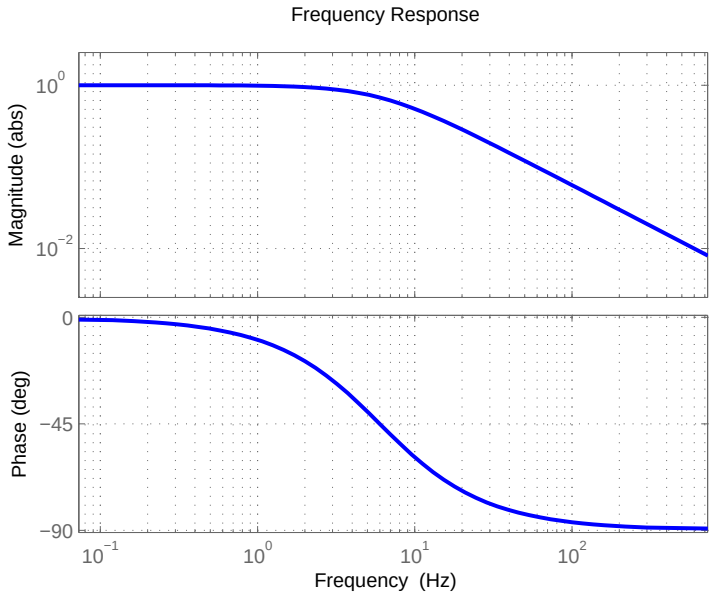

Figure 5.9: Frequency response of the air dynamic model, the pole of this 1^{st} order system is at 5.99Hz

5.3.2. Modelling solenoid valve

A solenoid valve is a spring-loaded mass actuated by a reluctance actuator. By applying voltage, the reluctance actuator will excite a force on the solenoid, pulling it away from the orifice. By controlling the distance between the solenoid and the outlet hole, it becomes possible for the solenoid to control the air flow, hence controlling the pressure inside the pressure regulator.

Figure 5.4a shows the schematic of the correspond subsystem. The solenoid core (not the valve) can be modelled as a mass-spring system connected to the external world, the force generated by the reluctance actuator has its own characteristic, which will be modelled as well.

A mass-spring system from the preloaded solenoid core has a certain resonance frequency, which is dependent on the mass of the solenoid and the stiffness of the spring. The transfer function of such a system is:

$$G(s) = \frac{x}{F} = \frac{1}{ms^2 + cs + k} \tag{5.8}$$

The parameters of the model are:

m	3.0×10^{-3}kg	Mass of the solenoid core
k	1.39×10^{4}N/m	Stiffness of the spring
c	0.8N s/m	Damping coefficient

The frequency response of the solenoid core model is shown in Figure 5.10

For the ASCO valves available in the lab, the reluctance actuator embedded in the valve has some special dynamic characteristic. In this case, ASCO has implemented a 3^{rd} order actuator to drive the solenoid core. Generally, a reluctance actuator is a first order system, which has a phase lag of -90°, but for the stability reason and reduce the noise a 2^{nd} low-pass filter can be implemented, at exactly the cut-off frequency of the reluctance actuator. However, this low-pass filter behavior is just an assumption as the ASCO valve does not provide any information about the extra -180° phase lag. In this model for the ASCO Posiflow valve, the cut-off frequency of the reluctance and the low pass filter is 400Hz.

The transfer function of the 3^{rd} order reluctance actuator can be approximated by a transfer function of a 3^{rd} order low pass filter: [15]

$$H(s) = \frac{k_0 G_o}{\prod_{k=1}^{n}(s - s_k)/\omega_c} \tag{5.9}$$

Where

$$s_k = \omega_c e^{\frac{j(2k+n-1)\pi}{2n}}, k = 1, 2, 3, ..., n$$

k_0 is the proportional gain between the input signal to the force on the solenoid core, the value of k can be determined during the design of a pneumatic actuator as a parameter.

The frequency response of the low-pass filter is also shown in Figure 5.10. The input is the input signal into the solenoid, the output is the displacement of the solenoid core.

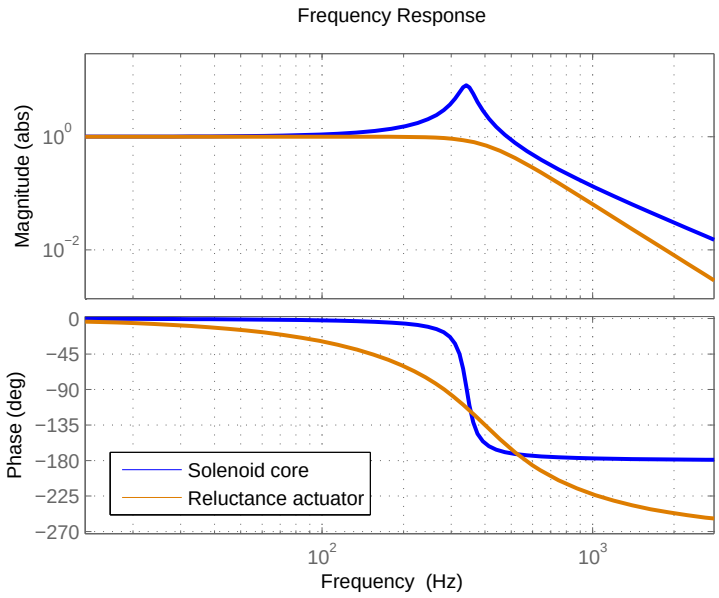

Figure 5.10: Preloaded solenoid sore, frequency response, shows up as a very common single mass-spring system with an eigenfrequency of 340Hz. Reluctance actuator model is approximated by a 3^{nd} order low pass filter, with a cut off frequency at 400Hz

Combining the transfer function of the mass-spring system and the reluctance actuator, the model of the solenoid valve is established:

$$G_{valve}(s) = G(s)H(s) \tag{5.10}$$

And the frequency response of the model of the valve is shown in Figure 5.11.

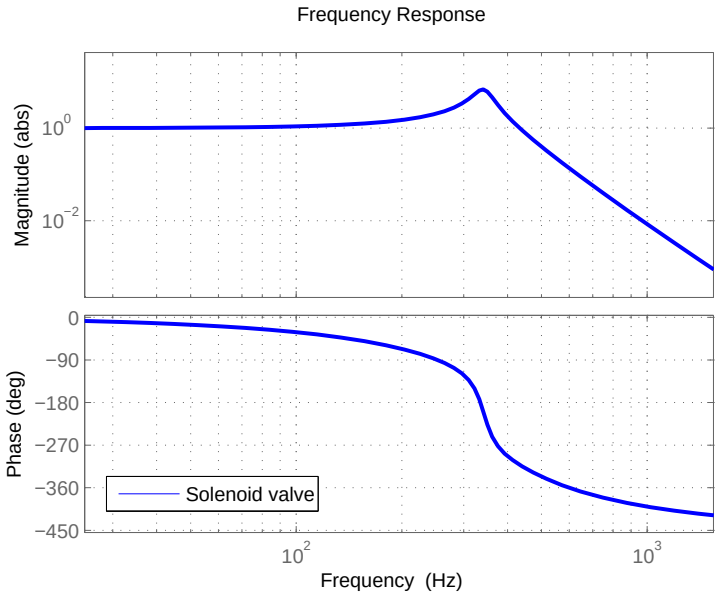

Figure 5.11: Frequency response of the model of a solenoid valve. It has a first eigenfrequency at 340Hz, and the phase after that goes down to -450°, indicating that it's a 5^{th} order system

A more detailed modelling of the solenoid valve can be found in Appendix C.

5.3.3. Modelling moving disk and external load

The moving disk and the steel spring are two mass-spring subsystems, and they are coupled together, form a new equivalent mass-spring system.

A COMSOL model in Figure 5.12a reveals the first eigenfrequency of the moving disk at 288Hz. The steel spring is made of a thin steel beam clamped on both sides, with the first eigenfrequency of 992Hz. The COMSOL model is shown in Figure 5.12b. These two subsystems are rigidly coupled, and they form a new 2^{nd} order mass-spring system with combined mass and stiffness.

The parameters of the subsystem are:

Diameter of the moving disk	20mm
Thickness of the moving disk	6mm
Diameter of the membrane	30mm
Thickness of the membrane	50μm
Length of the beam	136.9mm
Width of the beam	20.4mm
Thickness of the beam	3.4mm

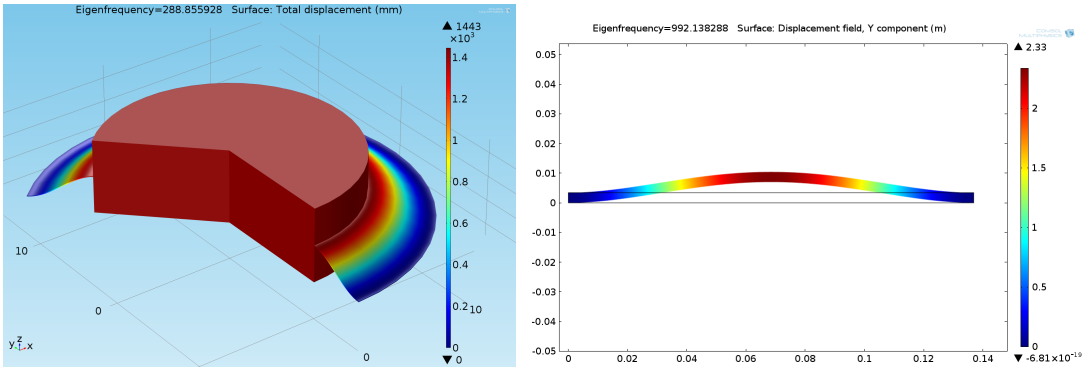

(a) COMSOL model of the moving disk (b) COMSOL model of the external load

Figure 5.12

After combining the moving disk and the beam, this subsystem has a first eigenfrequency around 800Hz. The frequency response of the load is shown in Figure 5.13. The input of the transfer function is the force on the moving disk, the output is the displacement of the moving disk.

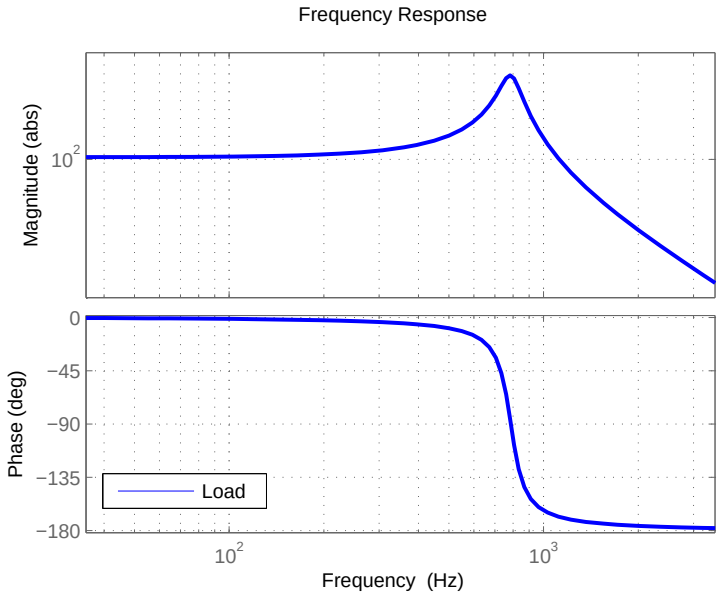

Figure 5.13: Frequency response of the moving disk with the external load

5.3.4. Pressure regulator model assembly

The pressure regulator model is a serial model combined with the air dynamics, solenoid core and the reluctance actuator, as shown in Figure 5.14. The transfer function of the pressure regulator can be obtained from Eq.5.11.

$$G_{regulator}(s) = G_{air}(s)G_{valve}(s) \tag{5.11}$$

where $G_{air}(s)$ is the transfer function of the air dynamic subsystem, $G_{valve}(s) = G(s)H(s)$ is the transfer function of the valve, G(s) is the transfer function of the solenoid core, H(s) is the transfer

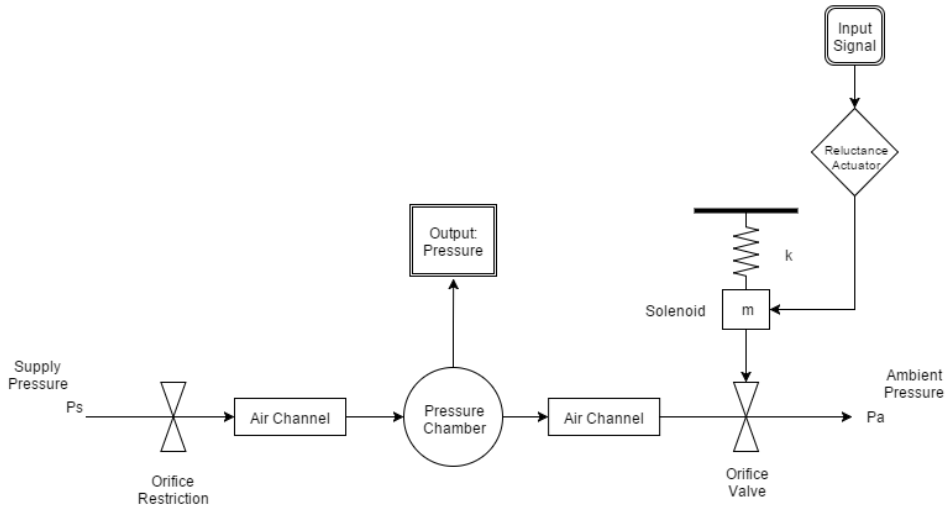

Figure 5.14: Schematic of the pressure regulator

function of the 3^{rd} order reluctance actuator.

The frequency response of the pressure regulator model is shown in Figure 5.15. The input is the input signal into the solenoid, the output is the pressure inside the pressure chamber. The characteristic of both the air dynamic and the solenoid valve subsystems are shown in the bode plot. The first order pole at 5.99Hz comes from the air dynamics subsystem, and the second order pole at 340Hz comes from the solenoid valve.

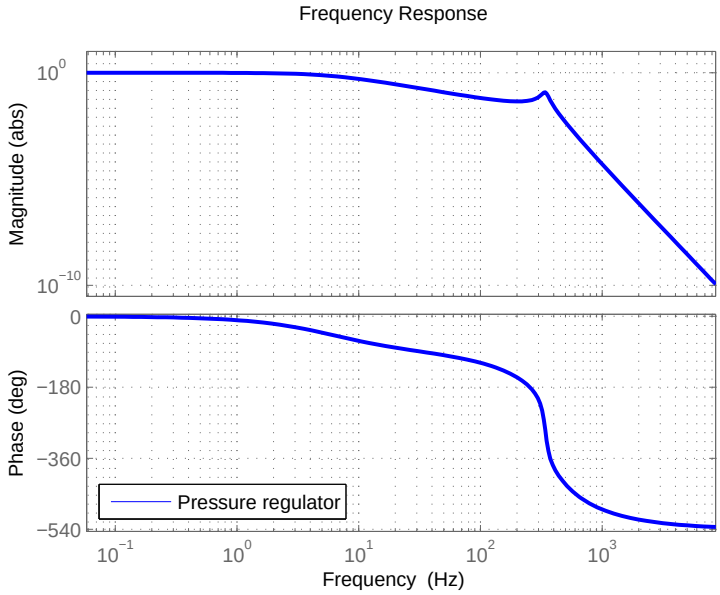

Figure 5.15: Pressure regulator model, frequency response. It contains the first order pole at 5.99Hz which is the characteristic of the air dynamic subsystem, and it has a second order pole at 340Hz which is the first eigenfrequency of the solenoid valve.

5.3.5. Pneumatic actuator model assembly

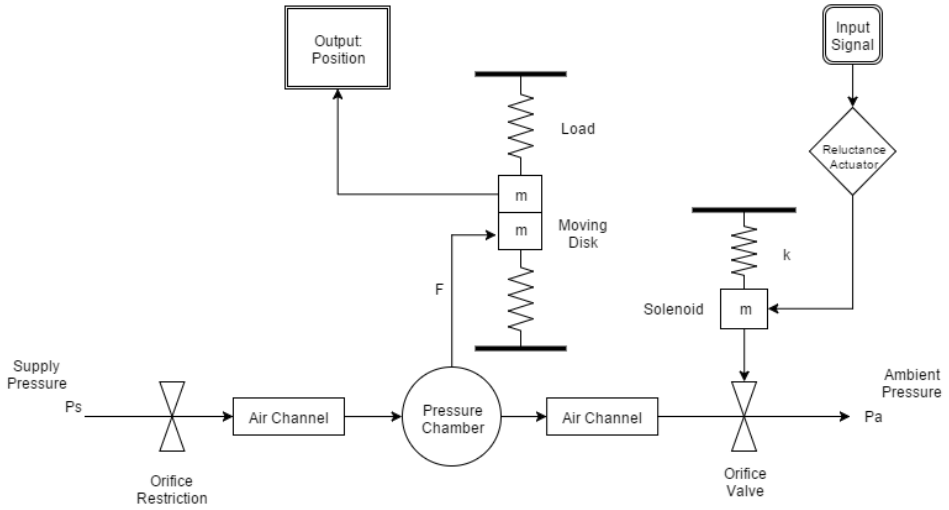

Figure 5.16: Schematic of the pneumatic actuator

The pneumatic actuator model is also a serial model combined with the pressure regulator and the load subsystem:

$$G_{actuator}(s) = G_{regulator}(s)G_{load}(s) = G_{air}(s)G_{valve}(s)G_{load}(s) \tag{5.12}$$

The frequency response of the pneumatic actuator is shown in Figure 5.17. The input is the input signal to the solenoid valve, the output is the displacement of the moving disk. This full assembled model contains information of all three subsystems, it has the first order pole at 5.99Hz which comes from the air dynamics subsystem, it has a second order pole at 340Hz which comes from the solenoid valve, and another second order pole at around 800Hz which comes from the load subsystem.

It should be noticed that the eigenfrequency of the load is so high that it in fact doesn't have any effect in the low frequency range. The bode plot is nearly identical to that of pressure regulator under a frequency of around 800Hz. It shows that the pressure regulator is in fact the most important part of the system because it determines the dynamic performance in the frequency range which is going to be focused in this research. The relation between the pneumatic actuator and the pressure regulator can even be simplified into a constant gain if needed, neglecting the load subsystem:

$$G_{actuator}(s) = k \cdot G_{regulator}(s) = k \cdot G_{air}(s)G_{valve}(s) \tag{5.13}$$

In this research, this simplification is not considered, thus the load subsystem will be included in the model.

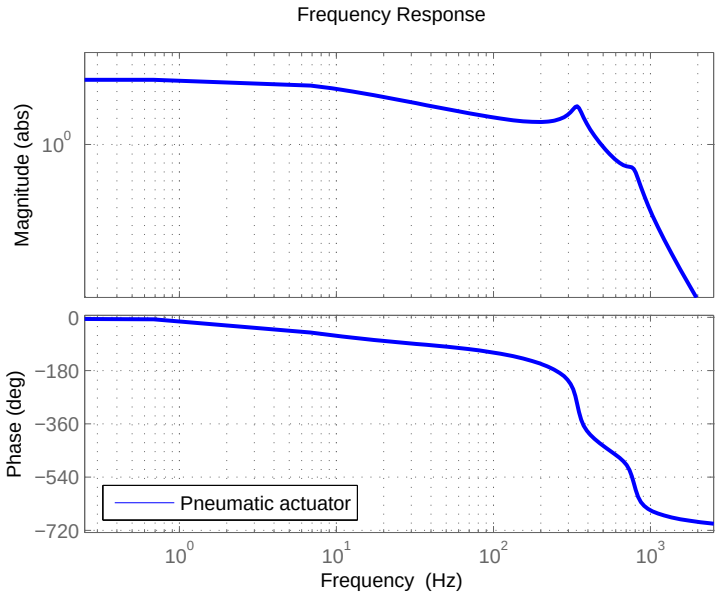

Figure 5.17: Pneumati actuator model, frequencyrResponse. It contains the first order pole at 5.99Hz which is the characteristic of the air dynamic subsystem, it has a second order pole at 340Hz which is the first eigenfrequency of the solenoid valve, and another second order pole at around 800Hz which is the first eigenfrequency of the load.

5.4. Model validation

Validation of a model is very important, as it determines whether the model succeeds in describing the reality and reveals the limit of the model. The validation of the model is done by the comparison between three test setups and the model: first test setup will be built to validate the model of the solenoid valve dynamics; second test setup to validate the model of the pressure regulator; third test setup to proof that the external load does not affect the dynamics of the actuator.

5.4.1. Test setup - solenoid valve

The solenoid valve is opened and mounted to an aluminium block for the test. The schematic is shown in Figure 5.18, the orifice component of the valve is removed, and the solenoid core is exposed to the capacitive sensor for measuring the displacement.

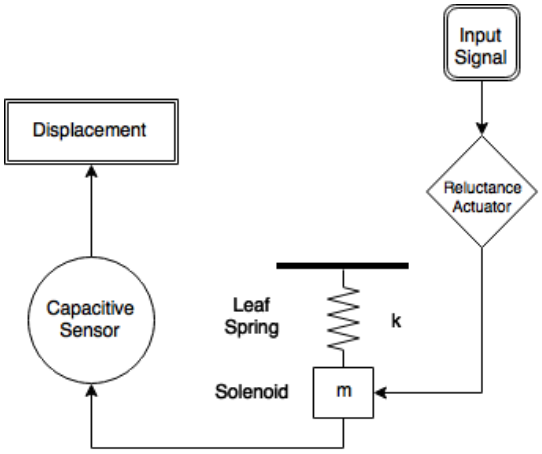

(a) Solenoid test schematic

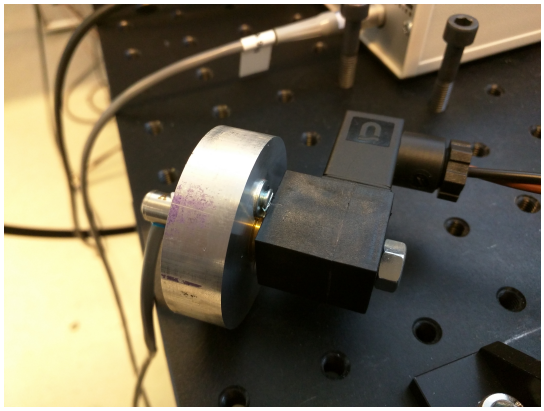

(b) Solenoid test setup, the orifice of the valve is removed and the solenoid core is couple to a capacitive sensor for measuring the displacement

Figure 5.18

The result is shown in Figure 5.19. The model with the special 3^{rd} order reluctance actuator matches the measurement from the test setup. The input is the signal for the reluctance actuator, and the output is the displacement of the solenoid core.

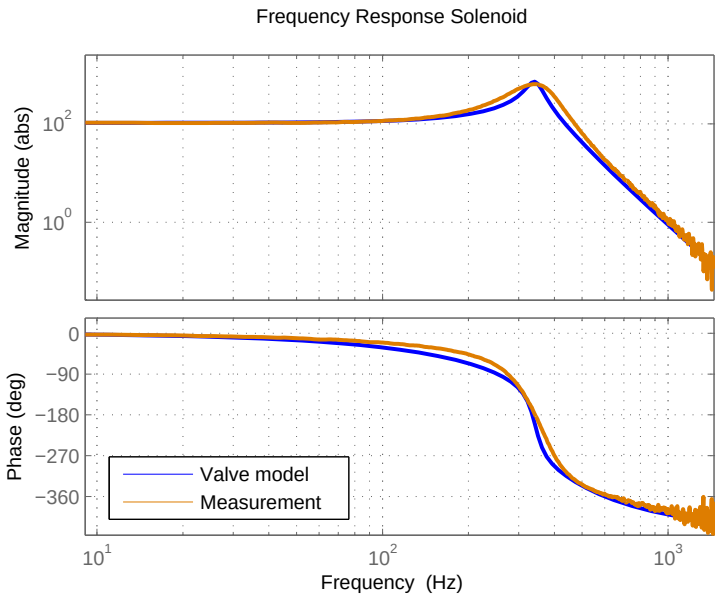

Figure 5.19: Frequency Response of the solenoid valve model and test setup, the result shows a good match between them, the eigenfrequency of the solenoid valve is 341Hz

5.4.2. Test setup - pressure regulator

A pressure regulator is built to verify the model. Figure 5.21 shows the internal construction and the actual assembly of the pressure regulator according to the schematic shown in Figure 5.20. This pressure regulator will be tested under 4 bar.

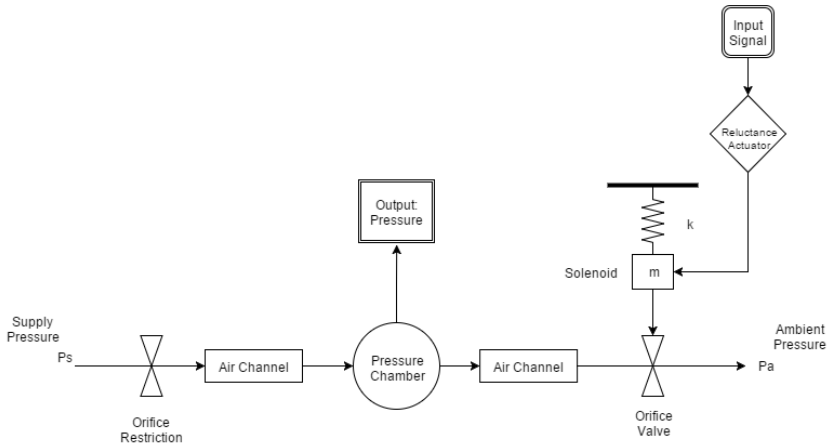

Figure 5.20: Schematic of the pressure pegulator

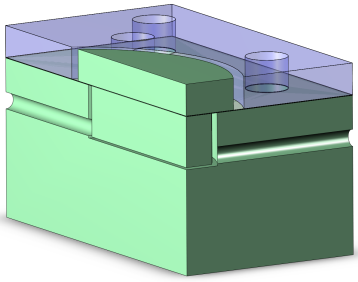

(a) CAD Model of the Pressure Regulator, cross section

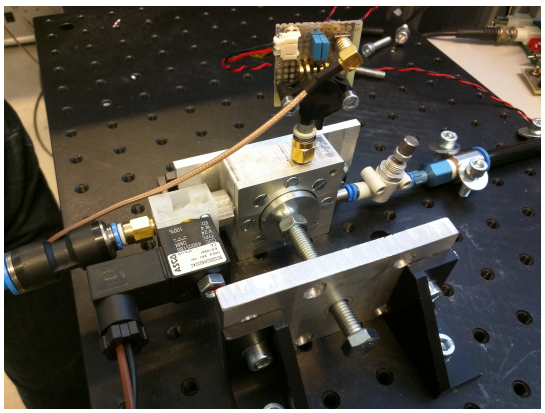

(b) Assembly of the Pressure Regulator

Figure 5.21

Figure 5.22 is the frequency response of the pressure regulator and the air dynamics models. By overlapping the frequency response of the pressure regulator and the model of air dynamic subsystem, as shown in Figure 5.22, The air dynamic model for low frequency is validated as the model and the measurement match each other. The air dynamic model has successfully described the low-frequency performance of the pressure regulator.

The model of the pressure regulator is obtained by combining the air dynamics model and the valve model described by Eq.5.11, Figure 5.23 shows the comparison between the measured frequency response of the test setup and the model of the pressure regulator. In the test setup, there is extra phase lag at higher frequencies and the magnitude of the bode plot start to differ a little bit. Unfortunately, it's not possible to measure deeper inside the pressure regulator because of the limit of space, but there are two hypothesis: The first one is that the pressure sensor has 1ms response time and 20ms of warm-up time, which cause the extra phase lag in the system, especially for higher frequency; the second one is the pressurized solenoid valve has extra dynamic characteristic because the orifice of the valve was excluded during the modelling and the previous test setup, this orifice has a plastic housing, it may generate some vibration of deformation and cause some extra phase lag and magnitude change in the system.

Judging from the results of the verification from the measurements, it can be concluded that the model has successfully predicted the dynamic performance of the pressure regulator.

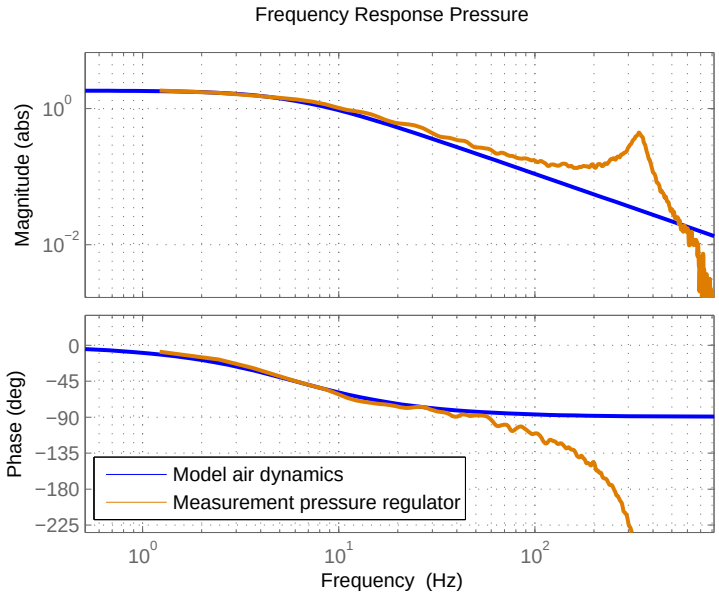

Figure 5.22: The air dynamics model is verified by the measurement, the pole of the model matches the test setup in low frequencies

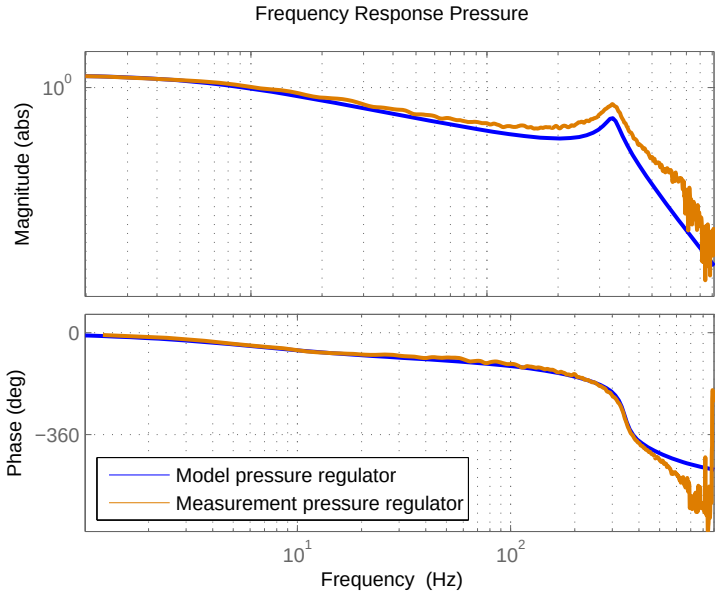

Figure 5.23: Frequency response, comparison of model and the test setup. The model can predict the dynamic performance very well up till the eigenfrequency of the system

5.4.3. Test setup - pneumatic actuator

A pneumatic actuator is built according to the schematics in Figure 5.24 to Justify the model of the moving membrane, which suggests that the existence of the moving membrane and the moving disk will not change the dynamic performance after including them in the actuator, and the pressure regulator model can represent the pneumatic actuator by implementing a static gain in the transfer function. The CAD model of the actuator is shown in Figure 5.25a and the parts are shown in Figure 5.25b.

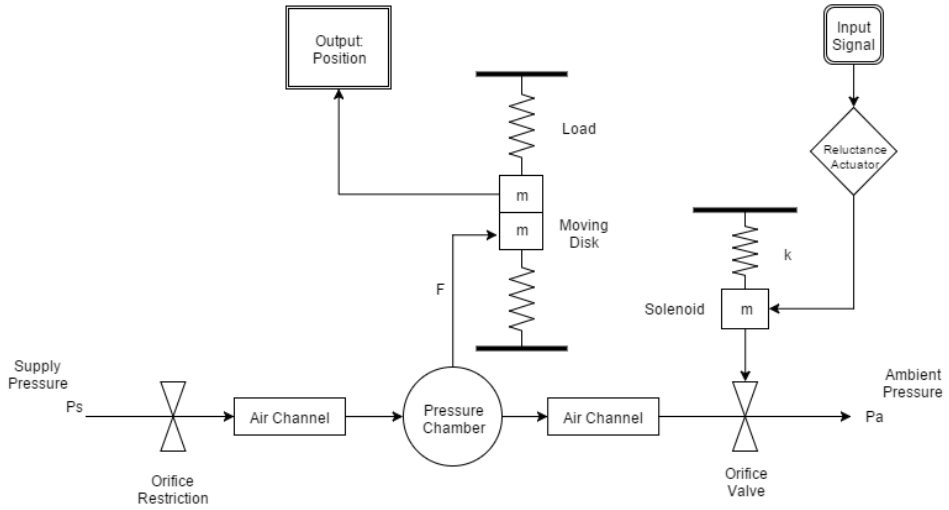

Figure 5.24: Schematic of the pneumatic actuator with load

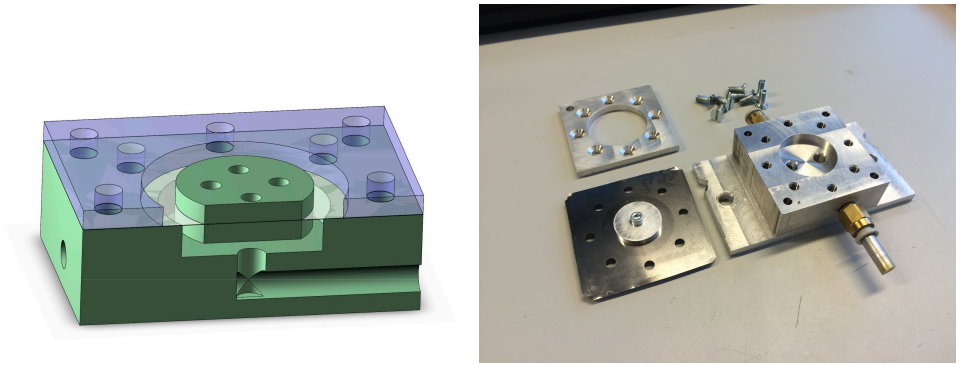

(a) CAD Model of the Actuator (b) Parts of the Actuator

Figure 5.25

The measurement of the test setup is shown in Figure 5.26. It can be seen that the frequency response of the pressure regulator and the pneumatic actuator match up very nicely, a good match for the phase up to a frequency of around 1000Hz, already past the eigenfrequency of the load subsystem. In this frequency, the noise becomes dominant, and the dynamic response past this frequency is in fact not affecting the system, therefore it should be concluded that the model is validated and is able to describe the dynamic performance of a pneumatic actuator.

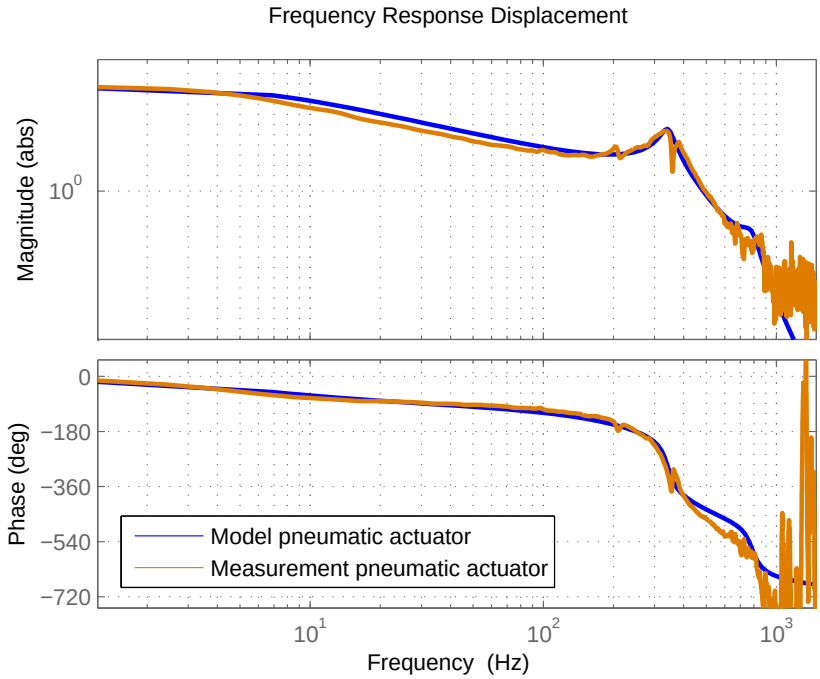

Figure 5.26: Frequency response, comparison of the model and the test setup of the pneumatic actuator. The measurement matches the model very well, it can be concluded that the model is able to predict the dynamic performance of the pneumatic actuator

5.5. Conclusion

In this chapter, a very successful model for the pneumatic actuator is accomplished by splitting the pneumatic actuator into subsystems and building separate models for them, then combining these models to form the model needed for the pneumatic actuator. There are assumptions for simplified models like the 1^{st} order lumped fluid dynamic model for the air flowing inside the actuator, and the performance equivalence between the pressure regulator and the pneumatic actuator under the requirements/conditions in this Flowerbed application. These models are validated by comparison with three test setups. To summarize, this model can precisely describe/predict the performance of a pneumatic actuator, regarding the requirements of this Flowerbed application.

In the next chapter, one very important component, the valve, will be discussed. A new type of valve will be introduced and studied. This new type of valve implements a piezo buzzer, and the advantage is that it can have a faster dynamic performance than the solenoid valve, and significant reduce the size at the same time, brings the possibility of integrating the valve into the pneumatic actuator.

6

Piezoelectric Valve Design

In the previous chapter, a model of the pneumatic actuator was established and validated. The model is accurate for designing a pneumatic actuator regarding the requirement of the Flowerbed, and can be used in the design. However, there is one more aspect of the pneumatic actuator to consider before starting designing - the size of the actuator, and its performance.

Solenoid valve, which is used in previous chapters, is a very common type of valve for pneumatic actuators due to the simple and reliable construction. Their dynamic performance can be easily predicted and they can work with very high pressure because of the strong actuation coming from the reluctance actuator. However, there are drawbacks of using the solenoid as the driving mechanism for a valve. The solenoid core has a certain mass which size is hard to reduce, the speed of the solenoid valves is limited by the mass-spring system. Stronger actuator can be used to drive the solenoid for faster performance, but the energy consumption and heating would be a problem. Furthermore, solenoid actuator consists a metal core and a reluctance actuator made from a copper coil, the stronger the actuator is, the bigger these components become. A big solenoid valve has a problem fitting in the 320x320mm space in the Flowerbed frame, and a big solenoid valve needs a strong current amplifier to drive, the cost of the strong valve with a heavy current amplifier can not be neglected and, in fact, the performance improvement from upgrading these components is very limited.

On the other hand, as already tested in the previous chapter, the piezo actuator, is very small and fast. As an actuator for driving the Flowerbed, it doesn't have enough stroke, but they can be used to drive a valve and, in fact, there are piezoelectric valves available on the market for very fast pressure regulation. One problem with such piezoelectric valves is, that they are expensive external components, they only solve the performance problem of the solenoid valve, but they still take a lot of space as an external component. Furthermore, they cost a lot, which is also a drawback when considering the cost of the project.

Therefore, the main focus of this chapter is to design a special low-cost piezoelectric valve and integrate this piezo valve into the pneumatic actuator.

6.1. Components

The most common type of piezo component used in a piezo valve is the bimorph piezo bender, as shown in Figure 6.1. The two layers in the piezo bender deform in a bending direction when a voltage is applied, and it provides a relatively large displacement at the tip of the bender. The large displacement with a small size is the advantage of the piezo bender, makes it very suitable in a valve application. Festo has come up with a piezo valve which utilize a piezo bender, [16] as shown in Figure 6.2

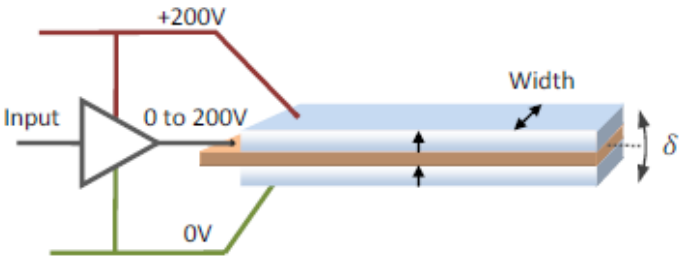

Figure 6.1: Schematic diagram of a bimorph piezo bender. Figure taken from www.piezodrive.com

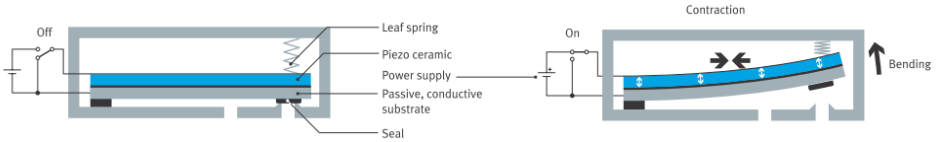

Figure 6.2: Festo piezoelectric valve schematic diagram [16]

Piezo buzzer, shown in Figure 6.3, is a type of piezo component commonly used as an audio device. It can be found in many small electric devices which gives simple tones to indicate their state or generate some warning sounds etc. The piezo buzzer is rarely used in valve application, but there is research that uses a similar type of piezo component in microfluidic microvalve. [17] Piezo buzzer is a very low cost actuator and can be easily obtained. In this research the piezo buzzer will be studied and the application of piezo valve using a buzzer will be investigated. The purpose of this part of research is to find a cost-effective alternative to the currently available solutions like the expensive piezo valve from Festo, or the expensive and very bulky solenoid valve from ASCO.

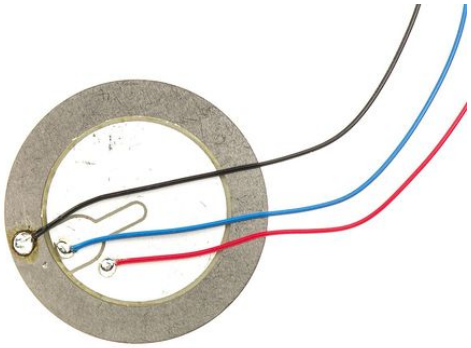

Figure 6.3: Picture of a piezo buzzer, taken from RS-online.com

6.2. Orifice modelling

Another important component of a valve is the orifice. As shown in Figure 6.4, an orifice is a small hole which air flows through, the flow rate is limited by a plate which holds against the orifice. The distance between the plate and the orifice determines the flow rate of the fluid.

The orifice model is constructed by a hole and a moving plate, air will flow out through the orifice hole then through the air gap. [18] Therefore, there are actually two equivalent orifices in this case. The hole is limiting the air flow, while the air gap is limiting the air flow as well. However, in the application of a piezo valve, the air gap is so small that the hole is no longer limiting the air flow, the

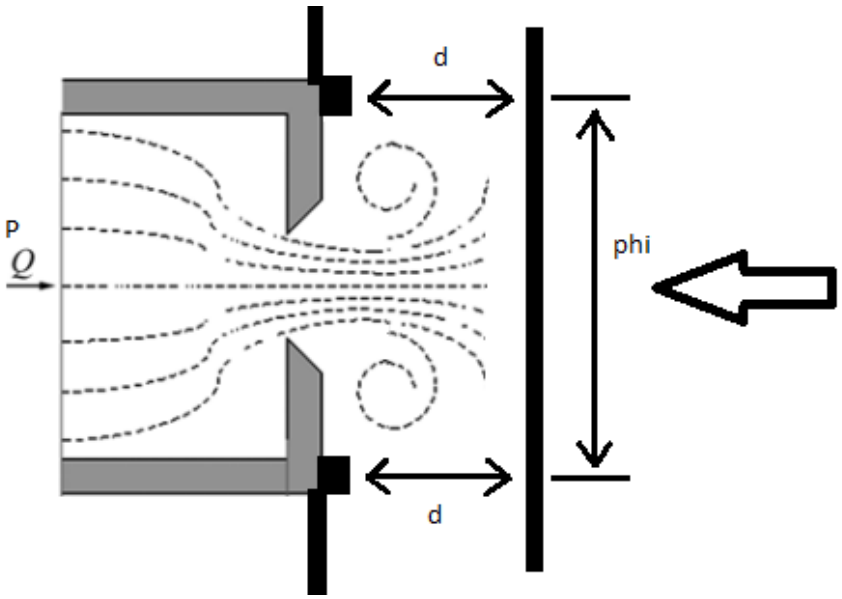

Figure 6.4: Orifice schematic diagram

air flow will only be limited by the air gap. The air gap is described as an equivalent 2-dimensional orifice. By unfolding the side area of the air gap, the equivalent area is

$$A = \pi \phi d \tag{6.1}$$

The orifice of the air gap forms a choking flow to limit the volumetric flow rate of air, it is wise to assume that the speed of the fluid is at the sound of speed, or Mach 1. The flow rate can be limited by the orifice hole or by the air gap. Therefore, the maximum flow rate is

$$Q = V\frac{\pi D^2}{4} \tag{6.2}$$

or

$$Q_2 = V\pi \phi d \tag{6.3}$$

where

$$Q = Flow\ Rate\ [m^3/s]$$
$$V = Speed\ of\ Sound\ [m/s]$$
$$D = Diameter\ of\ the\ Orifice\ [m]$$
$$\phi = Diameter\ of\ the\ Air\ Gap\ [m]$$

The speed of sound can be obtained by

$$V = \sqrt{kR_{specific}T} \tag{6.4}$$

where

$$k = Specific\ Heat\ Ratio\ for\ Air$$
$$R_{specific} = Specific\ Gas\ Constant\ [m^2/(s^2\,K)]$$
$$T = Absolute\ Temperature\ [K]$$

Given the outlet pressure as atmosphere $P_2 = 1$bar, the inlet pressure of the orifice can be obtained by [14]

$$P_1 = P_2(1 + 0.2Ma^2)^{3.5} \tag{6.5}$$

With the obtained flow rate and pressure, the linearized fluid resistance becomes

$$R = \frac{P_1 - P_2}{Q_2} \tag{6.6}$$

where

$$R = Fluid\ Resistance\ [\text{Pa s/m}^3]$$

The result of the piezoelectric valve resistance is shown in Figure 6.5.

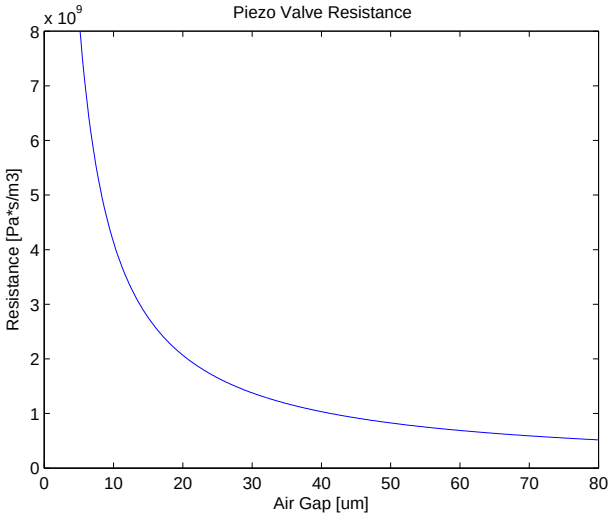

Figure 6.5: Piezoelectric valve resistance regarding to the air gap

6.3. Force compensating piezo actuator

The pressure of the air at the orifice will apply a force on the piezo bender, which will, in turn, reduce the displacement of the piezo, limiting the maximum opening of the valve. There are different ways to reduce this negative effect, one example is to use stiff piezo component, another example is to apply a counter force. The second method is widely used, it can be implemented by preloading using a spring or a force, as shown in the Festo piezoelectric valve schematic in Figure 6.2.

6.3.1. Limited closing force

The weakness of the piezo benders is the limited stiffness. The typical blocking force of a bimorph piezo bender can be around 0.1-2N. The closing force needed to close the outlet depends on the area of the outlet and the pressure, as shown in Figure 6.6. This blocking force limits the outlet diameter and the applied pressure. By applying a counter force on the piezo, the total force acting on the piezo can be reduced, which allows larger outlet diameter or higher pressure.

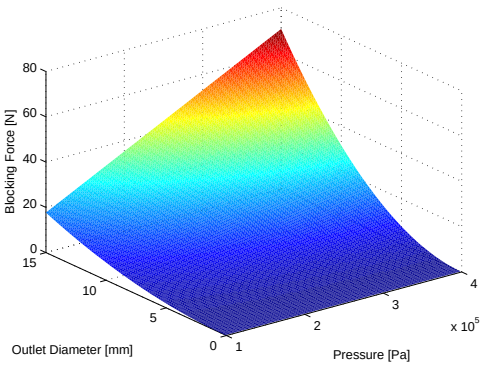

(a) 3D plot of the relation between blocking force, orifice/outlet diameter and pressure. The increase of required blocking is quadratic with increased diameter, and linear with increased pressure

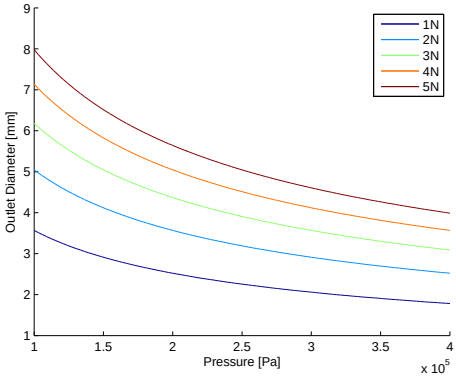

(b) Contour plor of the relation between the pressure and the orifice/outlet diameter under a constant blocking force. This graph illustrate the feasible pressure/orifice combination under a certain blocking force of the piezo

Figure 6.6: Blocking force piezo bender against orifice/outlet diameter and Pressure

6.3.2. Closing force compensation

There are many ways to apply the counter force, a very common solution is preloaded spring. Preloaded spring has a lot of advantages under such application, such as linear behaviour, constant stiffness and low hysteresis, depending on the design. However, the small dimension of the piezo valve and the spring require a precision fabrication and assembly, the tolerance would be very critical if all the components are integrated into a very small product. In this project, another approach of force compensating will be studied, the counter pressure force compensation.

Counter pressure force compensation, which means that the counter force will be applied, not through springs or any other mechanical contact, but straight through the compressed air, providing pressure on the surface at the other side of the piezo. Figure 6.7 shows the concept of the counter pressure force compensation with a cross-section of the valve with a piezo buzzer. The buzzer is sealed on the top surface, which a volume with a constant pressure is formed to provide a force that works against the other force coming from the bottom. This counter force is not able to fully compensate the force from the bottom due to the variance of the chamber pressure. However, the compensation will be sufficient if the pressure difference drops under the maximum allowed for the given blocking force.

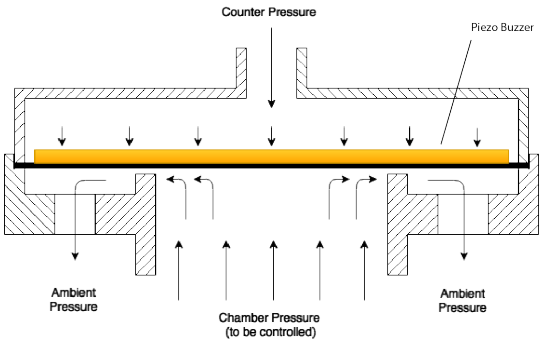

Figure 6.7: Piezo buzzer schematic concept

6.3.3. COMSOL simulation for the orifice valve

A finite element model is established with COMSOL to demonstrate the counter pressure concept, using a 2D axisymmetric geometry shown in Figure 6.8 and 6.9. The involved package is the Fluid Structure Interaction physics. The model tries to predict the pressure distribution at the outlet of the chamber and the displacement of the buzzer under the chamber pressure. Two different models are built for comparison, one without counter pressure and one with.

The parameters used in this model are:

Diameter of the air channel	10mm
Diameter of the copper plate, piezo buzzer	33mm
Thickness of the copper plate, piezo buzzer	0.2mm
Diameter of the ceramic plate, piezo buzzer	25mm
Thickness of the ceramic plate, piezo buzzer	0.3mm
Thickness of the air gap	5µm
Pressure of the inlet channel	0.4kPa
Counter pressure	0.1kPa

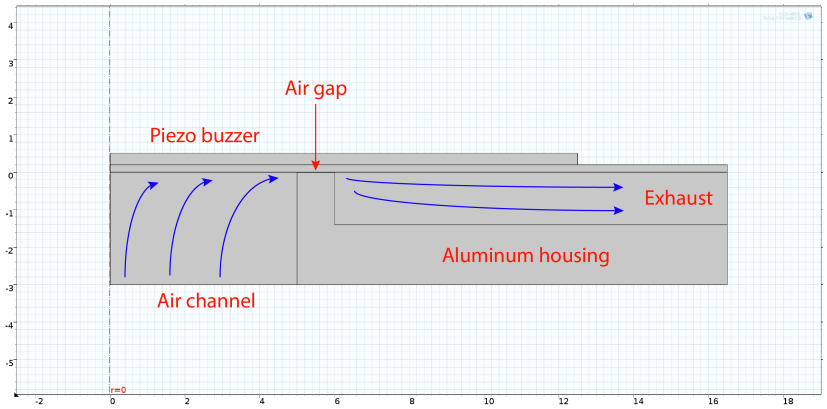

Figure 6.8: COMSOL model geometry without counter pressure

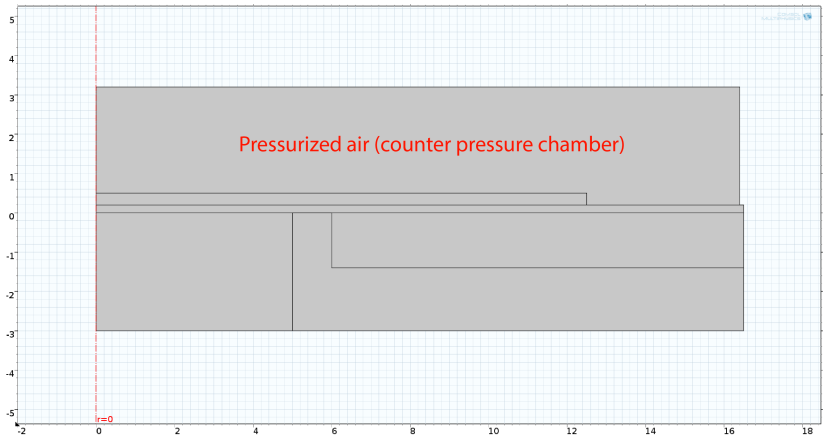

Figure 6.9: COMSOL model geometry with counter pressure

The Fluid-Structure Interaction Physics struggles to converge in this geometry, the simulation in this geometry hits its limit at a maximum inlet pressure of 0.4kPa. One possible reason is the existence of the small air gap which gives some difficulty in the algorithm. If the pressure is set higher, COMSOL

will not finish the simulation and interrupts it with an error, indicating that there are solutions which becomes complex numbers. The result is shown in Figure 6.10 and 6.11. Under a very small pressure the buzzer will only deform with a maximum displacement of 0.09µm without counter pressure, and 0.03µm with counter pressure.

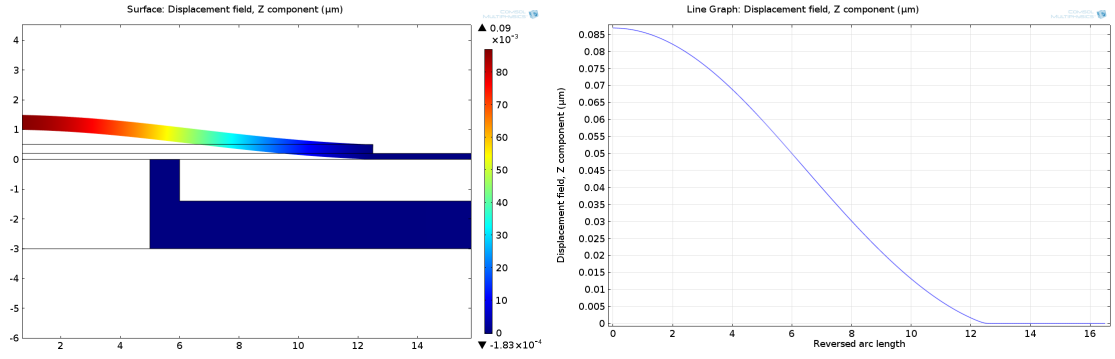

Figure 6.10: COMSOL simulation without counter pressure, the figure shows the deformation of the piezo in z direction

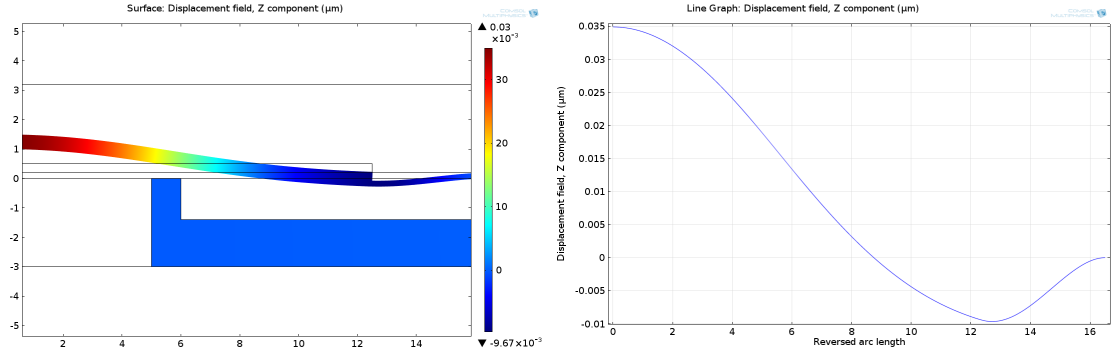

Figure 6.11: COMSOL simulation with counter pressure, the figure shows the deformation of the piezo in z direction

After changing the geometry, reducing the inlet channel diameter to 1.3mm, the simulation becomes more reliable and is able to simulate under an inlet pressure of 4bar without counter pressure. However the simulation is not able to finish the computing with any counter pressure, it gives the same type or error indicating a complex number as solution. The simulation result without counter pressure is shown in Figure 6.12. The piezo deforms with a maximum displacement of about 10µm without applying counter pressure.

This simulation is not able to describe precisely what the actual situation will be, but it can generally give an idea of what is happening when pressure and counter pressure is applied and how the piezo buzzer is going to deform. It has provided valuable information for further design of the prototype.

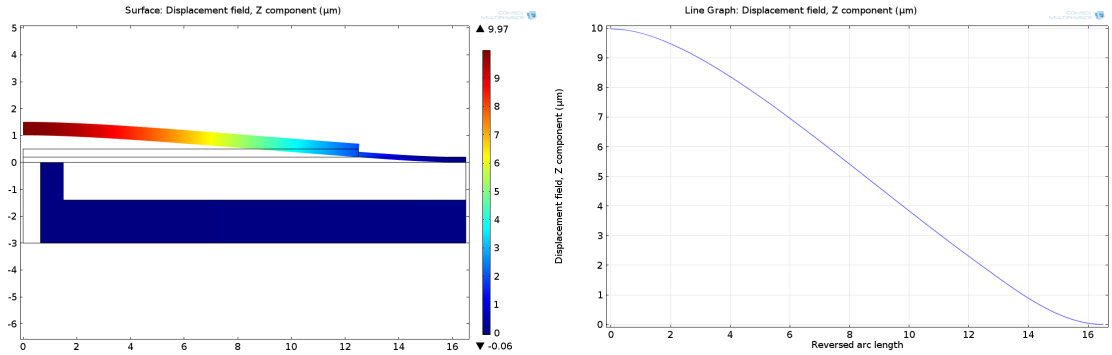

Figure 6.12: COMSOL simulation without counter pressure, the figure shows the deformation of the piezo in z direction

6.4. Piezo buzzer study

Some important parameters of a buzzer in this application are stroke, stiffness, frequency response. Most of the buzzers are meant to emit sound only, their detailed parameters are mostly unknown, therefore, they must be tested to obtain the parameters in order to determine whether it's suitable for the application. Three piezo buzzers, one steel membrane with 35mm diameter and two copper membrane with 35mm and 50mm diameter, shown in Figure 6.13, are put to a test.

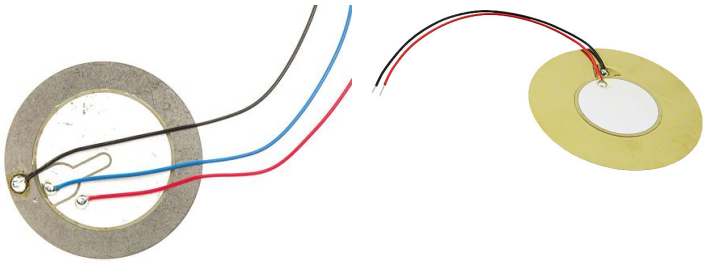

(a) Steel buzzer (b) Copper buzzer

Figure 6.13: Photos of the piezo buzzers

The membrane of a piezo buzzer are mostly flat when observed by naked eye, however, it's not the case under a microscope. The surface profile is critical for the application, as the unevenness of the surface may cause the orifice to stay largely opened and orifice valve will not be able to control the flow rate under such situation. A Bruker white light interferometer is used to measure the surface height of both buzzers, the results are shown in Figure 6.14 and 6.15. A full surface scan is done for the 35mm steel buzzer, a 6mm wide area scan is done for the 50mm copper buzzer due to the limit of the data size and scanning time. The result is very critical. The maximum height difference of the 35mm steel buzzer is about 120µm, while the 50mm copper buzzer has approximately 350µm.

The ceramic-metal layer construction of a buzzer could be the cause of the height difference. During the manufacturing, there is internal stress between these two layers, which causes some deformation even without applying voltage on the piezo material. Such height difference is at least 5 times larger than the stroke of a buzzer. Special treatment is required during assembly to adjust the position of the buzzer and the air gap, otherwise, the buzzer will not be able to close the orifice, hence unable to control the pressure.

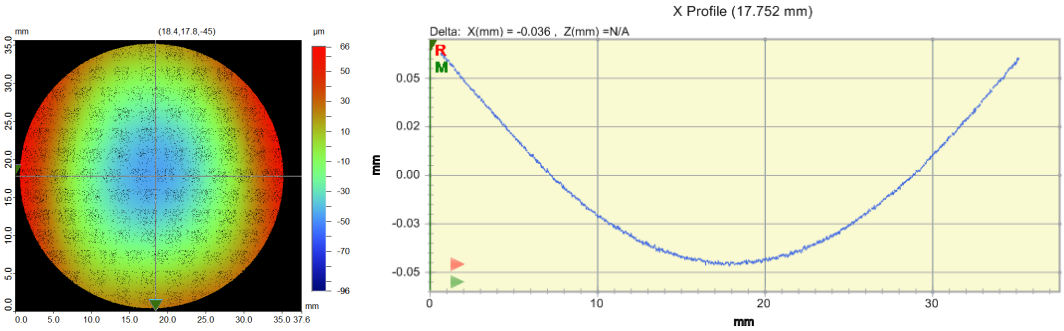

Figure 6.14: Surface profile of 35mm steel buzzer

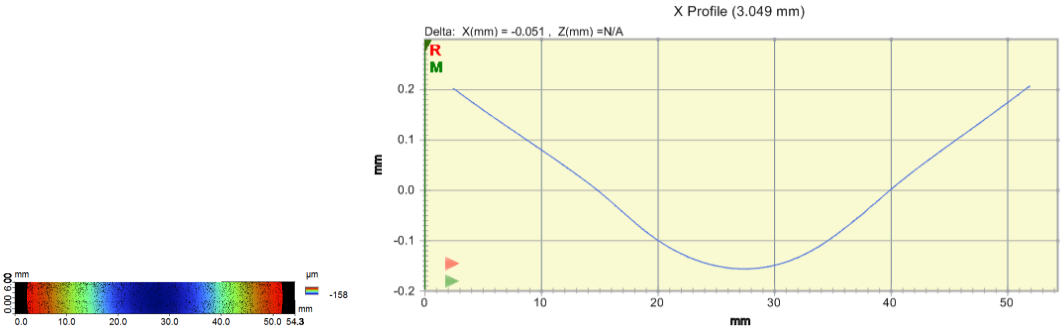

Figure 6.15: Surface profile of 50mm copper buzzer

The buzzers are mounted on a test setup, shown in Figure 6.16, to test the stroke and frequency response. The ground wire of the buzzer is removed, the clamping aluminium block will become the ground terminal, which will make the wiring much easier.[19] A capacitive sensor is mounted in the middle to measure the displacement at the center of the piezo buzzer.

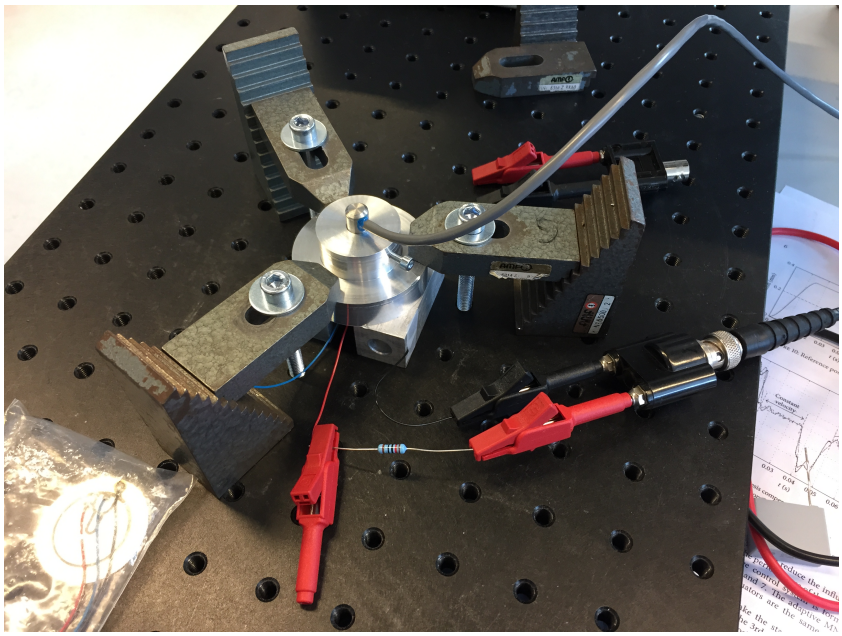

Figure 6.16: Test setup for the buzzer

The result is shown in Figure 6.17, 6.18 and 6.19. The input is the voltage signal from dSpace, the

output is the displacement of the buzzer in the center.

The frequency response is very similar between two buzzers up to 1kHz, but the steel buzzer has a very small stroke of less than 8µm, while the copper buzzer has about 52µm, under a clamped diameter of 35mm. Notice that the steel buzzer can only handle a maximum voltage of only 50V, while the copper buzzer can handle up to 140V.

The steel membrane is very stiff compared to copper, the undesired deformation under pressure will be much smaller than the copper buzzer, however, the less than 8µm stroke makes it unable to overcome any tolerance issue during assembly and also unable to change the air gap. This test concludes that the 35mm steel buzzer is not suitable for the application. The copper buzzers are very suitable to be used as a valve, however, the 50µm buzzer has its trade-off. The stroke is at a high number of 90µm, however, the large copper membrane introduces an undesired vibration mode at 381Hz. This vibration mode will reduce the bandwidth of the pressure regulator, but the benefit of 90µm stroke is largely preferred. This 50mm copper buzzer will be chosen as the valve.

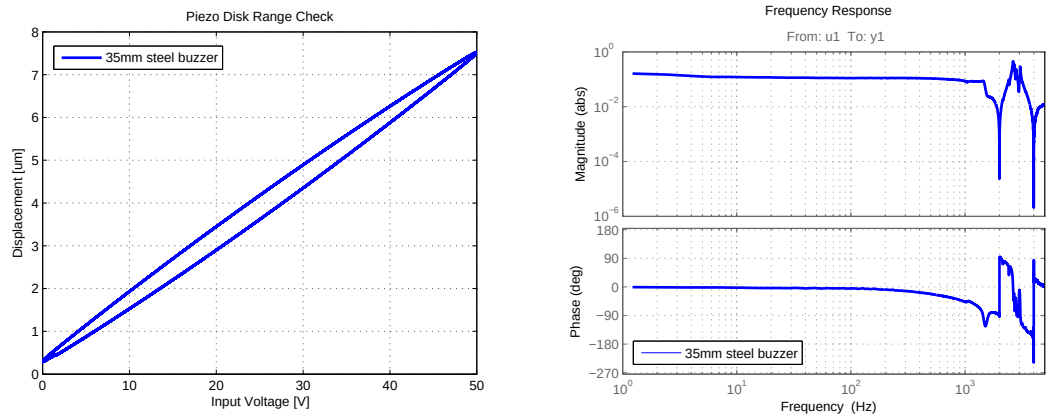

(a) Stroke and Hysteresis of the 35mm Steel Buzzer (b) Frequency response of the 35mm steel buzzer

Figure 6.17

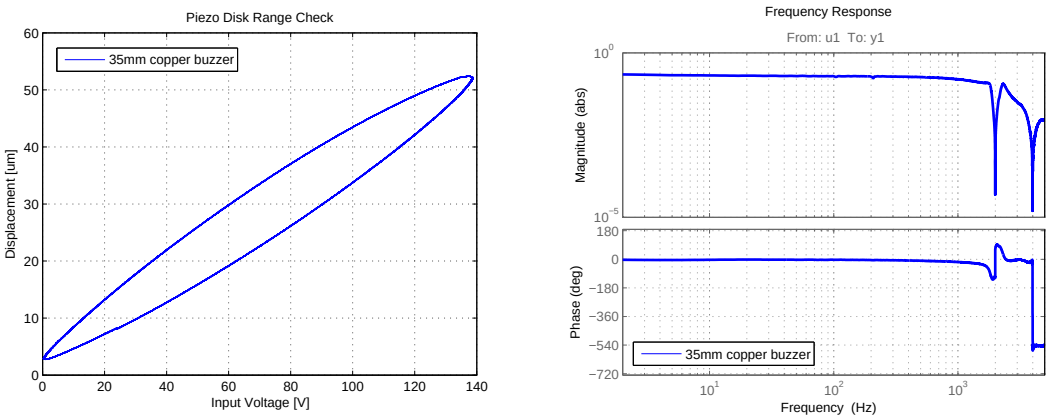

(a) Stroke and hysteresis of the 35mm copper buzzer (b) Frequency response of the 35mm copper buzzer

Figure 6.18

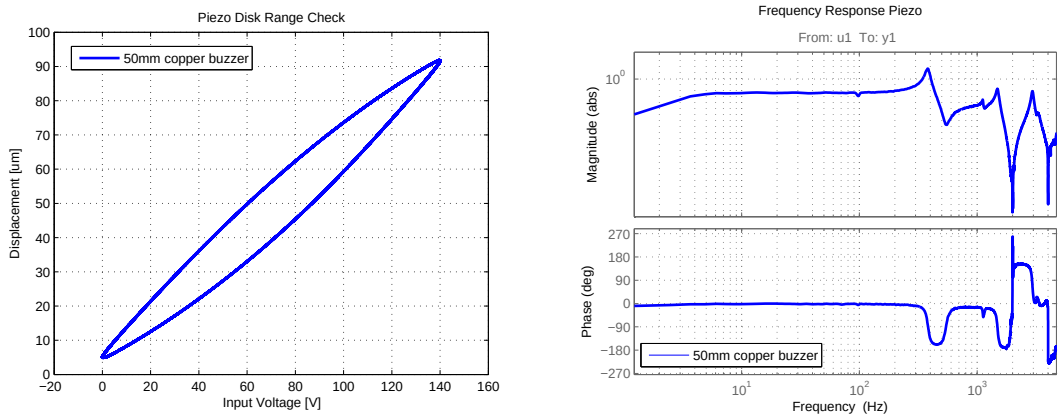

(a) Stroke and hysteresis of the 50mm copper buzzer (b) Frequency response of the 50mm copper buzzer

Figure 6.19

6.5. Conclusion

In this chapter, the principle of an orifice valve is studied, and the concept of a piezo controlled valve is brought up. Using the piezo buzzer to control the valve can provide a better dynamic performance for the pneumatic actuator, at the same time, it's possible to integrate the piezo valve into the actuator, significantly reducing the size.

The piezo buzzer is a very weak actuator and it has low blocking force, which means it has difficulty in controlling the air gap of the orifice when it's pressurized. The solution is to implement a counter pressure on the piezo, this counter pressure will compensate the force applied by the compressed air from the orifice. With the counter pressure concept, the piezo buzzer becomes a feasible valve component, and is able to regulate the pressure inside the pneumatic actuator. Although the COMSOL model can not precisely predict the behaviour of such a design, it shows what the piezo buzzer valve concept can achieve, and shows the way of how to implement it.

One prototype will be built according to the model and the piezo valve concept, the process of the design and manufacturing, as well as the controller design will be discussed in the next chapter.

7

Prototype Pneumatic Actuator

In the previous chapters, a model for the pneumatic actuator was established and verified, and a piezo buzzer valve concept was proposed. The required theory for designing a compact, fast and strong pneumatic actuator with a small stroke for the Flowerbed is completed.

Recall the requirement of the actuator:

- The actuator should have a stroke of 80μm.
- The actuator should be able to generate a maximum force of 140N.
- The actuator should be able to reach a bandwidth of 150Hz.
- The actuator should be as cost effective as possible.
- The actuator should be compact so that it can fit into the Flowerbed system.

Part of the requirements is already met. Piezo buzzer valve concept introduced in the previous chapter has reduced the cost of the valve from more than on hundred euros for a solenoid valve down to only 50 cents for one piezo buzzer. The piezo buzzer can be integrated into the actuator housing, reducing the size of the actuator.

In this chapter, a pneumatic actuator will be designed and manufactured using the models and the piezo valve concept discussed in the previous chapters. One prototype is made for this research, the design and the performance of this prototype will be discussed, together with the design of the controller.

7.1. Design parameters

As already discovered in the model, the most important parameters for the actuator during the design are:

1. supply pressure
2. inlet orifice resistance
3. outlet valve resistance
4. total internal volume

5. dynamic response of the valve
6. diameter of the pressure chamber

Among these parameters, the resistance of the valve is the most important for this special type of pneumatic actuator. It's the bottleneck of the system because it greatly determines the time needed for the pressure chamber to build up the pressure, which is the slowest part of the system. However finding the resistance is tricky, because the minimum resistance is determined by three factors: orifice diameter, stroke of the piezo buzzer, blocking force of the piezo buzzer. The larger the stroke is, the more deformation it is under stress, hence the lower blocking force. However the piezo preloading and counter pressure will partially eliminate the force on the piezo, the blocking force problem can be partially solved.

Figure 7.1 and 7.2 are results of a COMSOL simulation which simulates the deformation of the piezo buzzer with an 1.3mm(inner) and 3mm(outer) orifice diameter under a pressure of 4bar. The blocking force of the piezo limits the maximum inner orifice diameter and the maximum pressure, but theses two parameters are correlated. At the extreme condition, increasing the inner orifice diameter will force the designer to decrease the maximum pressure, and vice versa. It's a balance to choose and it's difficult to find the optimal parameters as a designer.

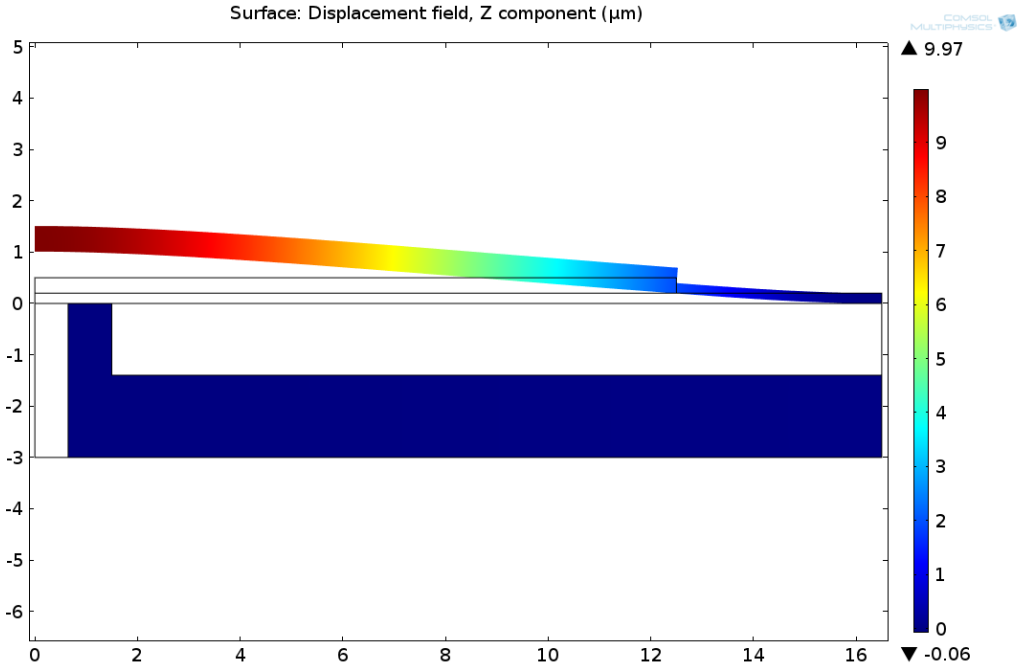

Figure 7.1: Deformation of a 50mm Piezo buzzer with 1.3mm(inner) and 3mm(outer) Orifice under a pressure of 4bar is about 10μm, about 10% of total stroke. This lost of stroke can be compensated by preloading and counter pressure

In this prototype a diameter of 1.3mm(inner) and 3mm(outer) is chosen for the orifice due to the limitation of the manufacturing precision and tolerance, with a supply pressure of 4bar and the diameter of the pressure chamber is 30mm. Figure 7.4 is the cross section of the CAD model built according to the schematics shown in Figure 7.3. The minimum drill diameter is 1.3mm during the manufacturing and this will be the diameter of the channels, as well as the inner diameter of the outlet orifice of the valve. The internal volume is kept as small as possible, but there must be attentions that the geometry of the internal construction will not introduce resistance into the system. For example, the very thin pressure chamber, once the thickness of the pressure chamber approaches zero, the resistance will start to increase and become unneglectable. Such geometry should be avoided but the internal volume should be kept as small as possible in order to achieve a faster response of the air dynamic subsystem as discussed in the previous chapters.

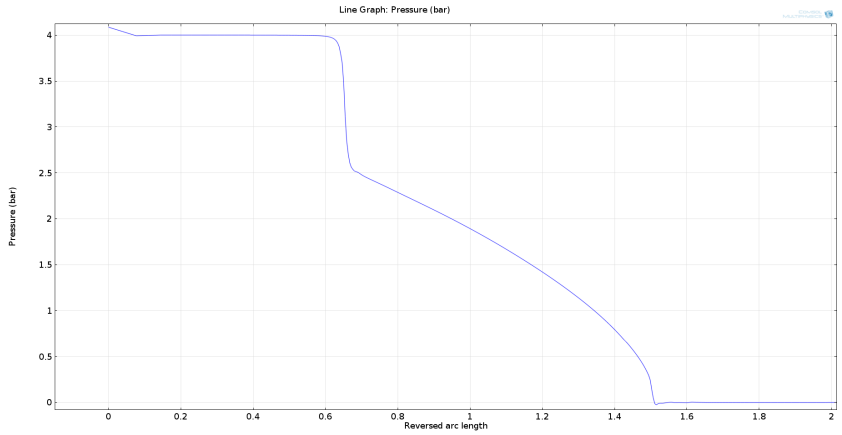

Figure 7.2: Pressure distribution on the piezo buzzer from center(0mm) to 2mm radius, with 1.3mm(inner) and 3mm(outer) Orifice. Pressure distribution depends on the inner and outer diameter of the orifice. As the inner diameter determines the resistance, the outer diameter should be as close to inner diameter as possible, so that the force applied on the piezo can be as reduced as much as possible

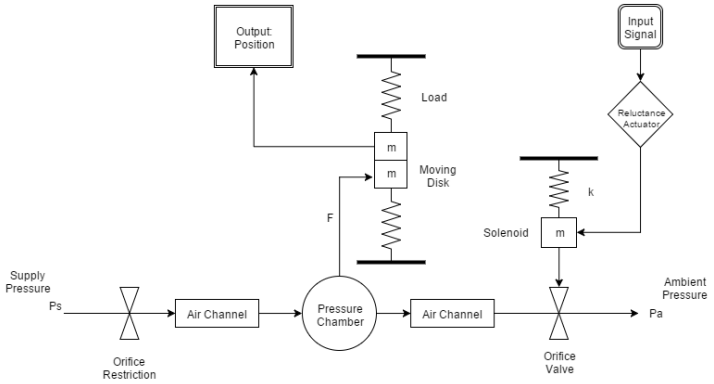

Figure 7.3: Schematic of the pneumatic actuator

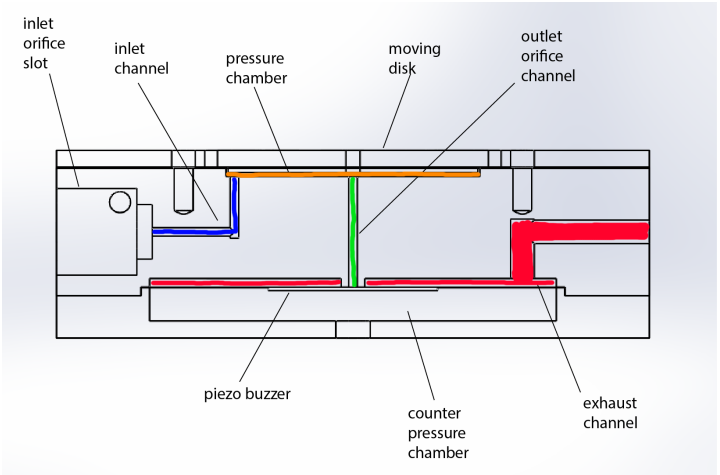

Figure 7.4: The CAD model of the actuator cross section

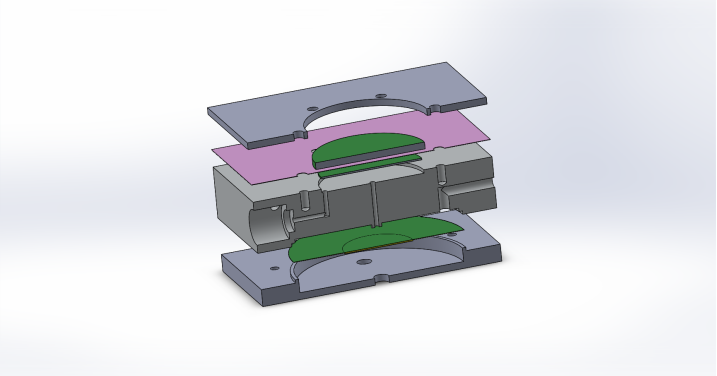

Figure 7.5: Exploded view of the actuator. The purple sheet is the moving membrane, the large green disk represents the piezo buzzer

7.2. Manufacturing of the prototype

The general approach of the design is to reduce the internal volume as much as possible to reduce the pressure build up time, and keep the channel as unobstructed as possible to prevent any unneglectable resistance appear in the channel. Most of the resistance should only exist in the inlet orifice and the valve.

There is some problem to solve during the manufacture. The piezo has a curved surface and it doesn't match the surface of the orifice, which means the piezo buzzer will not be able to close the air gap because their geometry doesn't fit. The surface of the piezo buzzer needs to be flattened by adding material between the piezo buzzer and the orifice.

This was achieved by adding a thin layer of epoxy in between during the assembly. However, this method is not reliable and is not very repeatable. If the amount of epoxy added on the gap is not exactly as much as needed, the applied epoxy will not able to fit the surface of the orifice, either the air gap stays open with if little epoxy applied, or the orifice gets permanently sealed with too much epoxy. Applying epoxy is therefore not the best option.

Instead, another approach is chosen, using a self-alignment method. Figure 7.6 shows the schematic of the self-alignment approach. The idea is to fill the gap with a piece of plastic folie which is thicker than the air gap, this thick layer will be clamped between the orifice and the piezo buzzer, and introduced some preload on the piezo. The plastic layer is sensitive to heat and it will soften under high temperature. By blowing hot air through the orifice, the plastic will soften and gradually deformed to fit the geometry of the air gap under the clamping force from the piezo. This fitting process is an easy way to achieve automatic alignment and fit the air gap between the orifice and the piezo buzzer, it's unlikely to fail with a well controlled hot air flow. This method yields a properly sealed air gap, without introducing any side effect, and it managed to reduce the difficulty in producing a piezo buzzer valve. Figure 7.7 shows the photo of the actual plastic sealing on the piezo buzzer.

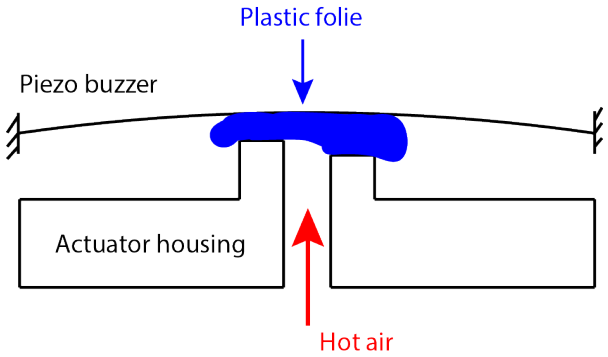

Figure 7.6: Schematic of the plastic seal between the piezo buzzer and the orifice, the plastic folie is heated by hot air flow, it will soften and automatically fit the air gap surface under the pretension of the piezo buzzer

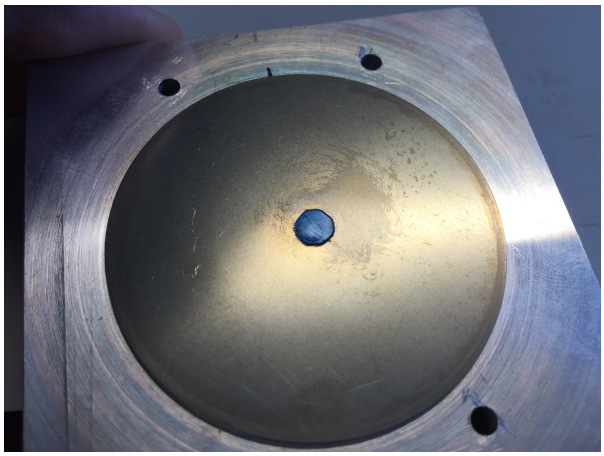

Figure 7.7: Photo of the actual plastic seal on the piezo buzzer

Another issue during the manufacturing is the fitting of the inlet restrictor. A Festo QS-4 restrictor is chosen and the core of this restrictor will be extracted and inserted into the inlet orifice slot of the actuator, as shown in Figure 7.8. The design was good, however, there was a compatibility problem occurred during the manufacturing. The screw thread used for the Festo QS-4 doesn't match the tapping tools in the workshop, hence, this QS-4 cannot be integrated into the actuator. Using another restrictor can solve this problem, but unfortunately, there aren't many choices at this stage, and due to the limitation of delivery time, no alternative approach is chosen and the QS-4 has to be used as an external component. Although the integration of the inlet orifice didn't succeed, in general, the concept is feasible, but it needs picking the components carefully. The result of this problem is that the actuator becomes slower, and it should be taken into account that the performance can be improved.

(a) Photo of a Festo QS-4 restrictor

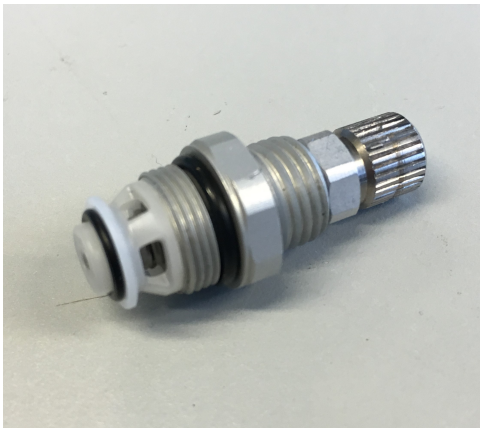

(b) Photo of the core of the Festo QS-4 restrictor. It should be installed into the pneumatic actuator to reduce the internal volume

Figure 7.8

The actuator shown in Figure 7.9 is fully assembled, and is ready for test.

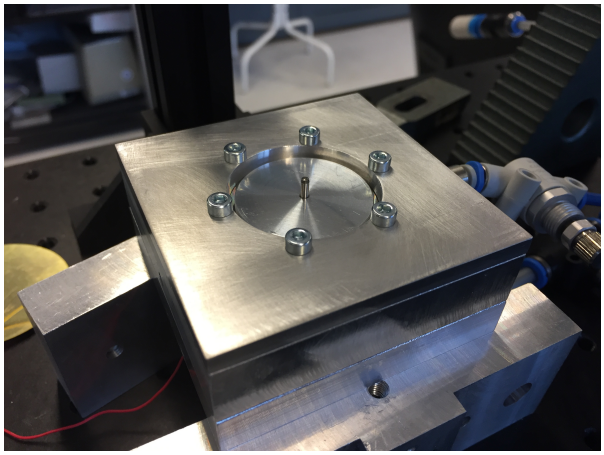

Figure 7.9: Assembly of the pneumatic actuator, with aligning pin for fitting measurement components. The aligning pin can prevent the components from slipping and it will make sure the components will receive a vertical force, preventing the membrane from twisting

7.3. Performance test of the prototype, openloop

The finished prototype will be tested in two major steps: First step is the pressure regulator test, which measures the performance of the piezo valve. The second step is the measurement of the pneumatic actuator itself.

In the first test, the moving disk will be removed and replaced by a pressure sensor, measuring the pressure inside the pressure chamber. Figure 7.10 shows the range of 1bar to 3.5bar inside the pressure chamber. The actuator is able to deliver a maximum force of 247N under 3.5bar. The input is the signal from dSpace, the output is the pressure inside the pressure chamber.

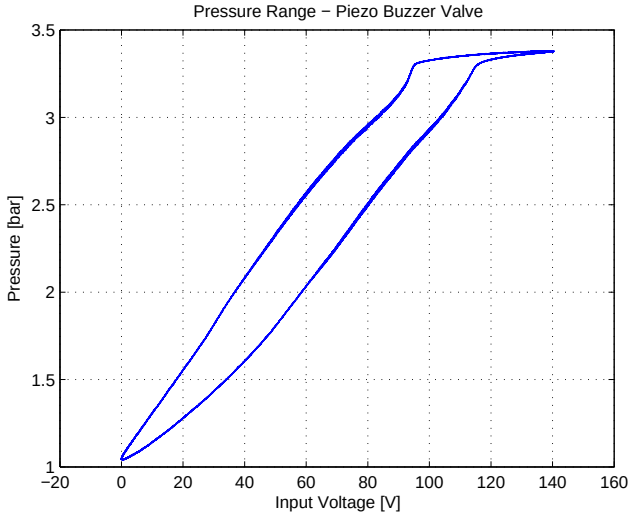

Figure 7.10: Working range and hysteresis of the pressure regulator of the prototype. A range of 1bar to 3.5bar shows a good sealing and enough opening of the air gap to ensure proper functioning of the pressure regulator. Response is slight non-linear

The frequency response of the pressure regulator in Figure 7.11 shows the first order characteristic of the air chamber model, as well as the characteristic of the piezo buzzer, which has a first eigenfrequency at around 500Hz. The input is the signal from dSpace, the output is the pressure inside the pressure chamber.

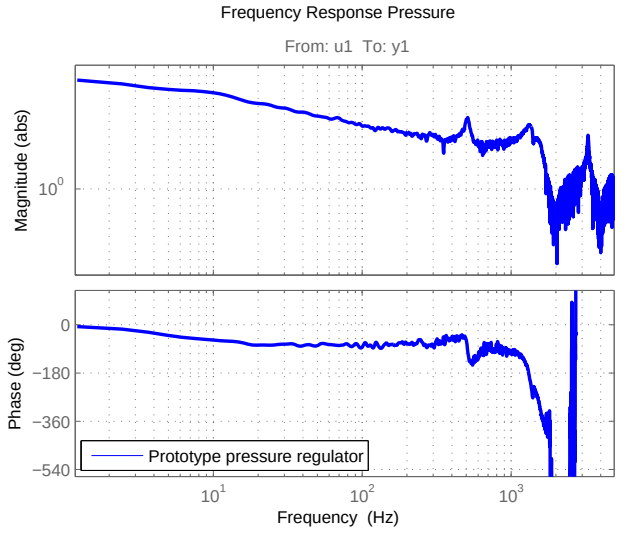

Figure 7.11: Frequency response of the pressure regulator. It clearly shows the 1st order behaviour of the air dynamics subsystem, and it also shows the dynamic behaviour of the piezo buzzer from the previous chapter

In the second test, the prototype will be fully assembled as a pneumatic actuator. The actuator will be preloaded with a spring and the displacement of the moving disk will be measured.

Figure 7.12 shows the stroke and the hysteresis of the actuator. The response is slightly non-linear which is expected from such a pneumatic system, but it's still a very good static response. Noticed the voltage only ranges from 0 to 100V to achieve the 80µm stroke. The purpose of this reserved voltage is to leave space for the controller to push the performance of the actuator by applying a reserved pressure which is higher in order to decrease the time to build up the pressure.

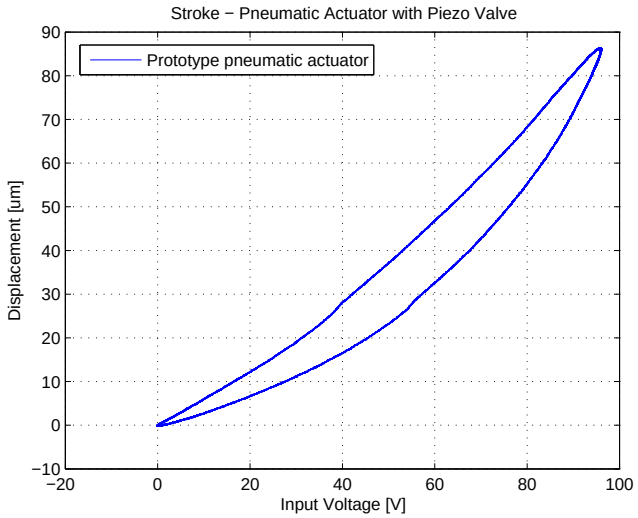

Figure 7.12: Working range and hysteresis of the actuator. Slightly non-linear response due to the non-linear pressure response shown from Figure 7.10. Voltage only ranges from 0-100V, 100-140V is reserved to speed up the performance shown in the next step

Figure 7.13 shows the step response of the actuator without any controller. As can be seen, it takes about 0.07 seconds to approach 80µm. This is caused by the characteristic of the air which is compressible. The air always needs time to build up the pressure after closing the valve. As was discussed in the previous chapter, the applied pressure, resistance and the internal volume determine the speed of this process.

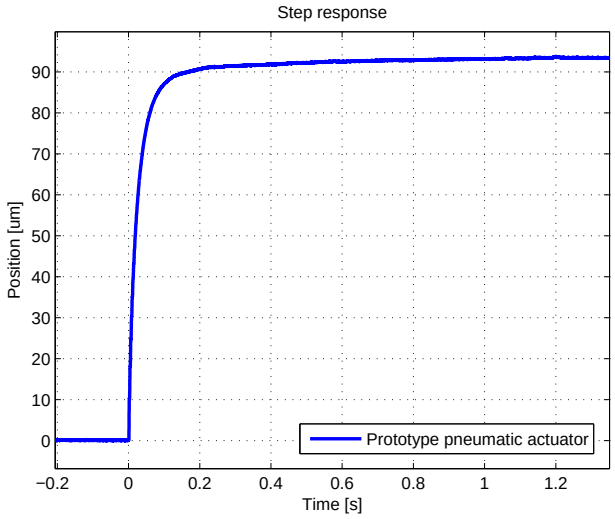

Figure 7.13: Step response of the actuator without controller. The response is not very fast due to the pressure build up, this can be improved by implementing a controller

Figure 7.14 shows the frequency response of the pneumatic actuator. The pole at 7.33Hz is the pole from the air dynamic subsystem. The first eigenfrequency at 490Hz, which matches the first eigenfrequency of the piezo buzzer. The input is the signal from dSpace, the output is the displacement of the moving disk.

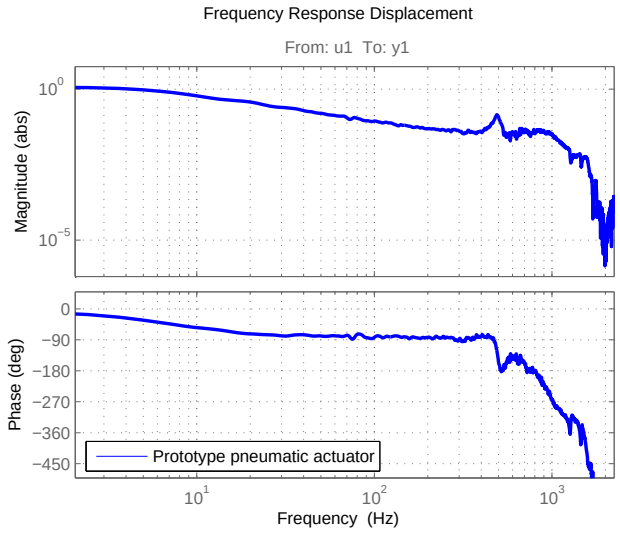

Figure 7.14: Frequency response of the actuator. The first pole of the system is at 7.33Hz, the first eigenfrequency is 490Hz, with a phase of -123°

7.4. Controller design

The prototype is successfully manufactured, a controller is needed to drive the prototype and improve the performance. A controller is a component in the dynamical system, which can sense the operation of a system, compares it against the desired behavior, computes corrective action based on a model of the system's response to external inputs and actuates the system to effect the desired change.[20]

The controller design for the prototype is based on a combination of filter and feedback PID controller, as shown in Figure 7.15. A feedback loop senses the output of the system, compares it to the input signal, then drive the system to reduce or eliminate the error. The filter is designed to compensate the dynamics of the system, it can improve the openloop dynamic performance of the actuator, reduce the resonance, compensate the magnitude of the frequency response in different frequencies, and attenuate the high frequency response, improve the the stability and disturbance rejection of the actuator. With a filter applied, the bode plot will show a smoother and flatter curve in the magnitude.

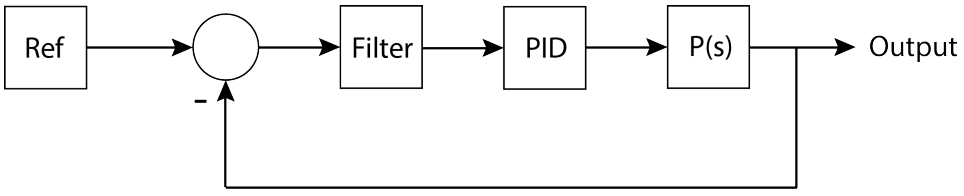

Figure 7.15: The control scheme of the prototype. It consist a PID feedback loop with a filter in the loop

Figure 7.16 shows the bode plot of the filtering, which consist three filters. It has two notch filters at 74.5Hz and 490Hz, which will reduce the peak shown in Figure 7.14. The 2^{nd} order low pass filter at 350Hz will reduce the magnitude above that frequency. These three filters together will deliver a smoother open loop frequency response. [21] [22]

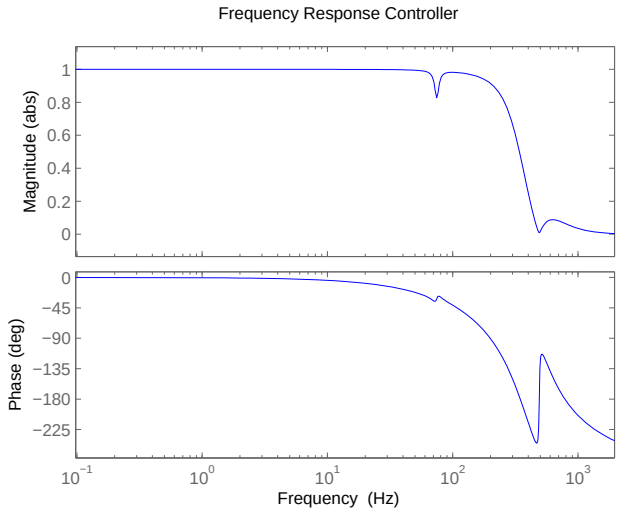

Figure 7.16: The filtering part consists two notch filters at 74.5Hz and 490Hz, and a 2^{nd} order lowpass filter with a cutoff frequency at 350Hz

Figure 7.17 shows a screenshot of a toolbox from TU/e called Shapeit, a toolbox that assists the design of controllers, and simulates the frequency response of a system with controllers implemented. From the simulation of the toolbox, the actuator is able to achieve a bandwidth around 100Hz. In practice, with further fine tuning of the PID controller and the filters, the actuator is able to achieve a bandwidth of 184Hz. Unfortunately, for the full range actuation, the bandwidth will reduce greatly. The cause of this reduction is the limited opening of the valve, it requires a minimum time for the air to build up the pressure. The more the actuator needs to move, the longer time it takes. The frequency response of the closed loop system is shown in Figure 7.18, the input is the reference signal from dSpace, the output is the displacement of the moving disk. The PID controller has a P gain of 9, D gain of 0.001, I gain of 200.

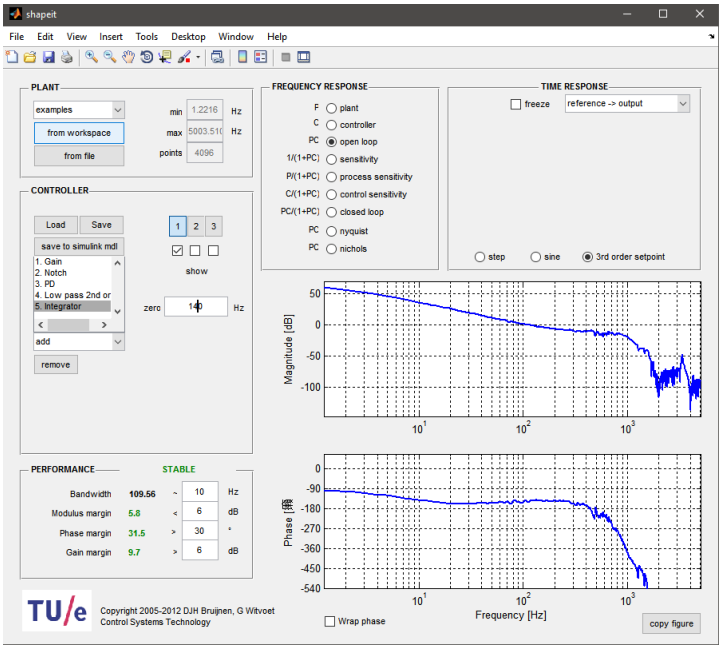

Figure 7.17: Openloop with filtering and PID controller. The response is very smooth thanks to the filtering which has reduced the peak and the magnitude of higher frequency. The toolbox simulation shows good margains of the system, and in practice the performance is even better, as can be seen in the frequency response of the close loop system

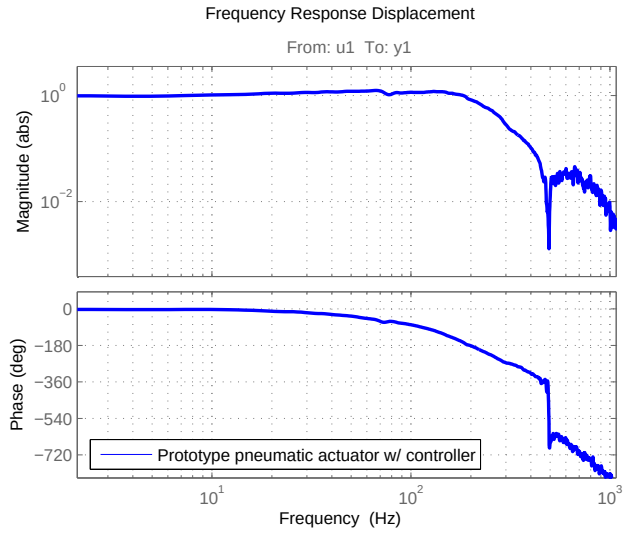

Figure 7.18: Closed loop of the actuator. The response is very nice and smooth, with a bandwidth of 183Hz

The step response of the actuator is shown in Figure 7.19 and 7.20. Noticed that the it only takes 0.0023s to reach the 1µm step position, there is some overshoot that cost some time to settle down. When the step size increase to 80µm, the time increases to about 0.013s. The reason is that the opening of the valve is limited, it requires the air inside the actuator to build up the pressure after the valve has closed and this process takes time. The larger the step size is, the more time it takes to reach the position. This is the weakness of the pneumatic actuator, the bandwidth is stroke-dependent.

Furthermore, during the manufacturing of the prototype, the inlet restrictor was not successfully integrated into the actuator housing and remained as an external component, it causes the internal volume to remain large and slows down the performance of the prototype. The bandwidth would have been greatly increased if the component was integrated into the housing.

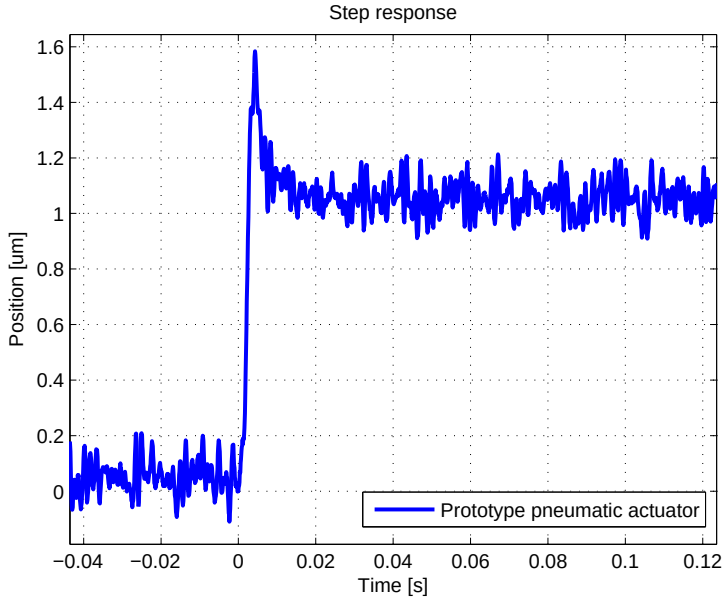

Figure 7.19: Step response of 1µm, it takes 0.0023s for the system to achieve the set point, however there is some overshoot, and it takes time to settle down

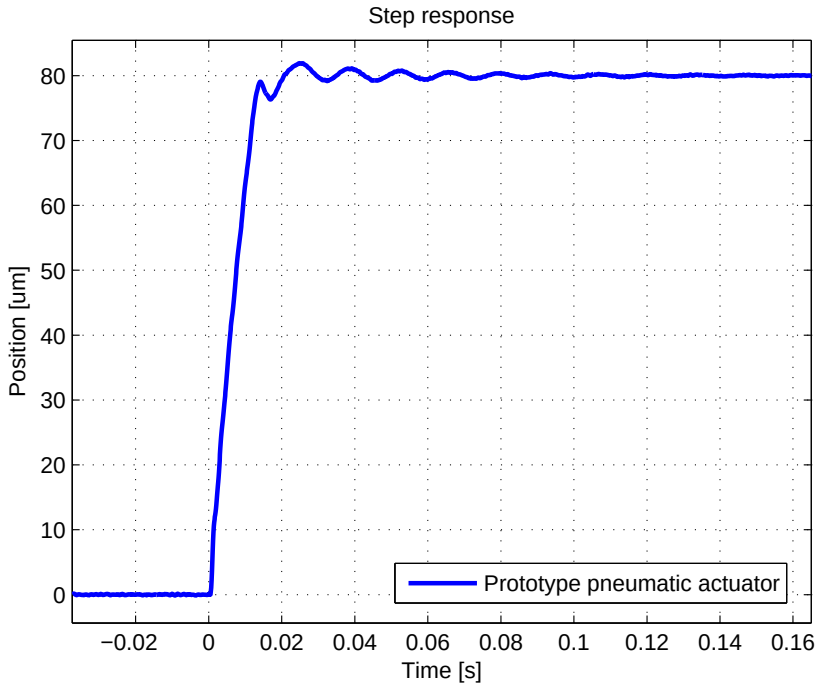

Figure 7.20: Step response of 80µm, it takes 0.0138s for the system to achieve the set point, more time is needed than the step response of 1µm due to the characteristic of pneumatic actuator

7.5. Conclusion

In this chapter, a prototype was successfully manufactured with the help of the model and the force compensated piezo valve concept. The design of the prototype was check by COMSOL before manufacturing. There are difficulties in the manufacturing, one of them being the surface profile of the piezo not matching the surface of the orifice. This was successfully solved by introducing a self-alignment assembly process with the help of a plastic folie and hot air.

A controller is designed for the prototype. The controller consists a filtering part with notch and low-pass filters, as well as a feedback PID controller.

The prototype has excellent performance:

- Stroke of more than 80µm, 80µm is required
- Maximum force of 247N, 140N is required.
- Bandwidth of 184Hz, 150Hz is required.
- Cost effective piezo buzzer valve.
- Integrated piezo valve inside the compact actuator housing.

However, the bandwidth of 184Hz is only valid under a very small range, once the actuator needs to move with a large step, the speed will slow down. The reason is that the change of pressure takes time, the compressed air needs to build up the pressure. The larger the difference is, the longer it takes. This weakness was amplified by the external inlet orifice which was not able to integrate into the actuator housing. This weakness can be solved by a stronger piezo component which can handle higher pressure, or have a larger opening of the air gap. However, there is always trade off between specification and cost. For the low-cost components implemented in the pneumatic actuator in this research, the result is remarkable.

The next chapter is the summary of the knowledge developed in this research. All the important theory and design will be summarized into a toolbox. This toolbox can be used for designing this kind of pneumatic actuator.

8

Design Toolbox

In the previous chapter, a prototype was successfully made, and it has met the requirement of the Flowerbed, and more importantly, it has proved that such a special pneumatic actuator can be made and it opens a way to manufacture a pneumatic actuator with small stroke and delivers a considerably large force and yet so cost effective, in fact, it's extremely low cost due to the implementation of a piezo buzzer.

This chapter, as the last part of the research, is to summarize the knowledge obtained during this research and conclude as a design method for this kind of actuator. The effects of the design parameters will be discussed, and finally, a toolbox made with the help of Matlab will be discussed.

8.1. Parameters

Parameters determine the performance of the actuator. Each of the parameters has to be considered during the design. Consider the schematic of the actuator shown in Figure 8.1, the important parameters derived from the schematic are:

1. Inlet orifice resistance
2. Inlet channel volume
3. Outlet valve resistance
4. Outlet channel volume
5. Pressure chamber volume
6. Valve dynamics
7. Supply pressure

These parameters have their effect to the system, and can be summarized into four categories:

1. Resistance
2. Volume
3. Valve dynamics
4. Supply pressure

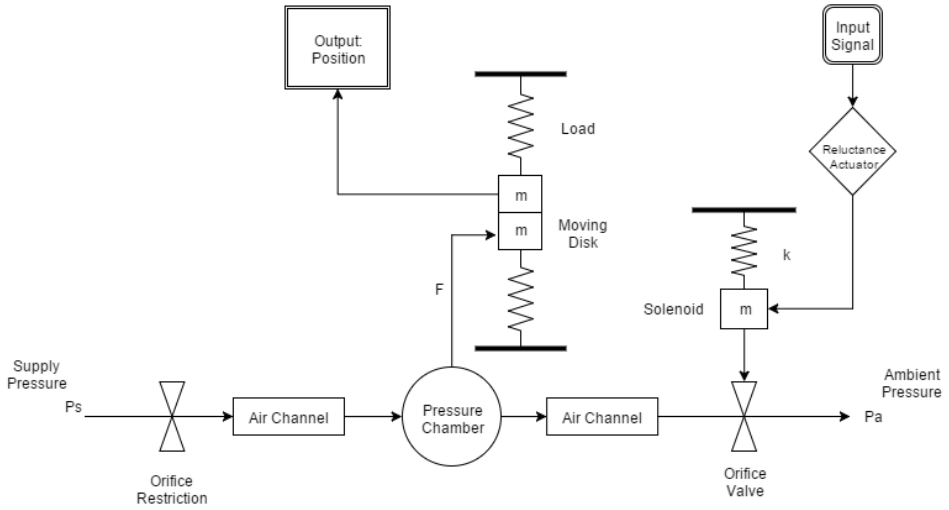

Figure 8.1: Schematic of the pneumatic actuator with load

Recall the results from the model of air dynamics, the pole of the transfer function is determined by

$$s = -\frac{\rho_o}{\rho_{chm}} \cdot \frac{1}{R_o C_{chm}} \tag{8.1}$$

To optimize the performance of the air dynamics, one can reduce internal volume, as well as the restriction of the orifice/valve. To demonstrate the effect, Figure 8.2 shows the difference in the frequency response of an actuator with different volume, while keeping other parameters equal. Reducing the internal volume will shift the pole of the system to a higher frequency, making it faster in response. In practice, this will reduce the time it needs for the chamber to build up the pressure. Figure 8.3 shows the effect of different resistance while keeping other parameters equal. Reducing the total resistance will also increase the performance of the actuator. A very important aspect of the improvement is that the low-frequency response will become flat, which indicates that the pole of the air dynamic system is shifting to a higher frequency.

Moreover, the model reveals that a change of 5 times in the resistance will yield to an equal result with one with a change of also 5 times in the volume. This shows that the change of resistance is comparable to the change of volume. In fact, this result does match what Eq.8.1 suggests, that the system is a 1^{st} order system. The proportional relationship between the resistance and the volume suggests that if one increases the volume 5 times and reduces the resistance 5 times, the system will behave exactly the same.

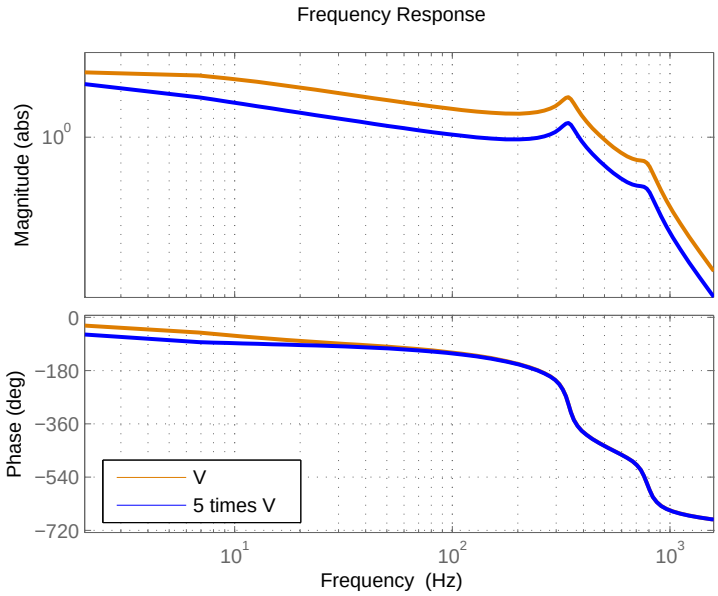

Figure 8.2: Dynamic response of a pneumatic actuator with 5 times volume difference

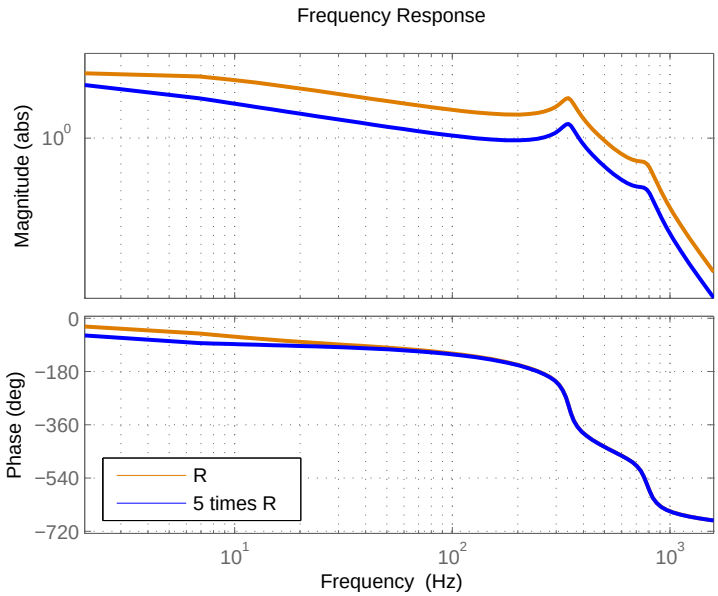

Figure 8.3: Dynamic response of a pneumatic actuator with 5 times resistance difference

On the other hand, increasing the supply pressure will also increase the performance as well. Figure 8.4 shows that a change of also 5 times in pressure will yield to a result comparable to the ones above. but this result depends a little bit on the resistance ratio between the inlet orifice and the outlet valve and, therefore, is not equal to the result mentioned above.

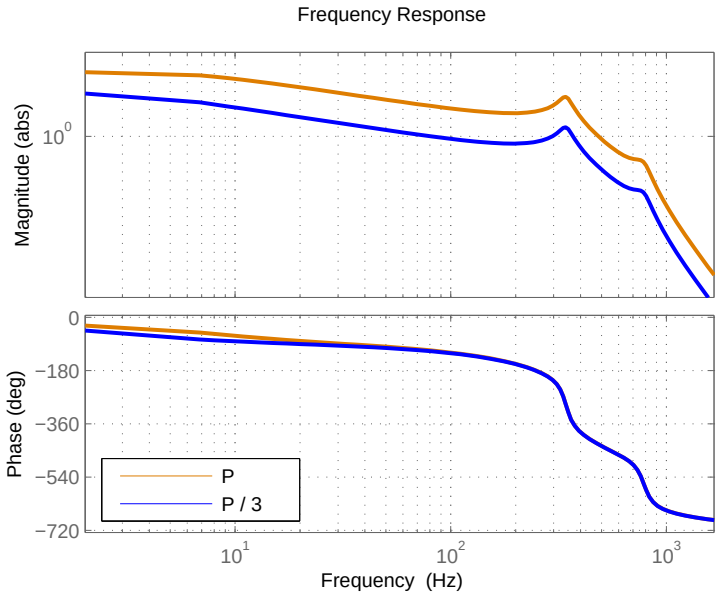

Figure 8.4: Dynamic response of a pneumatic actuator with 3 times difference in supply pressure

The last important parameter to the system is the valve dynamics. By improving the valve, one can improve the high-frequency performance of the actuator while keeping the low-frequency response unchanged as shown in Figure 8.5. When the eigenfrequency of the valve is increased, the peak of the Bode plot will shift to a higher frequency, increasing the bandwidth of the system.

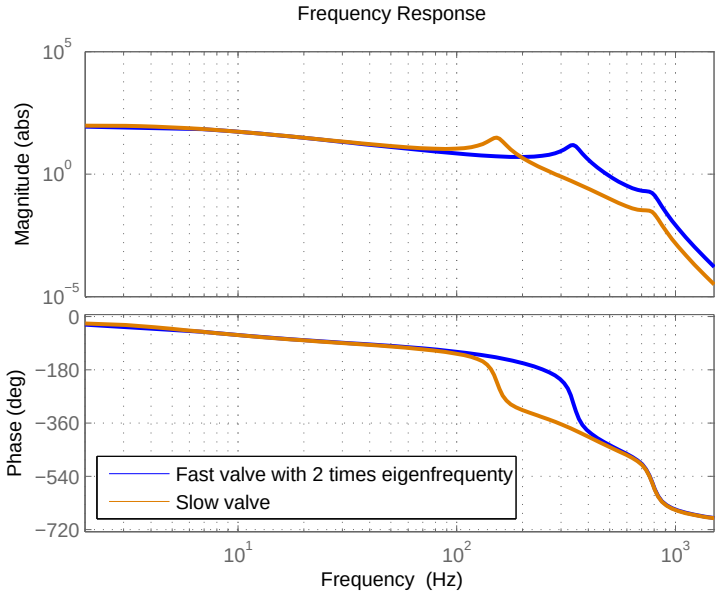

Figure 8.5: Dynamic response of an pneumatic actuator with a faster valve with 2 times the eigenfrequency. The eigenfrequency of the actuator is shifted also to 2 times, resulting a higher possible bandwidth

Figure 8.6 demonstrates the above-mentioned effects except the pressure by changing the ASCO PreciFlow valve into an ASCO PosiFlow. These two valves have different internal volume, different resistance and different dynamic response. Posiflow has larger internal volume but much smaller resistance, it shifts the pole of the air dynamic system to a higher frequency and maintains a flatter

response at a lower frequency. Meanwhile, the eigenfrequency of the solenoid is higher and it pushes the bandwidth of the system higher.

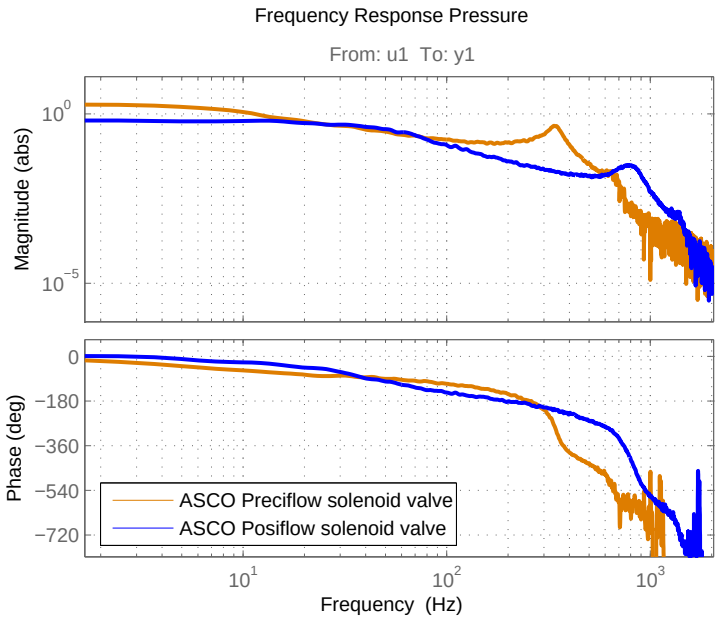

Figure 8.6: Dynamic response of a pressure regulator with a faster valve. This valve not only changes the eigenfrequency, it changes the internal volume and the resistance as well, affecting the performance from different aspects

The above tests showed the improvement of the performance by changing different parameters. However, these improvements will have their limits. Some of the limits come from the model, some of them come from the specifications of the components.

When the volume is decreased greatly to a level that it starts to approach zero, the geometry may start to introduce resistance into the system, in this case, the model is not valid any more and it can not be used for such extreme design.

Reducing the inlet resistance can greatly improve the performance of the actuator, however, the range of the pressure depends on both the inlet resistance and the outlet resistance. The outlet resistance depends on the outlet valve. If the range of the variable resistance of the valve, namely the stroke of the piezo buzzer, is very small, then, as a result, the range of the pressure inside the pressure chamber will be very small and this leads to a very small stroke of the actuator. Therefore, the resistance of the inlet restrictor and the valve must be balanced, so that the actuator can have a balance between stroke and speed.

Increasing the dynamic performance of the valve has also a similar limitation. Piezo buzzer as an example, a faster piezo buzzer generally means smaller stroke and that leads to a smaller range of pressure/force, as well as slower performance for large displacement.

Therefore, considering the limitations and the relations between the components, as a guideline, when designing such actuator, using the following steps would be recommended:

1. Choose the piezo buzzer regarding the required bandwidth of the system. In this case, it is recommended to choose a piezo buzzer which has at least an eigenfrequency 2 times of required bandwidth.

2. Determine the valve orifice diameter, using the orifice model, so that the minimum resistance can

be determined. Use COMSOL to simulate the deformation of the piezo buzzer, and determine the supply pressure which the buzzer can handle with the help of counter pressure.

3. Determine the resistance of the inlet orifice, find a balance between the range of the pressure inside the chamber and the dynamic performance, then design a restrictor and integrate it into the actuator housing. There is another possibility for the inlet restrictor, which is using another piezo buzzer, making this inlet orifice also controllable. The controllable inlet restrictor will not be discussed in this research but more information can be found in Appendix E.
4. Determine the diameter of the pressure chamber, so that the actuator can deliver required force.
5. Design the internal channel and pressure chamber of the actuator. Avoid difficult geometry which may lead to an increase in the resistance inside the actuator.
6. Evaluate the performance using the toolbox, and compare to the requirement. Iterate when necessary.

The above mentioned design method is only a general approach, there are some important aspects to consider before choosing a certain piezo buzzer:

- Generally for a piezo buzzer, the higher eigenfrequency it has, the smaller stroke it can deliver. A fast piezo buzzer may have a very small stroke which is not suitable for the valve design. On the other hand, a piezo buzzer with large stroke may have an eigenfrequency lower than required. Designer has to test the piezo buzzer first in order to determine whether he/she should choose that certain piezo buzzer.
- At the moment there is very little information about the performance of the piezo buzzer regarding the stroke and eigenfrequency, even the datasheet doesn't provide this information. But the datasheet does provide some specification for an initial guess: Maximum frequency, diameter and thickness. Larger diameter and smaller thickness leads to larger stroke, while higher maximum frequency indicates a higher first eigenfrequency.

With all the information provided in this research, it is still difficult to design such a pneumatic actuator with the performance exactly as required. There are difficulties in the design of the valve, and difficulties in the manufacturing. The designer still has to test the actuator to make sure how the actuator performs. In order to make the process less difficult, a toolbox will be introduced in the next section. This toolbox can provide a simulation of the pneumatic actuator, which can help the designer predict the performance of their design.

8.2. Design Toolbox

To summarize the results and findings of this research project, a toolbox is created using Matlab GUI. Figure 8.7 shows a screenshot of the toolbox. Once the parameters are filled in, the toolbox will generate a visualized schematic to show how much volume each component takes, together with a Bode plot to show the open loop performance of the pressure regulator. The designer can also change the type of the valve between solenoid and piezo, to evaluate the performance of different types of valve.

This toolbox only provides simulation for the pressure regulator, thus the pneumatic actuator with the moving disk locked. The reason is that the load subsystem has minimal affect in the dynamic performance, and the pressure regulator determines the dynamic performance of the whole system in the frequency range that the designer will be interested in.

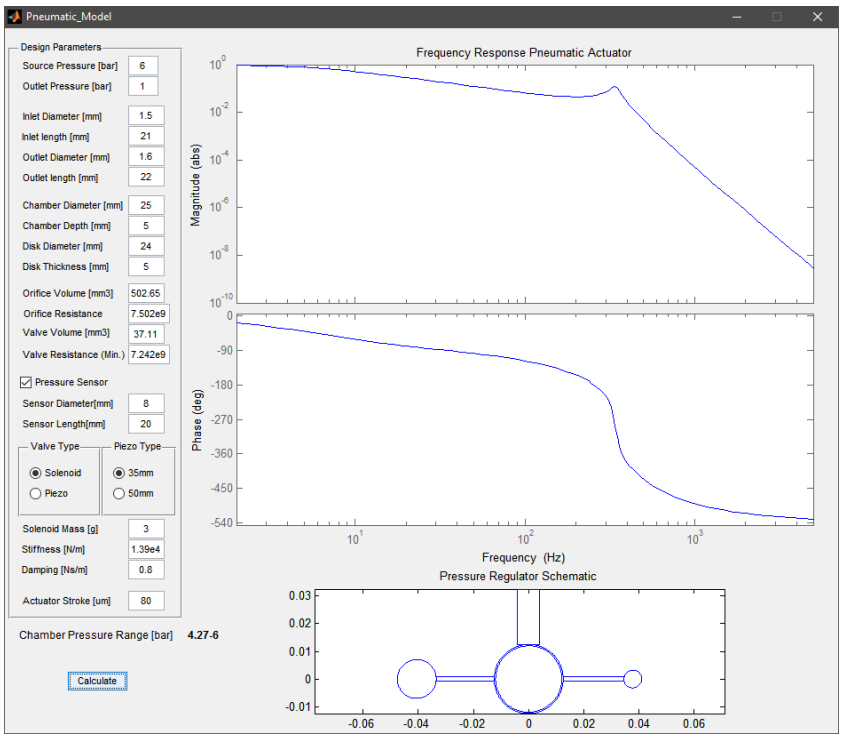

Figure 8.7: A screenshot of the toolbox.

To use the toolbox, first recall the construction of the actuator:

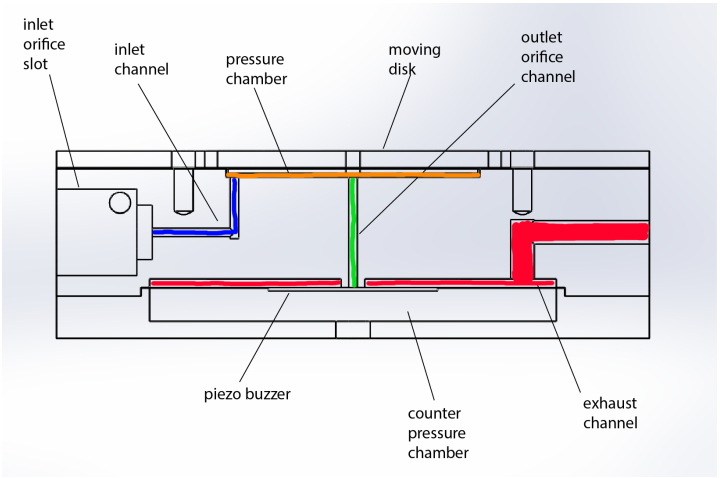

Figure 8.8: The CAD model of the actuator cross section

The components and properties of the actuators should be considered:

- Inlet orifice
- Inlet channel
- Pressure chamber
- Pressure sensor channel
- Outlet channel

- Outlet orifice/valve

On the left side of the toolbox, a list of parameters has to be filled in and they are categorized in components. For example, the inlet channel is defined as an equivalent tube, with two parameters: inner diameter and length. These two parameter should be filled in the section of the inlet channel. Other components, for example the inlet restriction, has parameters of internal volume and the resistance etc. These parameters must be filled in for each component.

There is a check box to choose whether a pressure sensor is implemented in the actuator. A pressure sensor has internal volume which should be included in the calculation, by checking the box this internal volume will be included. The internal volume of the pressure sensor is defined as an equivalent tube with two parameters: inner diameter and length.

Further more, two types of valves are provided: solenoid and buzzer. If solenoid valve is chosen, then the parameters of the mass-spring system of the solenoid valve must be filled in. The toolbox will calculate the dynamic performance of the solenoid valve and includes it into the simulation. If piezo buzzer is chosen, then the predefined model of the specific piezo will be loaded. There are two different piezo buzzer to choose from, and the designer can always add his/her own model for the buzzer he/she needs.

After filling in the parameters, click at the calculate button, the schematic of the pressure regulator and Bode plot will be updated. The schematic at the bottom shows how much internal volume each component takes, and it provides a visual feedback and a global judgement for the designer, then he/she can determine which component has the possibility for further improvement regarding internal volume. At the top right side is the bode plot of the model of the pressure regulator, simulated by the parameters given at the left side. The bode plot provides the information of the dynamic performance of the pressure regulator.

With the simulation provided by the toolbox, the designer can analyse the performance regarding the three subsystems discussed in the previous chapters, so that he/she can determine whether the design is fast enough.

Figure 8.9 shows a example of a pressure regulator with piezo buzzer as the type of valve, without pressure sensor installed.

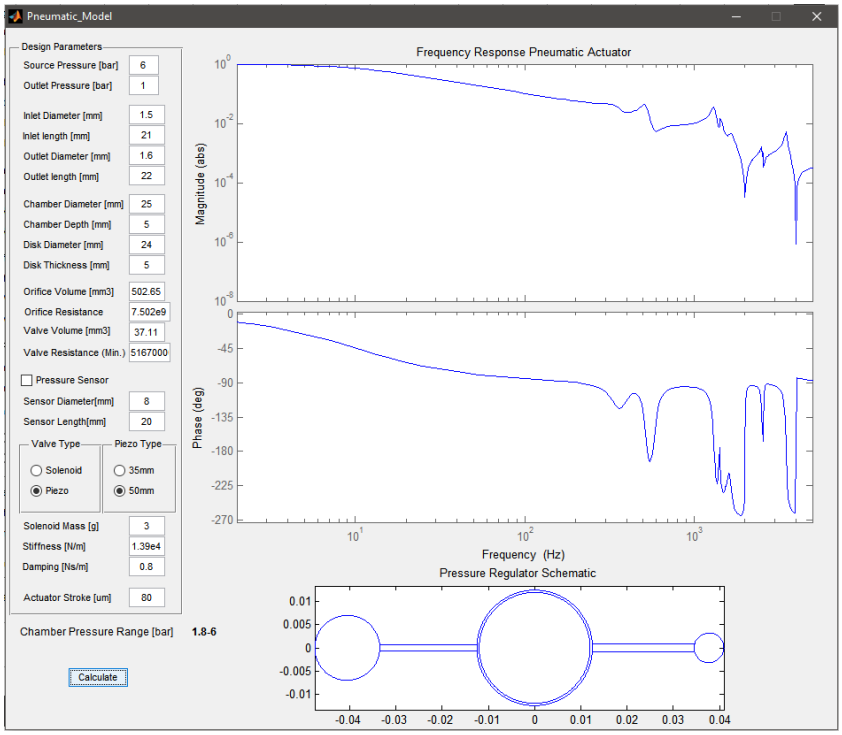

Figure 8.9: A screenshot of the toolbox with 50mm piezo buzzer chosen as valve type and pressure sensor is not installed

9

Conclusion

This MSc research project focuses on the design of an actuation system for the Flowerbed contactless wafer stage. The Flowerbed is a special stage because it has a high stiffness in the x-y-θ direction, which requires a relatively strong actuation system to control its displacement. The requirement of the Flowerbed is:

- The actuation system should be able to provide 3 degrees of freedom (x-y-θ) control to the Flowerbed.
- The actuation system should be able to reach the displacement limit of the Flowerbed, which is ±40μm translational and ±0.7mrad rotational.
- The actuator of the system should be able to generate a maximum force of 140N.
- The actuator of the system should be able to reach a bandwidth of 150Hz.
- The actuation system should be as cost effective as possible.

For the requirement different actuators and configurations are studied and the combination of pneumatic actuator and 3-RPR parallel manipulator configuration is chosen for this research. The 3-RPR configuration is simple and very strong, it only needs 3 actuators to achieve x-y-θ actuation. With this combination, the requirement of the actuator is defined:

- The actuator should have a stroke of 80μm.
- The actuator should be able to generate a maximum force of 140N.
- The actuator should be able to reach a bandwidth of 150Hz.
- The actuator should be as cost effective as possible.
- The actuator should be compact so that it can fit into the Flowerbed system.

A model for the pneumatic actuator is successfully established and is validated by simulation as well as lab testing. This model splits the pneumatic actuator into subsystems: air dynamic subsystem; valve subsystem and load subsystem. Each subsystem is separately established and by combining the models of the subsystems the full model of the pneumatic actuator is obtained.

Apart from the model, a study in the pneumatic valve is carried out. In this study, a concept of force compensated piezo buzzer valve is proposed, this concept utilizes an extremely low-cost piezo buzzer in the valve, providing excellent performance, it can reduce the size of the valve and significantly lower the cost.

A control system with filtering, together with PID feedback controller is designed for the actuator. The filtering consist notch filters and low pass filters, its purpose is to optimize the open loop frequency response of the actuator, while the PID feedback controller pushes the performance and stabilizes the system.

As a result, the prototype is successfully made, with excellent performance:

- Stroke of more than 80µm, 80µm is required
- Maximum force of 247N, 140N is required.
- Bandwidth of 184Hz, 150Hz is required.
- Cost effective piezo buzzer valve.
- Integrated piezo valve inside the compact actuator housing.

The greatest achievement of this project is having discovered the possibility to produce a pneumatic actuator with small stroke in the scale of micrometer, yet it can deliver relatively large force, and at the same time with components integrated into a very small package, yet the cost is reduced to an extremely low level, with a piezo buzzer costs 50 cents only.

The final part of this project is to summarize the knowledge developed in this research and create a Matlab toolbox. This toolbox is made to simulate the performance of a pneumatic actuator during the design stage, it will become a useful tool to assist engineer designing a fast pneumatic actuator with small stroke and large force.

10

Recommendation

This research is successfully completed, yet there are still many possibilities in this field and there are some recommendations can be made for further research.

The actuation configuration is chosen to be 3-RPR parallel manipulator, but the control algorithm is not discussed. Further research is recommended, together with the actuator created by this thesis.

The analytical model of the pneumatic actuator is a lumped 1^{st} order fluid dynamic model, with the resistance of most components neglected. This model is valid for most of the situations, but if the design is pushed to an extreme when the internal geometry starts to form some internal resistance, the model will become invalid. Further research for a much-refined model is recommended as it could be useful when the performance of the actuator can be pushed to a higher level. Furthermore, this model is established in frequency domain, and is not able to predict the transient response of the pneumatic actuator. A model in time domain can be very helpful because it can predict the slowdown for large stroke, hence, it can provide the possibility to optimize the speed of the actuator for large stroke as well, so that the performance can be further improved.

The pneumatic actuator discussed in this research is based on a fix inlet restrictor and a controllable outlet valve configuration. There is another configuration which is based on two controllable valves. In this case the inlet restrictor will be replaced by another valve, these two valves cooperate and controls the air flow with a larger range of variable resistance. The pneumatic actuator can benefit from this configuration, obtaining a higher performance. This kind of configuration is called differential valves. There are difficulties of this configuration, part of which is discussed in Appendix E, still it is recommended that further research should be carried out regarding this configuration.

In the final prototype, the pressure sensor is not implemented due to the large internal volume introduced by the pressure sensor with the connection. There are ways of integrating a piezo component and use it as a pressure sensor. Although the benefit of having a pressure sensor is not significant, it is still a good idea to have a pressure sensor inside the actuator to help to monitor the condition of the actuator, and achieve faster performance with further research.

Although the self-aligned piezo sealing layer is very convenient and works very well, it still increases the difficulty during manufacturing. It is recommended to investigate the manufacturing method, and reduce the difficulty.

A

Parallel Robot Modelling

This appendix explains the model and the matlab codes of the 3-RRR and 3-RPR parallel manipulator.

A.1. 3-RRR parallel manipulator

For the kinematics, the model is based on ideal revolute joints. This assumption defines the degree of freedom of the joints, allows it for only rotation movement, thus further constraint the end-effector to have only planar movement. Furthermore, the links are assumed to be rigid in the kinematics model. Figure A.1 and A.2 show the general configuration of a 3-RRR parallel manipulator and the configuration used in the Flowerbed application. A_i $(i = 1, 2, 3)$ denotes the position of the compliant joints that connect the links with the outside world, B_i $(i = 1, 2, 3)$ denotes the position of the compliant joint that connect the links A_iB_i and B_iC_i, C_i $(i = 1, 2, 3)$ are the joints that connect the links B_iC_i and the moving platform. θ_{1i} $(i = 1, 2, 3)$ denotes the initial angle of the links A_iB_i and θ_{2i} $(i = 1, 2, 3)$ denotes the initial angle of the links B_iC_i. l_1 denotes the length of the joints A_iB_i and l_2 denotes the length of the joints B_iC_i

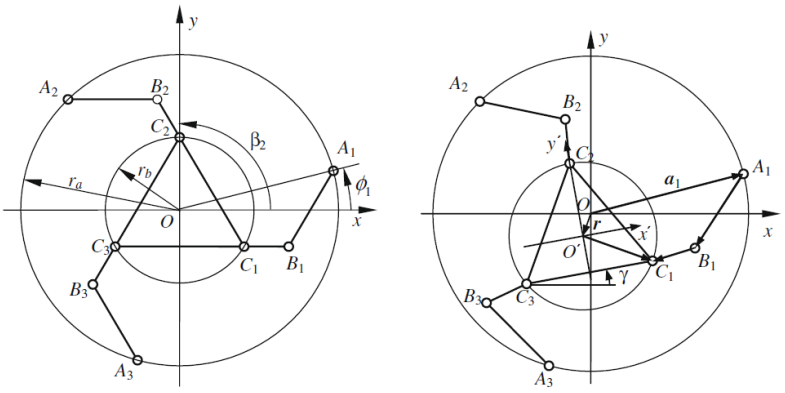

Figure A.1: Schematic of a general 3-RRR parallel manipulator

Based on the geometric and the movement constraints, the close-loop constraint equation can be written as

$$\mathbf{r} + \mathbf{R}\mathbf{b}_i - \mathbf{a}_i - l_1\mathbf{u}_i = l_2\mathbf{w}_i \tag{A.1}$$

where $\mathbf{r} = (x, y)^T$ is the position of the end-effector, which is the center of the moving platform; $\mathbf{u}_i$ and $\mathbf{v}_i$ are the unit vectors of the links A_iB_i and B_iC_i, respectively; $\mathbf{a}_i$ and $\mathbf{b}_i$ are the position of the joints A_i and B_i in the coordinate of O-xy and O'-x'y', respectively.

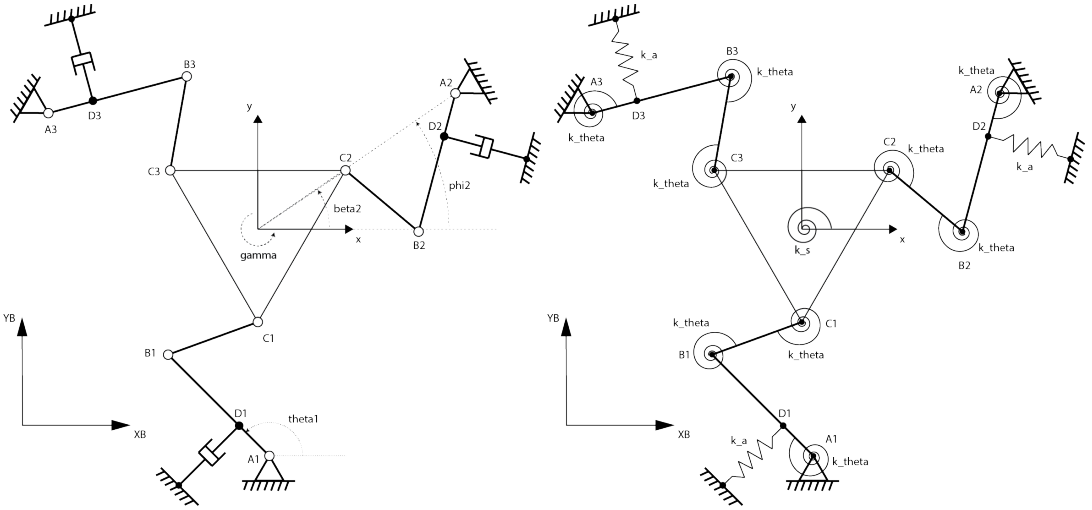

Figure A.2: Schematic of the 3-RRR configuration for the Flowerbed

furthermore,

$$\mathbf{R} = \begin{bmatrix} cos\gamma & -sin\gamma \\ sin\gamma & cos\gamma \end{bmatrix}$$

$$\mathbf{a}_i = r_a[cos\phi_i \ sin\phi_i]^T, \ \mathbf{b}_i = r_b[cos\beta_i \ sin\beta_i]^T$$

$$\mathbf{u}_i = r_b[cos\theta_{1i} \ sin\theta_{1i}]^T, \ \mathbf{w}_i = r_b[cos\theta_{2i} \ sin\theta_{2i}]^T$$

where $\beta_i = \beta_1 + \frac{2(i-1)\pi}{3}$, $\phi_i = \phi_1 + \frac{2(i-1)\pi}{3}$ $(i = 2, 3)$ are the position angles of the joints A_i and B_i in the coordinate of O-xy and O'-x'y', respectively; γ is the orientation of the end-effector.

By taking the dot product of its own on both sides, Eq.A.1 becomes

$$(\mathbf{r} + \mathbf{R}\mathbf{b}_i - \mathbf{a}_i - l_1\mathbf{u}_i)^T \ (\mathbf{r} + \mathbf{R}\mathbf{b}_i - \mathbf{a}_i - l_1\mathbf{u}_i) = l_2^2 \tag{A.2}$$

Further rewritten in the form of

$$A_i sin\theta_{1i} + B_i cos\theta_{1i} + C_i = 0 \tag{A.3}$$

where

$$A_i = -2l_1[y + r_b sin(\gamma + \beta_i) - r_a sin\phi_i]$$

$$A_i = -2l_1[x + r_b cos(\gamma + \beta_i) - r_a cos\phi_i]$$

$$C_i = r^2 + r_b^2 + l_1^2 + 2\mathbf{r}^T\mathbf{R}\mathbf{b}_i - 2\mathbf{a}_i^T\mathbf{R}\mathbf{b}_i - 2\mathbf{a}_i^T\mathbf{r} - l_2^2$$

The solution of Eq.A.2 is

$$\theta_{1i} = 2arctan\frac{-A_i \pm \sqrt{A_i^2 - C_i^2 + B_i^2}}{C_i - B_i} \tag{A.4}$$

Thus $\mathbf{u}_i$ can be determined. However θ_{2i} is still unknown, but $\mathbf{w}_i$ can be derived from Eq.A.1

$$\mathbf{w}_i = \frac{\mathbf{r} + \mathbf{R}\mathbf{b}_i - \mathbf{a}_i - l_1\mathbf{u}_i}{l_2} \tag{A.5}$$

Differentiating Eq.A.1 with respect to time:

$$\mathbf{v} + \mathbf{QRb}_i\omega - l_1\dot{\omega}_{1i}\mathbf{Qu}_i = l_2\dot{\theta}_{1i}\mathbf{Qw}_i \tag{A.6}$$

where $\mathbf{v}$ is the velocity vector of the end-effector.

Pre-multiplying both sides with $\mathbf{w}_i^T$, taking account to $\mathbf{w}_i^T\mathbf{Qw}_i = 0$, finally $\dot{\theta}_{1i}$ can be obtained:

$$\dot{\theta}_{1i} = \frac{\mathbf{w}_i^T\mathbf{v} + \mathbf{w}_i^T\mathbf{QRb}_i\omega}{l_1\mathbf{w}_i^T\mathbf{Qu}_i} = \frac{(\mathbf{w}_i^T + \mathbf{w}_i^T\mathbf{QRb}_i)(\dot{x}\ \dot{y}\ \dot{\gamma})^T}{l_1\mathbf{w}_i^T\mathbf{Qu}_i} \tag{A.7}$$

In the same way, pre-multiplying both sides with$\mathbf{u}_i^T$, $\dot{\theta}_{2i}$ can be obtained:

$$\dot{\theta}_{2i} = \frac{\mathbf{u}_i^T\mathbf{v} + \mathbf{u}_i^T\mathbf{QRb}_i\omega}{l_2\mathbf{w}_i^T\mathbf{Qu}_i} \tag{A.8}$$

Introducing vectors $\dot{\mathbf{P}} = (\dot{x}\ \dot{y}\ \dot{\gamma})^T$ and $\dot{\theta}_1 = [\dot{\theta}_{11}\ \dot{\theta}_{12}\ \dot{\theta}_{13}\ ]^T$, Eq.A.7 can be rewritten in a matrix form

$$\dot{\theta}_1 = \mathbf{J}\dot{\mathbf{P}} = \mathbf{B}^{-1}\mathbf{A}\dot{\mathbf{P}} \tag{A.9}$$

where $\mathbf{J}$ is the Jacobian matrix defined by

$$\mathbf{A} = \begin{bmatrix} \mathbf{w}_1^T & \mathbf{w}_1^T\mathbf{QRb}_1 \\ \mathbf{w}_2^T & \mathbf{w}_2^T\mathbf{QRb}_2 \\ \mathbf{w}_3^T & \mathbf{w}_3^T\mathbf{QRb}_3 \end{bmatrix},\ \mathbf{B} = l_1 diag(\mathbf{w}_1^T\mathbf{Qu}_1\ \mathbf{w}_2^T\mathbf{Qu}_2\ \mathbf{w}_3^T\mathbf{Qu}_3)$$

Due to the implementation of the linear actuators for driving the system, the angular velocity $\dot{\theta}_i$ can be transformed to linear displacement of the actuators

$$\dot{\mathbf{q}} = \mathbf{J}_a\dot{\mathbf{P}} \tag{A.10}$$

where $\dot{\mathbf{q}} = [\dot{s}_1\ \dot{s}_2\ \dot{s}_3\ ]^T$ is the vector of the linear velocity of the actuators, $\mathbf{J}_a = \mathbf{J}l_d$, l_d is the distance between A_i and D_i.

When the displacement of the actuators and the end-effector is very small, the relation between the displacement of the actuator and the displacement of the end-effector can be linearized:

$$\Delta\mathbf{q} = \mathbf{J}_a\Delta\mathbf{P} \tag{A.11}$$

The stiffness of the revolute joints of the parallel manipulator must be translated to a form that can be described by the displacement of the linear actuator:

$$\mathbf{K}\Delta\mathbf{P} = \mathbf{J}_a^T\mathbf{F} \tag{A.12}$$

where $F = [F_1\ F_2\ F_3]^T$ is the vector of the linear actuators, and $\mathbf{K}$ can be defined as

$$\mathbf{K} = k_\theta\sum_{i=1}^{3}\mathbf{J}_i^T\mathbf{J}_i + k_a\mathbf{J}_a^T\mathbf{J}_a \tag{A.13}$$

where $\mathbf{J}_1 = \mathbf{J}$, $\mathbf{J}_2 = -l_2^{-1}\mathbf{B}^{-1}\mathbf{C}$, $\mathbf{J}_3 = l_1l_2^{-1}\mathbf{B}^{-1}\mathbf{D}$. $\mathbf{C}$ and $\mathbf{D}$ are defined by

$$\mathbf{C} = \begin{bmatrix} l_1\mathbf{u}_1^T + l_2\mathbf{w}_1^T & l_1\mathbf{u}_1^T\mathbf{QRb}_1 + l_2\mathbf{w}_1^T\mathbf{QRb}_1 \\ l_1\mathbf{u}_2^T + l_2\mathbf{w}_2^T & l_1\mathbf{u}_2^T\mathbf{QRb}_2 + l_2\mathbf{w}_2^T\mathbf{QRb}_2 \\ l_1\mathbf{u}_3^T + l_2\mathbf{w}_3^T & l_1\mathbf{u}_3^T\mathbf{QRb}_3 + l_2\mathbf{w}_3^T\mathbf{QRb}_3 \end{bmatrix}$$

$$\mathbf{D} = \begin{bmatrix} \mathbf{u}_1^T & \mathbf{u}_1^T\mathbf{QRb}_1 + l_2\mathbf{w}_1^T\mathbf{Qu}_1 \\ \mathbf{u}_2^T & \mathbf{u}_2^T\mathbf{QRb}_2 + l_2\mathbf{w}_2^T\mathbf{Qu}_2 \\ \mathbf{u}_3^T & \mathbf{u}_3^T\mathbf{QRb}_3 + l_2\mathbf{w}_3^T\mathbf{Qu}_3 \end{bmatrix}$$

Above is the modelling of the modified 3-RRR parallel manipulator with linear actuator attached to the link A_iB_i.

The matlab code of the modelling is shown below:

```
1
2  % RRR_kinematics_model.m
3  % Kinematics model of a modified 3-RRR parallel manipulator
4
5  clc
6  clear all
7  close all
8
9  %% initial parameters, length input unit is mm
10
11 L = 320;          % length of the square mounting plate
12 ra = 140;         % distance of joint A to center
13 rb = 50;         % diatance of joint C to center      (default 120-140)
14
15 l1 = 70;
16 l2 = 70;
17 %la = 10;
18
19 for counter=1:70;
20
21 la(counter) = counter;
22 l = [l1 l2 la(counter)];      % length of the links AB AC and AD, where D is the piezo ...
       driving point
23
24 x = 0;
25 y = 0;
26 r = [x y]';      % position of the end-effector
27 gamma = 0;       % orientation of the end-effector
28
29 phi(1) = -pi/3;        % position of the A1 joint
30 for i=2:3;
31 phi(i) = phi(1) + 2*(i-1)*pi/3;
32 end
33
34 beta(1) = -pi/2;   % position of the B1 joints
35 for i=2:3;
36 beta(i) = beta(1) + 2*(i-1)*pi/3;
37 end
38
39 % stiffness of the components, [N/mm]
40 k_x = 1e3;           % X-Y stiffness of the platform
41 k_y = 1e3;
42 k_theta = 20;        % theta stiffness of the platform
43 k_j = 0;            % stiffness of the joints [N/rad]
44 %k_c = 5000;          % stiffness of the piezo connection
45 k_pzt = 100e3;         % stiffness of the piezo actuator
46 %k_a = k_c*k_pzt/(k_c + k_pzt) *2;  % serial stiffness of piezo actuator + connector, ...
       pair
47 k_a = k_pzt;
48
49 % here comes the input for static positioning calculation
50 % input1 is stroke of piezo
51 % input2 is X Y theta of the platform
52 ds1 = -16e-3;
53 ds2 = 8e-3;
54 ds3 = 8e-3;
55 input1 = [ds1 ds2 ds3]';
```

```
56
57 dP1 = 0e-3;
58 dP2 = 98e-3;
59 dP3 = 0e-3;
60 input2 = [dP1 dP2 dP3]';
61
62 %% geometric, initial position
63
64 % Rotation matrix
65 R = [cos(gamma) -sin(gamma); sin(gamma) cos(gamma)];
66
67 % Position vector of points A, a(:,i) = [xa ya]'
68 for i=1:3;
69 a(:,i) = ra .* [cos(phi(i)) sin(phi(i))]';
70 end
71
72 % Position vector of points C, b(:,i)
73 for i=1:3;
74 b(:,i) = R*( rb .* [cos(beta(i)) sin(beta(i))]' ) + r;
75 end
76
77 % Calculate AB orientation, theta1(i)
78 for i=1:3;
79 A(i) = -2*l(1)* ( y + rb*sin(gamma+beta(i)) - ra*sin(phi(i)) );
80 B(i) = -2*l(1)* ( x + rb*cos(gamma+beta(i)) - ra*cos(phi(i)) );
81 C(i) = r'*r + rb^2 + ra^2 + l(1)^2 + 2*r'*R*b(:,i)...
82 - 2*a(:,i)'*R*b(:,i)...
83 - 2*a(:,i)'*r...
84 - l(2)^2;
85
86 var(i) = sqrt( A(i)^2 + B(i)^2 - C(i)^2 );
87 end
88
89 theta1(1) = 2*atan( (-A(1) + var(1) )/(C(1)-B(1)) );
90 theta1(2) = 2*atan( (-A(2) + var(2) )/(C(2)-B(2)) );
91 theta1(3) = 2*atan( (-A(3) + var(3) )/(C(3)-B(3)) );
92
93 % Unit vector of link AB, U(:,i)
94 for i=1:3;
95 u(:,i) = [cos(theta1(i)) sin(theta1(i))]';
96 end
97
98 % Position vector of Joints B, c(:,i)
99 for i=1:3;
100 c(:,i) = a(:,i) + l(1)*u(:,i);
101 end
102
103 % Unit vector of link BC, w(:,i)
104 for i=1:3;
105 w(:,i) = (r + R*b(:,i) - a(:,i) - l(1)*u(:,i)) / l(2);
106 end
107
108 % Check the constrain, passed if constrain = [1 1 1] and no complex numbers in
109 % equation
110 % only useful for large displacement, so not for this project
111 for i=1:3;
112 if(r + R*b(:,i) - a(:,i) - l(1)*u(:,i) == l(2)*w(:,i))
113 constrain(i) = 1;
114 else
115 constrain(i) = 0;
116 end
117 end
118 %constrain
119
120 %% Calculate Jacobian
121
122 Q = [0 -1; 1 0];
123
124 A = [ w(:,1)' w(:,1)'*Q*R*b(:,1);...
125 w(:,2)' w(:,2)'*Q*R*b(:,2);...
126 w(:,3)' w(:,3)'*Q*R*b(:,3);...
```

```
];

B = l(1) * diag([ w(:,1)'*Q*u(:,1) w(:,2)'*Q*u(:,2) w(:,3)'*Q*u(:,3) ]);

C = [ l(1)*u(:,1)' + l(2)*w(:,1)'   l(1)*u(:,1)'*Q*R*b(:,1) + l(2)*w(:,1)'*Q*R*b(:,1);...
l(1)*u(:,2)' + l(2)*w(:,2)'   l(1)*u(:,2)'*Q*R*b(:,2) + l(2)*w(:,2)'*Q*R*b(:,2);...
l(1)*u(:,3)' + l(2)*w(:,3)'   l(1)*u(:,3)'*Q*R*b(:,3) + l(2)*w(:,3)'*Q*R*b(:,3);...
];


D = [ u(:,1)'   u(:,1)'*Q*R*b(:,1) + l(2)*w(:,1)'*Q*u(:,1);...
u(:,2)'   u(:,2)'*Q*R*b(:,2) + l(2)*w(:,2)'*Q*u(:,2);...
u(:,3)'   u(:,3)'*Q*R*b(:,3) + l(2)*w(:,3)'*Q*u(:,3);...
];

J(:,:,1) = B\A;                 % J1, a more accurate way to use inv(B)*A
J(:,:,2) = -1/l(2) * B\C;       % J2
J(:,:,3) = l(1)/l(2) * B\D;     % J3
J_a = J(:,:,1) * l(3);          % Ja

%% Calculate stiffness
%disp('stiffness')

K_j = zeros(3,3);

for i = 1:3;
K_j = K_j + k_j * J(:,:,i)'*J(:,:,i);
end

K_s = [k_x 0 0; 0 k_y 0; 0 0 k_theta];
K_j;
K = K_j + K_s;
K_a = k_a * (J_a')*J_a;

%% Static displacement without stiffness
%disp('static displacement without stiffness')

% input:    ds, displacement of piezo before deformation
% output:   dp, displacement of the end-effector
dP = inv(J_a)*input1;
dP_X(counter) = dP(1);
dP_Y(counter) = dP(2);
dP_G(counter) = dP(3);

% input:    dp, displacement of the end-effector
% output:   ds, displacement of piezo before deformation
dS = J_a*input2;
dS_X(counter) = dS(1);
dS_Y(counter) = dS(2);
dS_G(counter) = dS(3);


%% Static displacement with stiffness
%disp('static displacement with stiffness')

% input:    ds, displacement of piezo before deformation
% output:   dp, displacement of the end-effector
dP_k = inv(K + K_a)*K_a*inv(J_a) * input1;
dP_k_X(counter) = dP_k(1);
dP_k_Y(counter) = dP_k(2);
dP_k_G(counter) = dP_k(3);

% input:    dp, displacement of the end-effector
% output:   ds, displacement of piezo before deformation
dS_k = J_a*inv(K_a)*(K + K_a) * input2;
dS_k_X(counter) = dS_k(1);
dS_k_Y(counter) = dS_k(2);
dS_k_G(counter) = dS_k(3);

end
```

```
%% Draw the geometric configuration

figure
hold on

%% Draw the square mounting plate
line([-L/2 -L/2], [-L/2 L/2],'lineWidth',2)
line([-L/2 L/2], [L/2 L/2],'lineWidth',2)
line([L/2 L/2], [L/2 -L/2],'lineWidth',2)
line([L/2 -L/2],[-L/2 -L/2],'lineWidth',2)

%% Draw the triangle platform
line([b(1,1) b(1,2)],[b(2,1) b(2,2)],'lineWidth',2)
line([b(1,2) b(1,3)],[b(2,2) b(2,3)],'lineWidth',2)
line([b(1,3) b(1,1)],[b(2,3) b(2,1)],'lineWidth',2)

%% Draw the link AB
line([a(1,1) c(1,1)],[a(2,1) c(2,1)],'lineWidth',2)
line([a(1,2) c(1,2)],[a(2,2) c(2,2)],'lineWidth',2)
line([a(1,3) c(1,3)],[a(2,3) c(2,3)],'lineWidth',2)

%% Draw the link BC
line([c(1,1) b(1,1)],[c(2,1) b(2,1)],'lineWidth',2)
line([c(1,2) b(1,2)],[c(2,2) b(2,2)],'lineWidth',2)
line([c(1,3) b(1,3)],[c(2,3) b(2,3)],'lineWidth',2)

xlim([-170 170]);
ylim([-170 170]);
axis square

%% Draw the strokes
figure
plot(la/l1,dP_k_Y*1e3,'lineWidth',2)
xlabel('Position of the actuator')
ylabel('Maximum stroke of flowerbed [um]')
```

A.2. 3-RPR parallel manipulator

The 3-RPR kinematic schematics is given in Figure A.3. The three revolute joints A_i connected to the external world are located in the world coordinate B, while the three revolute joints C_i, which connect the moving platform and the links A_iC_i are located in the moving coordinate H. $X = [x\ y\ \phi]^T$ is the position of the end-effector and $L = [L_1\ L_2\ L_3]^T$ is the length of the link A_iC_i, or so called prismatic joints.

Given the position of the end-effector X, the closed-loop equation of the chains can be described from the aspect of inverse kinematics by

$$ {}^B\mathbf{C}_i = {}^B\mathbf{P}_H + {}^B_H\mathbf{R}\,{}^H\mathbf{C}_i = {}^B\mathbf{A}_i + L_i e^{i\theta_i} \tag{A.14} $$

where: $ {}^B\mathbf{P}_H = \begin{Bmatrix} x \\ y \end{Bmatrix}$ and $ {}^B_H\mathbf{R} = \begin{bmatrix} cos\phi & -sin\phi \\ sin\phi & cos\phi \end{bmatrix}$

The joint angle θ_i can be determined by

$$ \theta_i = atan2({}^BC_{iy} - {}^BA_{iy}, {}^BC_{ix} - {}^BA_{ix}) \tag{A.15} $$

From the forward kinematics, Eq.A.14 can be rewritten into

$$ \begin{bmatrix} L_i cos\theta_i \\ L_i sin\theta_i \end{bmatrix} = \begin{bmatrix} x \\ y \end{bmatrix} + \begin{bmatrix} cos\phi & -sin\phi \\ sin\phi & cos\phi \end{bmatrix} \begin{bmatrix} {}^HC_{ix} \\ {}^HC_{iy} \end{bmatrix} - \begin{bmatrix} {}^BA_{ix} \\ {}^BA_{iy} \end{bmatrix} \tag{A.16} $$

From the velocity kinematics, Eq.A.16 can be further rewritten into

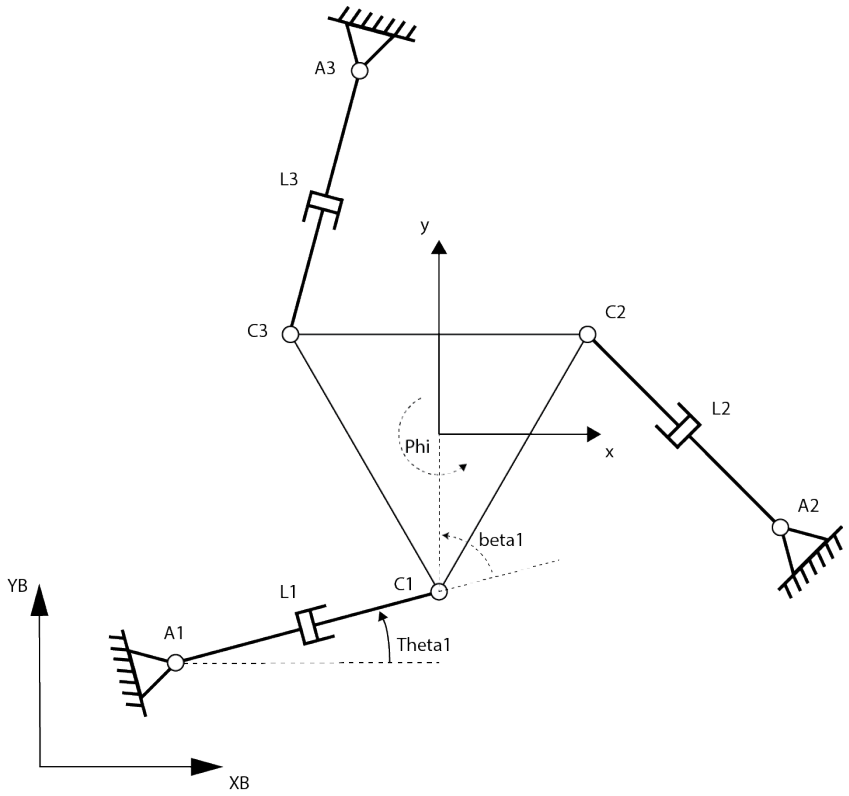

Figure A.3: Schematic of a general 3-RRR parallel manipulator

$$^{B}\mathbf{P}_{H} = ^{B}\mathbf{A}_{i} + L_{i}e^{i\theta i} + l_{Hi}e^{i(\theta_{i}+\beta_{i})} \tag{A.17}$$

where l_{Hi} is the length from C_i to the end-effector and β_i is the variable angle from C_i to the end-effector.

The overall Jacobian relationship for the 3-RPR parallel manipulator is defined as

$$\dot{L} = \mathbf{J}^{-1}\dot{X} \tag{A.18}$$

where $\dot{L} = [\dot{L}_1\ \dot{L}_2\ \dot{L}_3]^T$, $\dot{X} = [\dot{x}\ \dot{y}\ \dot{\phi}]^T$, and

$$\mathbf{J}^{-1} = \begin{bmatrix} cos\theta_1 & sin\theta_1 & l_{H1}sin\beta_1 \\ cos\theta_2 & sin\theta_2 & l_{H2}sin\beta_2 \\ cos\theta_3 & sin\theta_3 & l_{H3}sin\beta_3 \end{bmatrix}$$

is called the inverse Jacobian matrix.

The matlab code of the modelling is shown below:

```
1
2  % RPR_kinematics_model.m
3  % Kinematics model of a 3-RPR parallel manipulator
4
5   clc
6   clear all
7   close all
8
9  %% initial parameters
10
11  Q = 320;              % length of the square mounting plate
```

```
l = 70;                 % distance of joint C to center
L = 80;                 % length of the link

x = 0;
y = 0;
r = [x y]';             % position of the end-effector
phi = 0;                % orientation of the end-effector

alpha(1) = phi -pi/2; % orientation of the joint C1
theta(1) = 0;           % angle of the link A1

% Rotation matrix
R = [cos(phi) -sin(phi); sin(phi) cos(phi)];

%% geometric, initial position

% orientation of the C joints
for i=2:3;
alpha(i) = alpha(1) + 2*(i-1)*pi/3;
end

% position of the C joints
for i=1:3;
C(:,i) = R*( l .* [cos(alpha(i)) sin(alpha(i))]' ) + r;
end

% orientation of the A joints
for i=2:3;
theta(i) = theta(1) + 2*(i-1)*pi/3;
end

% position of the A joints
for i=1:3;
A(:,i) = C(:,i) - L.* [cos(theta(i)) sin(theta(i))]' ;
end

%% calculate jacobian, constant
for i=1:3;
beta(i) = alpha(i) + pi - theta(i);
end

% inverse Jacobian mataix, J^(-1)
M = [cos(theta(1))  sin(theta(1))  l*sin(beta(1));
cos(theta(2))  sin(theta(2))  l*sin(beta(2));
cos(theta(3))  sin(theta(3))  l*sin(beta(3))];

gamma = linspace(0, pi*2, 600);

for i=1:600;
X(:,i) = [40*cos(gamma(i)); 40*sin(gamma(i)); 0];
dL(:,i) = M * X(:,i);
end

%  dL = M*X

%% Plot

%%Draw the square mounting plate
line([-Q/2 -Q/2], [-Q/2 Q/2],'lineWidth',2)
line([-Q/2 Q/2], [Q/2 Q/2],'lineWidth',2)
line([Q/2 Q/2], [Q/2 -Q/2],'lineWidth',2)
line([Q/2 -Q/2],[-Q/2 -Q/2],'lineWidth',2)

%%Draw the triangle platform
line([C(1,1) C(1,2)],[C(2,1) C(2,2)],'lineWidth',2)
line([C(1,2) C(1,3)],[C(2,2) C(2,3)],'lineWidth',2)
line([C(1,3) C(1,1)],[C(2,3) C(2,1)],'lineWidth',2)

%%Draw the links
line([A(1,1) C(1,1)],[A(2,1) C(2,1)],'lineWidth',2)
line([A(1,2) C(1,2)],[A(2,2) C(2,2)],'lineWidth',2)
```

```
line([A(1,3) C(1,3)],[A(2,3) C(2,3)],'lineWidth',2)

xlim([-170 170]);
ylim([-170 170]);
axis square

%%Draw the stroke with circle
hFig = figure;
set(hFig, 'Position', [100 100 1100 370])
hold on
h1 = plot(gamma/pi/2*360, dL(1,:),'b','lineWidth',2);
h2 = plot(gamma/pi/2*360, dL(2,:),'g','lineWidth',2);
h3 = plot(gamma/pi/2*360, dL(3,:),'r','lineWidth',2);
plot(X(1,:)-40, X(2,:), 'c','lineWidth',2)

xlim([-100 370]);
ylim([-80 80]);
line([0 0], ylim,'Color','k'); %x-axis
line([0 370], [0 0],'Color','k'); %y-axis
legend([h1 h2 h3],{'Actuator 1','Actuator 2','Actuator 3'})
% axis equal tight
```

B

Air Dynamics Modelling

B.1. Modelling

In this appendix, the modelling of the air dynamics will be shown, explaining how the model is built, and how it corresponds to the frequency response. Furthermore, the Matlab code is attached.

Known parameters:

$$\rho_{air_s} = 1.205 kg/m^3$$
$$\mu_{air} = 18.27 \times 10^{-6}$$
$$R_{specific} = 287.058$$
$$T = 293.15K$$
$$P_s = 6 \times 10^5 Pa$$

Design parameters:

1) Orifice properties

$$R_{orifice} = 7.502 \times 10^9 Pa \cdot s/m^3$$
$$V_{orifice} = 5.02 \times 10^{-7} m^3$$

2) Inlet channel dimensions

$$\phi_{inlet} = 1.5mm$$
$$l_{inlet} = 21mm$$

3) Outlet channel dimensions

$$\phi_{outlet} = 1.5mm$$
$$l_{outlet} = 21mm$$

4) Chamber dimensions

$$\phi_{base} = 25mm$$
$$\phi_{disk} = 24mm$$
$$d_{base} = 5mm$$
$$d_{disk} = 5mm$$

5) Pressure sensor channel dimensions

$$\phi_{sensor} = 8mm$$

$$l_{sensor} = 20mm$$

6) Valve properties

$$R_{valve} = 7.242 \times 10^9 Pa \cdot s/m^3$$

$$V_{valve} = 3.711 \times 10^{-8} m^3$$

The design parameters will be converted into SI before calculation.

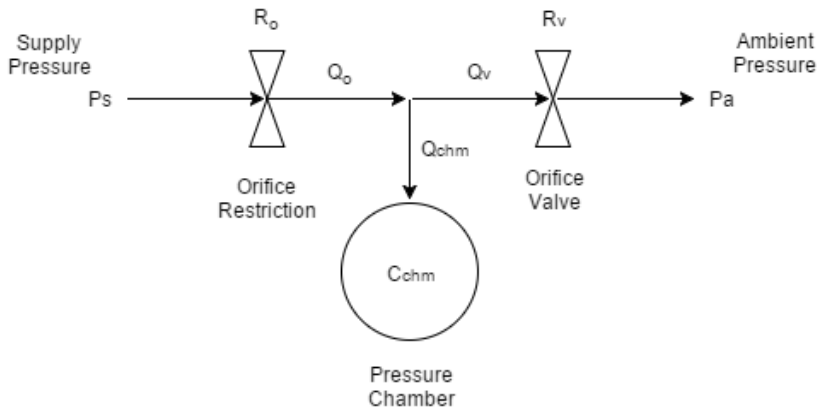

Figure B.1: Simplified Fluid Dynamic Model

Linearized situation at working point:

$$\dot{m}_c = 0$$

$$\dot{m}_o = \dot{m}_v$$

$$Q_o \rho_o = Q_v \rho_v$$

Where

$$Q_o = \frac{P_s - P_c}{R_o}$$

$$Q_v = \frac{P_v - P_a}{R_v}$$

$$\rho_o = \frac{(P_s + P_c)/2}{R_{specific} T}$$

$$\rho_v = \frac{(P_c + P_a)/2}{R_{specific} T}$$

Substitute and the equation becomes

$$\frac{P_s - P_c}{R_o} \frac{(P_s + P_c)/2}{R_{specific} T} = \frac{P_c - P_a}{R_v} \frac{(P_c + P_a)/2}{R_{specific} T}$$

$$\frac{P_s^2 - P_c^2}{R_o} = \frac{P_c^2 - P_a^2}{R_v}$$

$$(\frac{1}{R_v} + \frac{1}{R_o}) P_c^2 = \frac{P_a^2}{R_v} + \frac{P_s^2}{R_o}$$

$$P_c^2 = \frac{R_o}{R_v + R_o} P_a^2 + \frac{R_v}{R_v + R_o} P_s^2$$

$$P_c = \sqrt{\frac{R_o}{R_v + R_o} P_a^2 + \frac{R_v}{R_v + R_o} P_s^2}$$

Capacitance of the pressure regulator:

$$V_{regulator} = V_{orifice} + V_{inlet} + V_{chamber} + V_{sensor} + V_{outlet} + V_{valve}$$

$$C_{regulator} = \frac{V_{regulator}}{P_{chamber}}$$

Flow rate:

$$\rho_{orifice} = \frac{(P_s + P_{chamber})/2}{R_{specific}T}$$

$$\rho_{valve} = \frac{(P_{chamber} + P_a)/2}{R_{specific}T}$$

$$\rho_{chamber} = \frac{P_{chamber}}{R_{specific}T}$$

$$Q_{orifice} = \frac{(P_s - P_{chamber})}{R_{orifice}}$$

$$Q_{valve} = \frac{P_{chamber} - P_a}{R_{valve}}$$

$$\dot{m}_{orifice} = Q_{orifice} \cdot \rho_{orifice}$$

$$\dot{m}_{valve} = Q_{valve} \cdot \rho_{valve}$$

Based on the simplified lumped model, a one dimensional fluid dynamic differential equation can be set up by mass conservation:

$$\dot{m}_o = \dot{m}_{chm} + \dot{m}_v$$

$$\rho_o Q_o = \rho_{chm} Q_{chm} + \rho_v Q_v$$

Substitute the linearized resistance into the equation:

$$\rho_o \frac{P_s - P_{chm}}{R_o} = \rho_{chm} C_{chm} \dot{P}_{chm} + \rho_v Q_v$$

Using Laplace transformation to turn the equation into Laplace domain:

$$\frac{\rho_o P_s}{R_o} - \frac{\rho_o}{R_o} P_{chm} = s\rho_{chm} C_{chm} P_{chm} + \rho_v Q_v$$

The transfer function of the model becomes

$$\frac{P_{chm}}{Q_v} = \frac{\rho_o P_s - R_o \rho_v Q_v}{Q_v(s\rho_{chm} R_o C_{chm} + \rho_o)}$$

The transfer function shows that the air dynamic system is first order, the pole of the system is

$$s = -\frac{\rho_o}{\rho_{chm}} \cdot \frac{1}{R_o C_{chm}}$$

The frequency response of the model is shown in Figure B.2. As is mentioned above, the transfer function is of first order, with the pole determined by the R_o and C_{chm}.

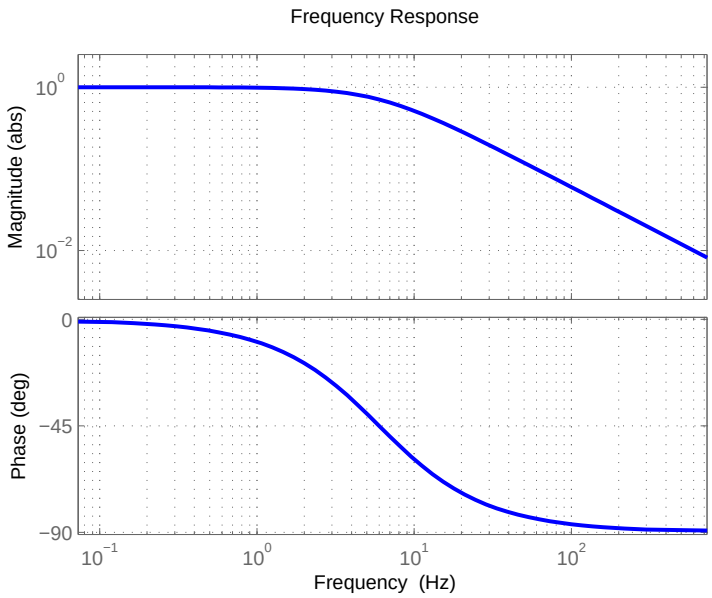

Figure B.2: Air Dynamic Model, Frequency Response

B.2. Simulation Nijveldt model

Thijs Nijveldt from TU Delft had developed a model during his research in pneumatic manifold design. This model can be used to predict the much more complicated dynamic response of the air channel design in contactless wafer handler. The air channel in the pressure regulator can be modelled as a simplified manifold, and the 1^{st} order air dynamic lumped model can be validated using the simulation from the Nijveldt model. [23]

The result of the simulation is shown in Figure B.3a. The model from Nijveldt shows the decrease of the phase in first order, and there is resonance in the air channel at a frequency of higher than 1000Hz. The simulation focus in the resonance of the air in the channel, and this resonance does not show up in the lumped first order ODE model of the air channel in Figure B.3b . The reason is that the ODE model only considers the simple RC effect in the system and only implement the first order behavior. The resonance in such an actuator has a very high frequency and has very little effect on the performance of the pressure regulator. The Nijveldt simulation, therefore, verified that the 1^{st} order lumped model is sufficient for predicting the air dynamics subsystem of the pressure regulator.

```
1
2  % model_air_dynamics.m
3
4  %clear all
5  %close all
6   clc
7
8  %% Parameters Pressure Regulator
9  rho_air_s = 1.205;  % normal air density [kg/m3]
10 mu_air = 18.27e-6;  % viscosity of air [Pa s]
11 R_specific_air = 287.058;    % specific gas constant for dry air [J/KgK]
12 t1 = 20;            % temperature in degree celcius
13 T1 = t1 + 273.15;   % absolute temperature in K
14
15 P_s = 4e5;          % inlet pressure [Pa]
16 P_a = 1e5;          % outlet pressure [Pa]
```

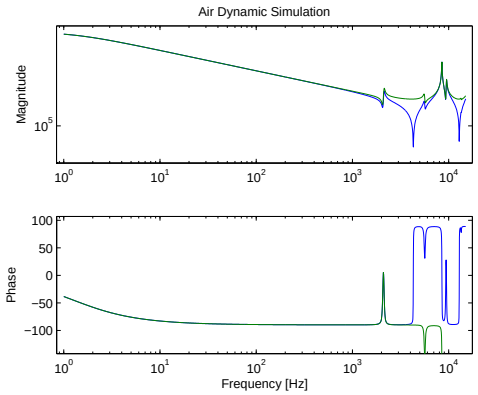

(a) Simulation Nijveldt model. The higher order air dynamics starts to show its existence after 1kHz, this frequency is so high and is neglectable, it proofs that the 1^{st} order model is already sufficient

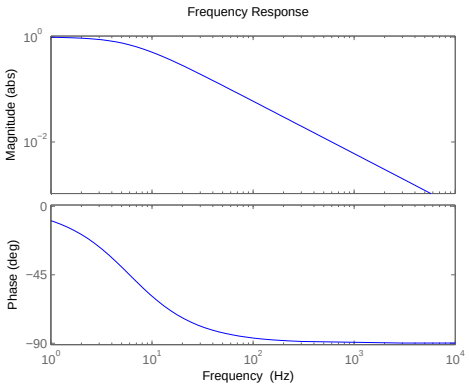

(b) Frequency response of the air dynamics model, it shows a very similar characteristic between this model and the Nijveldt model for low frequency. It has proofed that the 1^{st} order lumped model is valid in this research

Figure B.3: Comparison between Simulation from Nijveldt model and the air dynamic model

```
17
18 %% Resistance
19 R_orifice = 7.502e9;% resistance [Pa*s/m3]
20 %     R_orifice = R_orifice * 5;
21 R_valve = 7.242e9;
22 %     R_valve = R_valve * 0.1;
23
24 %% Volume
25 % volume of inlet channel
26 phi_inlet = 1.5e-3;        % 1.5mm diameter
27 l_inlet = 21e-3;          % 21mm length
28 A_inlet = 1/4 * pi * phi_inlet^2;
29 V_inlet = A_inlet * l_inlet
30
31 % volume of outlet channel
32 phi_outlet = 1.6e-3;        % 1.5mm diameter
33 l_outlet = 22e-3;          % 21mm length
34 A_outlet = 1/4 * pi * phi_outlet^2;
35 V_outlet = A_outlet * l_outlet
36
37 % Volume of the chamber
38 phi_chamber = 25e-3;
39 phi_disk = 24e-3;
40 d_chamber = 5e-3;
41 d_disk = 4e-3;
42 V_chamber = 1/4 * pi * (phi_chamber^2 - phi_disk^2) * d_chamber
43
44 % volume of the pressure sensor
45 phi_sensor = 7.2e-3;              % internal diameter of the tube
46 l_sensor = 10e-3;
47 % V_press_sensor = 0
48 V_sensor = 1/4 * pi * phi_sensor^2 * l_sensor
49
50
51 % correction for volume in the orifice
52 % V_orifice = 0.5*V_sensor
53 V_orifice = 5.0265e-07;
54
55 % correction for volume in the valve
56 % V_valve = 1*V_inlet
57 V_valve = 3.7110e-08;
58
59 % total volume inside the pressure regulator
60 V_actuator = V_orifice + V_chamber + V_inlet + V_outlet + V_sensor + V_valve
```

```
% V_actuator = V_actuator *5;


%% Calculate P_chamber
% a = 1/R_valve;
% b = P_s/R_orifice - P_a/R_valve;
% c = -P_s^2/R_orifice;
%
% P_chamber = (-b + sqrt(b^2 - 4*a*c))/2/a;

P_chamber = sqrt( R_orifice/(R_valve + R_orifice) * P_a^2 ...
+ R_valve/(R_valve + R_orifice) * P_s^2)

%% Capacitance
C_actuator = V_actuator / P_chamber;

%% Calculate Flow rate
% rho_orifice = P_s / R_specific_air / T1;
% rho_valve = P_chamber / R_specific_air / T1;

rho_orifice = (P_s + P_chamber)/2 / R_specific_air / T1;
rho_valve = (P_chamber + P_a)/2 / R_specific_air / T1;
rho_chamber = P_chamber / R_specific_air / T1;

Q_orifice = (P_s - P_chamber) / R_orifice
Q_valve = (P_chamber - P_a) / R_valve

m_orifice = Q_orifice * rho_orifice;
m_valve = Q_valve * rho_valve;

%% construct transfer function of air dynamics
s = tf('s');
F1 = rho_orifice * P_s - R_orifice * rho_valve * Q_valve;
F2 = Q_valve * (s * rho_chamber * C_actuator * R_orifice + rho_orifice);

sys_air_dynamics = F1 / F2;

% normalize the transfer function (mag=1 at 0.1rad/s)
w = 0.1;
s = 1j*w;
mag = abs( evalfr(sys_air_dynamics, s));
sys_air_dynamics = sys_air_dynamics / mag;

% mag = 1.84;
% sys_air_dynamics = sys_air_dynamics * mag;

%% Bodeplot

figure
h = bodeplot(sys_air_dynamics);
opts = getoptions(h);
opts.FreqUnits = 'Hz';
opts.MagUnits = 'abs';
opts.MagScale = 'log';
% opts.MagLowerLimMode = 'manual';
% opts.MagLowerLim = 0.01;
% opts.Xlim = [1e-1 1000];
opts.Xlim = [1 10000];
opts.Grid = 'on';
opts.Title.String = 'Frequency Response';
setoptions(h,opts)
hold on
```

C

Modelling and System Identification of the Solenoid Valve

The solenoid valve consists a mass-spring sub-system, which is a mass preloaded with a leaf spring, actuated by reluctance force. Figure C.1 shows that the orifice of the valve is removed and only the solenoid is put into measurement.

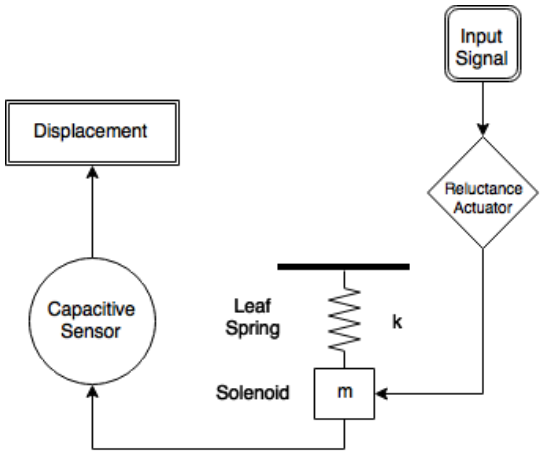

(a) Solenoid Test Schematic

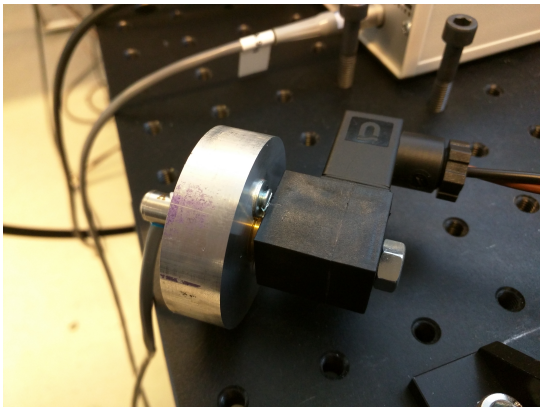

(b) Solenoid Test Setup

Figure C.1

The model of the solenoid can be constructed by a single mass-spring system. The solenoid core weight 3g, with an eigenfrequqncy of 342Hz. The stiffness k of the leaf spring is $1.39 \times 10^4 N/m$, obtained from the equation:

$$\omega = \sqrt{\frac{k}{m}}$$

The transfer function of the mass-spring system is:

$$\frac{x}{V} = \frac{1}{2.158 \times 10^{-7} s^2 + 5.755 \times 10^{-5} s + 1}$$

The input of the transfer function is the voltage coming out from dSpace, the output of the transfer function is the displacement of the solenoid core.

The frequency response of the model is shown in Figure C.2

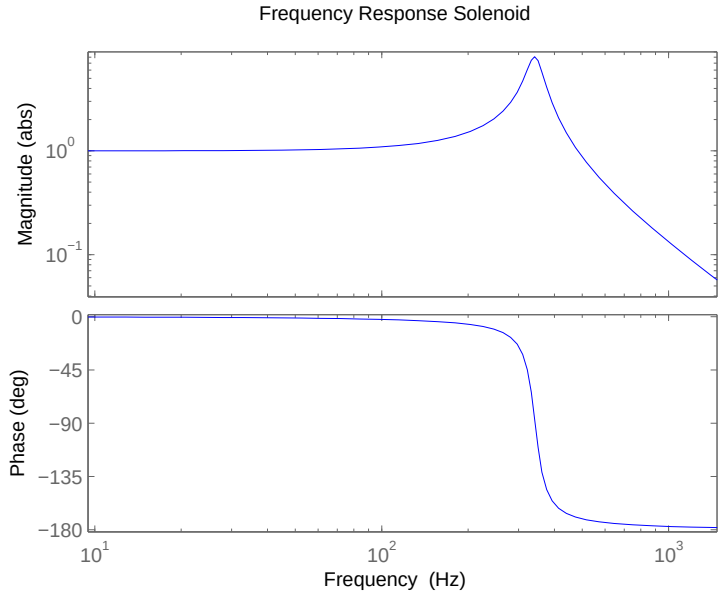

Figure C.2: Frequency Response Solenoid Model, with Eigenfrequency 342Hz

A sine wave input signal is given into the solenoid by current amplifier. Figure C.3 shows the working range and hysteresis of the solenoid. Hysteresis is small and the full range can be used as approximately linear.

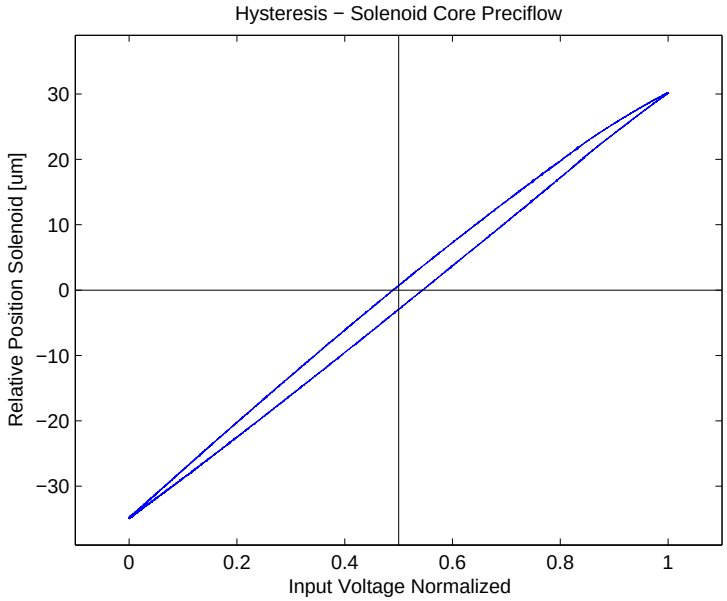

Figure C.3: Stroke and Hysteresis of Solenoid Core

The Solenoid is put in a frequency response test to verify the mass-spring model. Figure C.4 shows

the comparison of the Bode plot between the mass-spring model and the actual solenoid. The first eigenfrequency of the model is at 342Hz, which matches the measurement. However the measurement revealed a phase lag of -180 degree at the eigenfrequency, and continues to drop to -450 degree towards infinity.

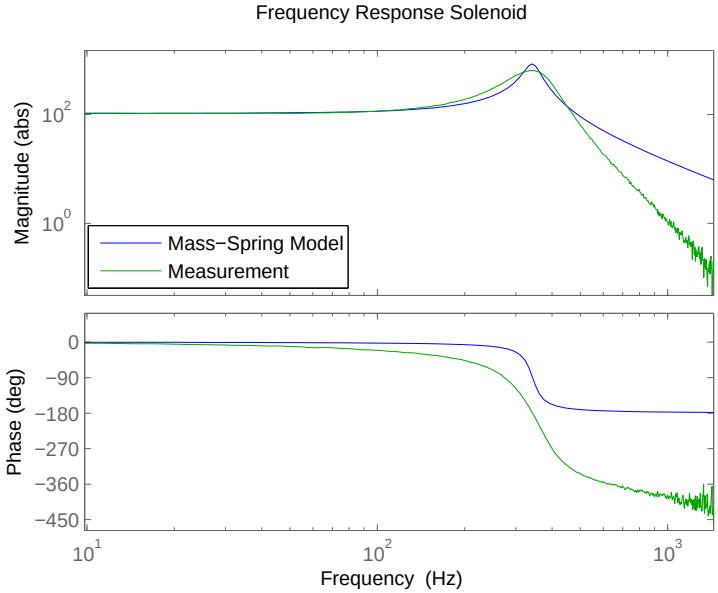

Figure C.4: Frequency Response of Mass-Spring Model and Measurement, First Eigenfrequency 342Hz, Large Difference in Phase

This difference occurs around the eigenfrequency, it makes the solenoid as a 5^{th} order system. The magnitude suffers from extra slope and decreases very rapidly.

Generally the reluctance actuator will introduce a phase lag of -90 degree, however in this case the phase lag is -270 degree. There is an unknown -180 degree phase lag in the system. No information can be found in the data sheet of the ASCO valve, but it's reasonable to assume there is be some characteristic of the circuit or component inside the reluctance actuator, with a cut off frequency slightly higher than the eigenfrequency of the solenoid core.

The most reasonable assumption in this case would be that the reluctance actuator is coupled with a 2^{nd} order low pass filter and they form a 3^{rd} order system together.

Therefore the identified low pass characteristic can approximated by 3^{rd} order butterworth low pass filter with a transfer function of

$$H(s) = \frac{G_0}{\prod_{k=1}^{n}(s - s_k)/\omega_c}$$

where

$$s_k = \omega_c e^{\frac{j(2k+n-1)\pi}{2n}}$$

with a constant gain $G_0 = 1$, 3^{rd} order $n = 3$, cut off frequency at $\omega_c = 2513$ rad/s.

The frequency response of the approximated reluctance actuator is shown in Figure C.5a.

Combining the mass-spring model and the low pass filter, a new modified solenoid model is obtained. This new modified model is able to describe the dynamic characteristic of the solenoid valve. The

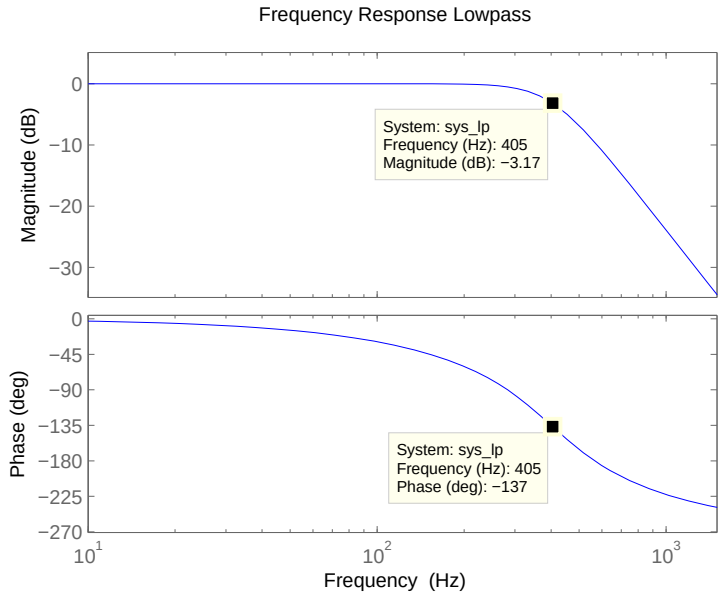

(a) Frequency Response of 3^{rd} order reluctance actuator with a cut off frequency at 400Hz

comparison of the frequency response between the model and the measurement is shown in Figure C.6. It should be noticed that the slight difference in the magnitude around the eigenfrequency is caused by the air-tight test setup, which introduces some damping in the measurement. This damping disappears when the solenoid core sit back into its own housing, which can be seen in the frequency response of the pressure regulator.

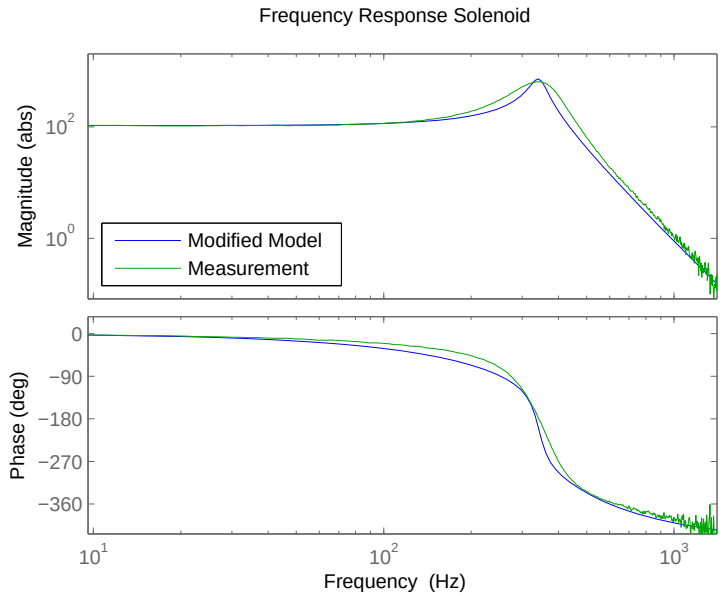

Figure C.6: Frequency Response of Modified Model and Measurement, Matching Result

D

Resistance of the Solenoid Valve and Orifice, Parameter Measurement and Correction

The resistance of the orifice and the solenoid valve is unknown, there is no direct numbers given by the manufacturer. Generally these components are defined as flow control components and that's exactly how they are designed to work in the most applications. These components takes control of the flow rate of the medium directly, and many of them are linear flow rate control components.

Instead of resistance, the flow coefficient Kv is commonly used in the industry. Kv can be obtained from the following equation together with measurements:

$$Kv = Q\sqrt{\frac{\Delta p_{Kv} \cdot \rho}{\Delta p \cdot \rho_w}}$$

where

$$Q: \ measured\ volumetric\ flow\ rate\ [m^3/h]\ or\ [L^3/m]$$

$$\Delta p_{Kv}: \ static\ pressure\ loss\ of\ 10^5\ Pa$$

$$\Delta p: \ measured\ static\ pressure\ loss\ across\ the\ valve\ in\ [Pa]$$

$$\rho: \ density\ of\ the\ fluid\ [kg/m^3]$$

$$\rho_w: \ density\ of\ water\ [kg/m^3]$$

The Kv value of the valve is given in the Datasheet. Since resistance is needed in the Flowerbed Application, it's possible to obtain the resistance from the Kv number, with the help of other parameters. Using the reference orifice formula sheet (Figure D.1) from ASCO, the flow rate can be calculated. It should be mentioned that other necessary parameters are already known or obtained in chapter of modelling.

The obtained values are

$$Q_v = 3.0863 \times 10^{-4}\ m^3/s$$

$$\dot{m}_v = 4.0751 \times 10^{-7}\ kg/s$$

Formula for liquid

$$Kv = Q \cdot \sqrt{\frac{(S.G.)}{\Delta p \cdot 1000}}$$

$$Q = Kv \cdot \sqrt{\frac{\Delta p \cdot 1000}{(S.G.)}}$$

$$\Delta p = (S.G.) \cdot \left(\frac{Q}{Kv}\right)^2 \cdot \frac{1}{1000}$$

Formula for gases (with temperature correction) (1)

$p_2 < \frac{p_1}{2}$

$$Kv = \frac{Q_N}{257 \cdot p_1} \cdot \sqrt{(S.G.)_N \cdot T_1}$$

$$Q_N = 257 \cdot Kv \cdot p_1 \cdot \frac{1}{\sqrt{(S.G.)_N \cdot T_1}}$$

$$\Delta p \neq f\,(Kv, Q_N, (S.G.)_N, p_2, T_1)$$

$p_2 \geq \frac{p_1}{2}$

$$Kv = \frac{Q_N}{514} \cdot \sqrt{\frac{(S.G.)_N \cdot T_1}{\Delta p \cdot p_2}}$$

$$Q_N = 514 \cdot Kv \cdot \sqrt{\frac{\Delta p \cdot p_2}{(S.G.)_N \cdot T_1}}$$

$$\Delta p = \frac{Q_N^2 \cdot (S.G.)_N \cdot T_1}{Kv^2 \cdot 514^2 \cdot p_2}$$

(S.G.)	(kg/m³)	: specific gravity related to water for liquids
(S.G.)N	(kg/m³)	: specific gravity related to air for gases
T1	(°C)	: fluid temperature at the valve inlet
T2	(°C)	: fluid temperature downstream of the valve
Q	(m³/h)	: flow
QN	(Nm³/h)	: volumetric flow across the valve
Kv	(m³/h)	: flow coefficient
p1	(bar)	: pressure at the valve inlet
p2	(bar)	: pressure downstream of the valve
Δp	(bar)	: pressure drop

(1) To calculate the volumetric flow **QN** we must know:
- the **Kv** coefficient
- the specific gravity **(S.G.)N** of the fluid
- the pressure loss **Δp** across the valve
- the fluid pressure **p2** downstream of the valve
- the fluid temperature **T1** at the valve inlet

Figure D.1: ASCO Formula Sheet

The flow rate and resistance can be linearized by the equation

$$R_v = \frac{P_{chm} - P_a}{Q_v} = 9.7203 \times 10^8\ Pa \cdot s/m^3$$

The situation of the Festo orifice is slightly a bit difficult. The Kv value of the orifice is unknown, it's not possible to calculate the flow rate directly. Alternatively, Festo provided a datasheet with a flow rate chart, which contains the direct relation between the control and the flow rate. Kv can be obtained by the chart from the datasheet of Festo (Figure D.2) using the reference formula from ASCO.

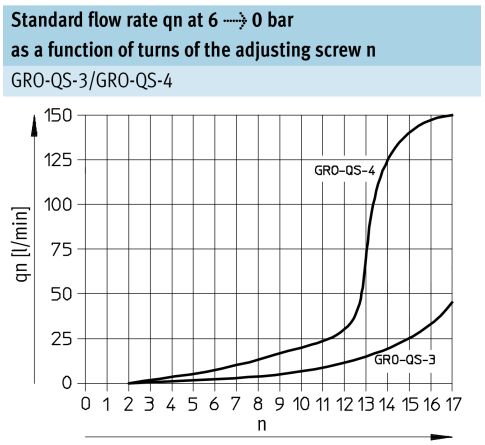

Figure D.2: Festo GRO-QS-4 Flow Rate Chart

The obtained parameters of the orifice are

$$K_{v_o} = 0.0085$$

$$Q_o = 2.4343 \times 10^{-4}\ m^3/s$$

$$\dot{m}_o = 4.0178 \times 10^{-7}\ kg/s$$

$$R_o = \frac{P_s - P_{chm}}{Q_o} = 4.1079 \times 10^8\ Pa \cdot s/m^3$$

A lab test is needed to verify the above calculation, as shown in Figure D.3b . Figure D.3a shows the schematic of the setup. The test setup consists a 2 Litre air tank charged with 6bar compressed air, connected with the orifice or the valve. At the moment the orifice or valve is opened, compressed air will surge out from the air tank through the tested component, the pressure inside the air tank will start to drop. By measuring the change of the pressure, one can obtain the needed parameters in further calculation.

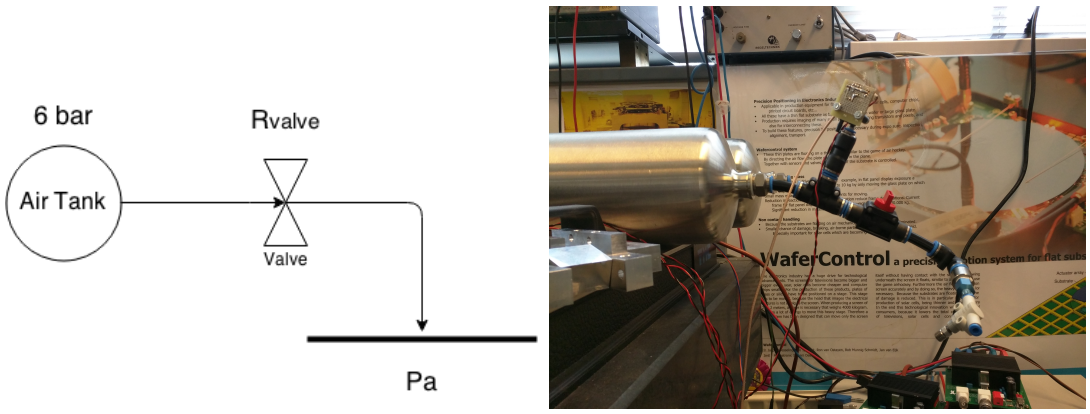

(a) Resistance Measurement Test Schematic (b) Resistance Measurement Test Setup

Figure D.3

Using the Ideal Gas Law

$$PV = nRT$$

Substitute with

$$R_{specific} = \frac{R}{M}$$

$$M = \frac{m}{n}$$

Differentiate both sides:

$$\dot{P}V = \dot{m}R_{specific}T$$

Finally the mass flow can be obtained:

$$\dot{m} = \frac{R_{specific}T}{\dot{P}V}$$

The measured pressure versus time needs to be curve fitted before obtaining the derivative. The pressure change is expected to be 2^{nd} order, thus a curve fit of 3^{rd} or higher order polynomial will be sufficient.

With the fitted polynomial, Figure D.4 shows the actual flow rate of the orifice and the valve, with the order of 10^{-5}, while the calculation following the ASCO reference formula comes out with a number in the order of 10^{-4}.

This difference of the resistance caused a mismatch of the modelling of the air chamber, as shown in Figure D.5. The first pole of the transfer function is 107Hz, compared to the measurement which is only 6.1Hz.

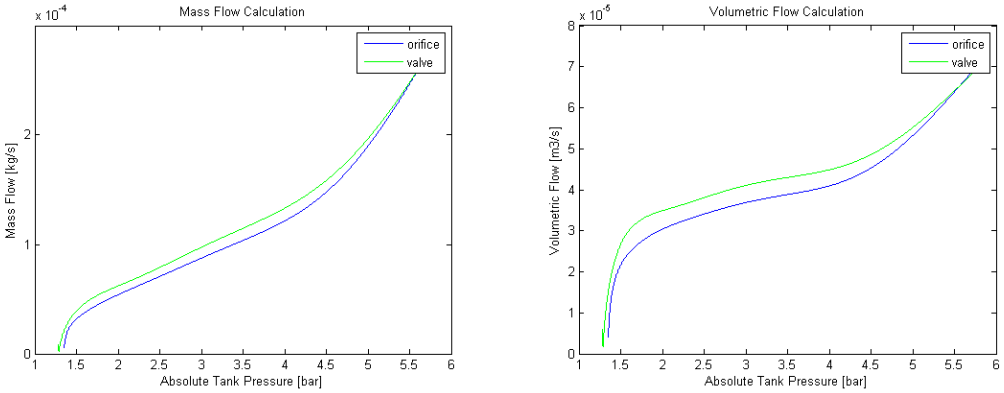

(a) Mass Flow Rate of the Components (b) Volumetric Flow Rate of the Components

Figure D.4: Measured Flow Rate of the Components

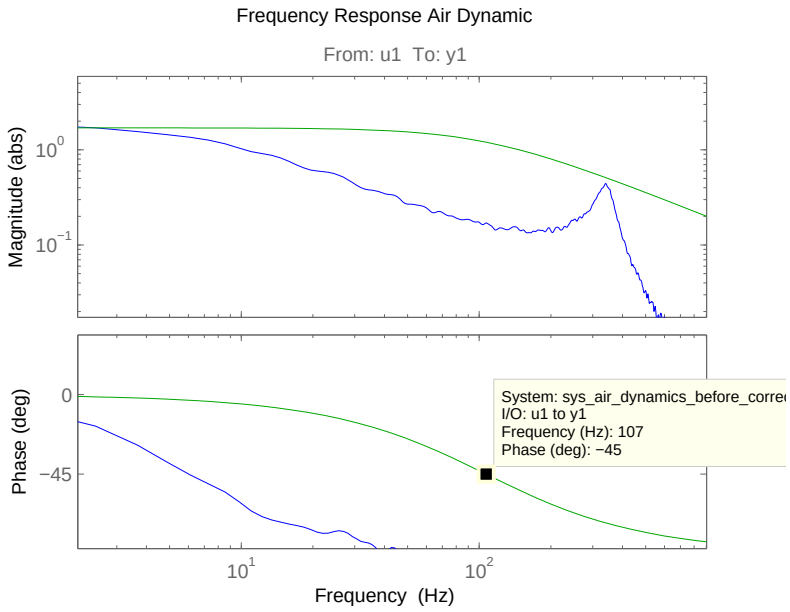

Figure D.5: Mismatched Frequency Response between Model and the Measurement

The cause of the difference in the theoretical resistance is unknown, one of the reason could be the valid condition is different for the equation, but still the difference of 10 times is not neglectable.

Using the flow rate obtained by measurements, Figure D.6 shows the resistance of the orifice and the valve.

Figure D.7 shows that the model matches the measurement with the correct resistance of the orifice and valve. The pole of the model is 5.7Hz, compared to 6.1Hz in the measurement, not a difference of 10 times any more and finally this result is acceptable.

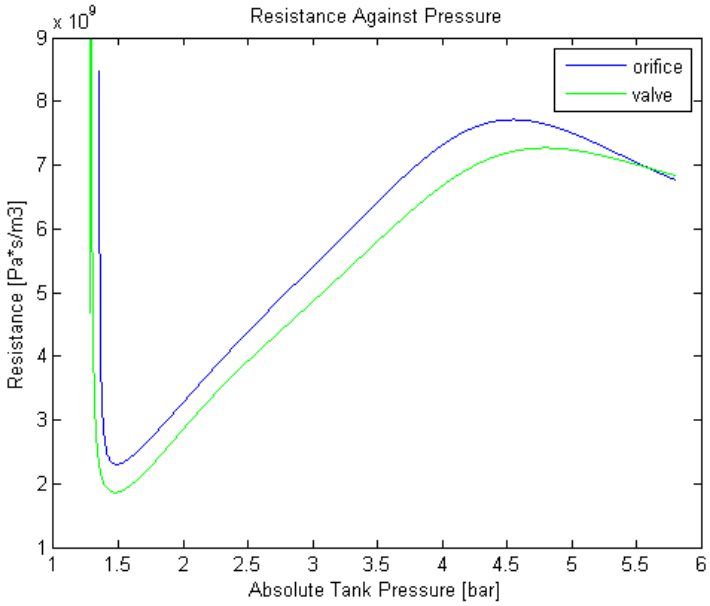

Figure D.6: Linearized Resistance of the Orifice and the Valve

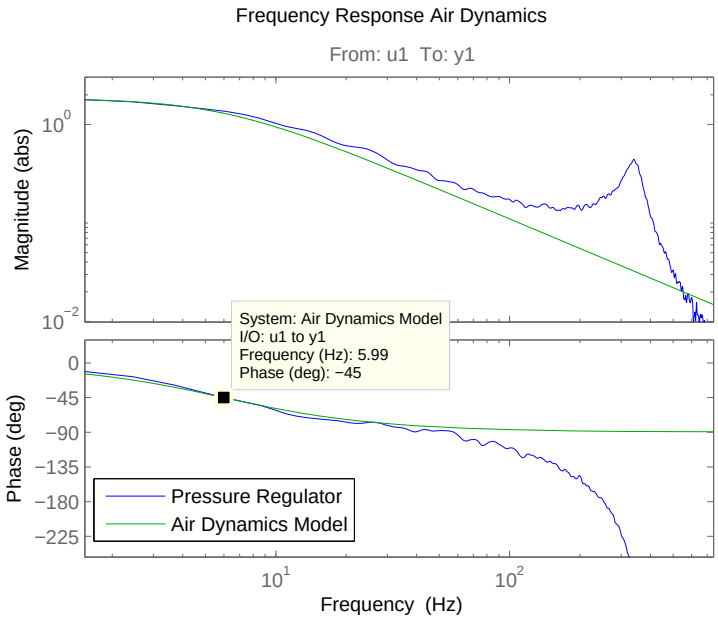

Figure D.7: Bode Plot of the Air Dynamic Transfer Function, with correct parameters

E

Pressure Regulator Configuration

There are different configurations of a pressure regulator, regarding to where the valve and the orifice restriction are located. In this appendix a basic performance is carried out to investigate the effect of different configuration for the Flowerbed application.

The pressure regulator is put under a frequency response test, where the valve will be actuated.The test will be carried out in two variants: a single orifice-valve (Festo QS-4 orifice and ASCO PreciFlow valve)configuration and a differential valve-valve (two ASCO PreciFlow valves)configuration.

E.1. Orifice-Valve Configuration

In this configuration, the resistance of the orifice will be adjusted to a certain value, more specifically, the same resistance as the full opened valve. The schematic was shown in Figure E.1.

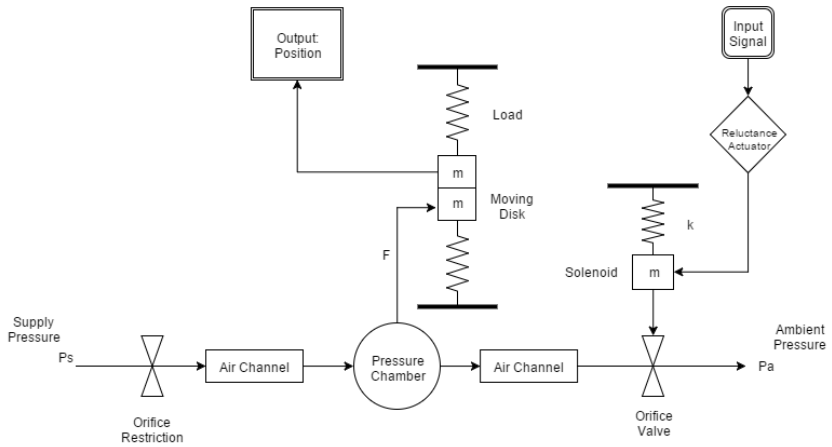

Figure E.1: Schematic of an Orifice-Valve Configuration

A sine wave is given as an input to the solenoid valve, Figure E.2 shows the working range of the valve, as well as the hysteresis. The valve has nearly full range linear static response from 0.6-0.85 normalized input voltage, where the frequency response test will be based on. Hysteresis is not neglectable, but it does not affect the performance of the frequency response test.

Figure E.3 is the frequency response of the system, it shows that there is a 1^{st} order pole at around 6.1Hz. There is a higher order pole around 342Hz. The 1^{st} order pole comes from air dynamics and the

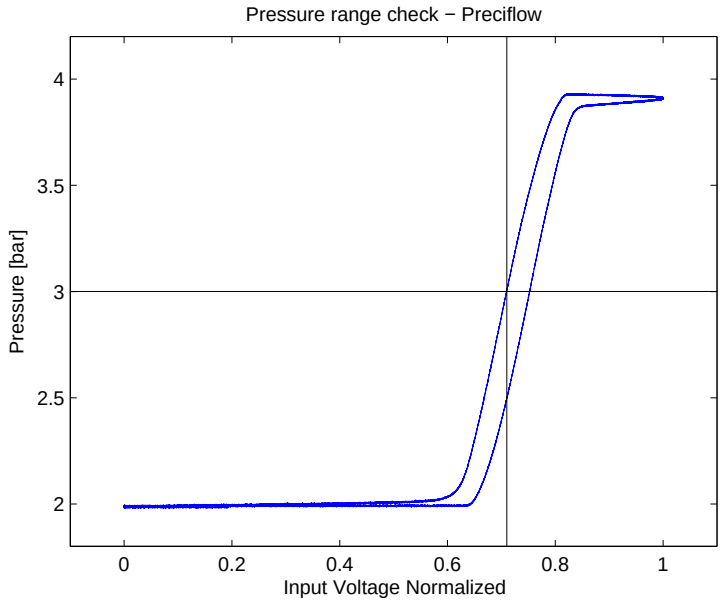

Figure E.2: Working Range and Hysteresis of Orifice-Valve Configuration

higher order pole comes from the solenoid valve. Another test is done with a larger chamber volume by increasing the volume of the pressure regulator. The new test shows that the 1^{st} order pole has shifted to 3.7Hz, while the higher order pole remains at 342Hz. This test shows that the internal space can influence the speed of the regulator, it's a feasible way to increase the performance.

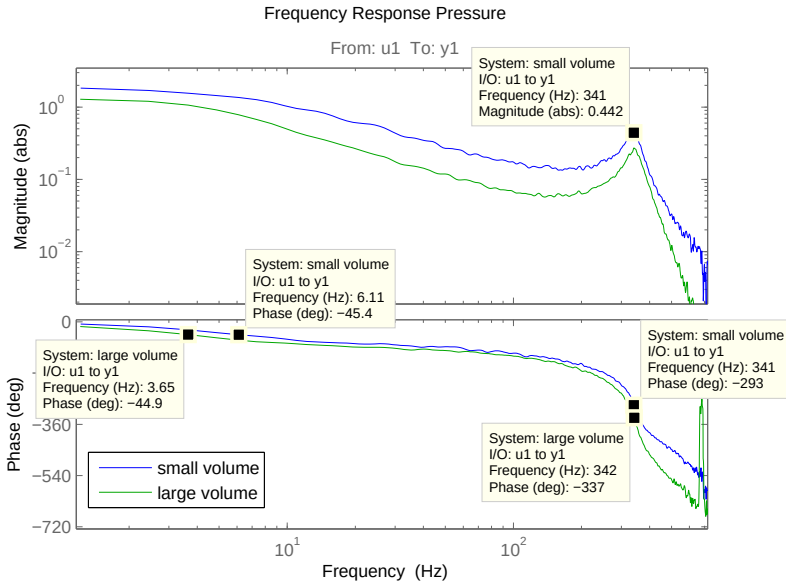

Figure E.3: Frequency Response of Orifice-Valve Configuration, Different Chamber Volume

Another comparison test is carried out, with two different solenoid valves. Figure E.4 Shows the difference in the frequency response of both systems. It can be seen that by using the faster valve, the eigenfrequency of the system is drastically improved, by a flatter curve in low frequency, and a higher first eigenfrequency.

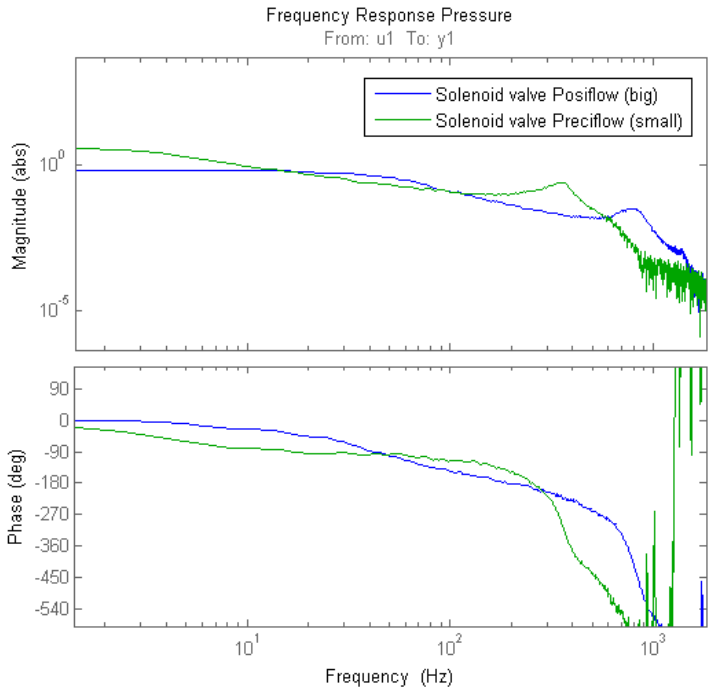

Figure E.4: Frequency Response of Orifice-Valve Configuration, Different Valves

E.2. Differential Valve-Valve Configuration

A valve-valve configuration has the same principle as orifice-valve, but it replace the constant orifice with a variable valve, and thus becomes a variable orifice. These two valves will form a differential operation, one opens, the other closes. Figure E.5 shows the schematic of the configuration. The known advantage is that the range of pressure will increase due to the larger range of the variable resistance in the system, it's commonly used in pneumatic actuators that requires a large range of variable pressure.

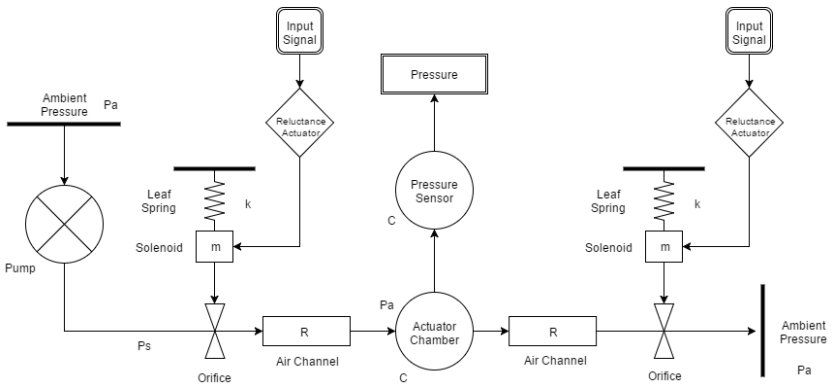

Figure E.5: Schematic of the Pressure Regulator with Differential Valves Configuration

In general it's difficult to have two valves with identical characteristic. Each of the ASCO valves are tested under the same orifice-valve configuration, the result is shown in Figure E.6a. The valves have different range under same input. If they're combined to form a differential configuration, the pressure response becomes very non-linear. Figure E.6b shows the non-linear pressure range and hysteresis. The obvious disadvantage of differential valves configuration is a much more complex system to control,

with an extra valve.

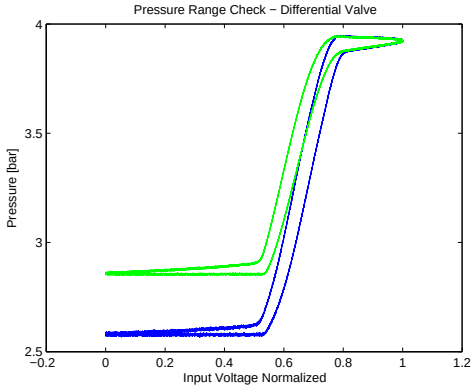

(a) Working Range and Hysteresis of each Valve in Single Valve Configuration

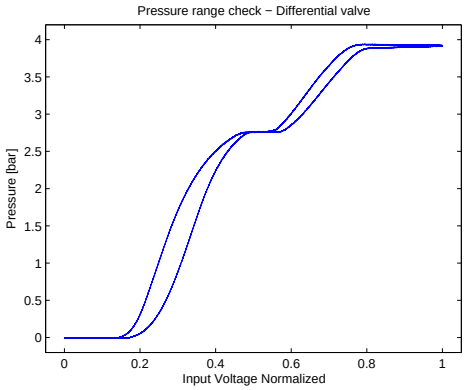

(b) Working Range and Hysteresis of Differential Valves Configuration Formed by Combining Two Valves

Figure E.6

The Bode plot in Figure E.7 shows that the frequency response doesn't have considerable improvement under differential valves configuration.

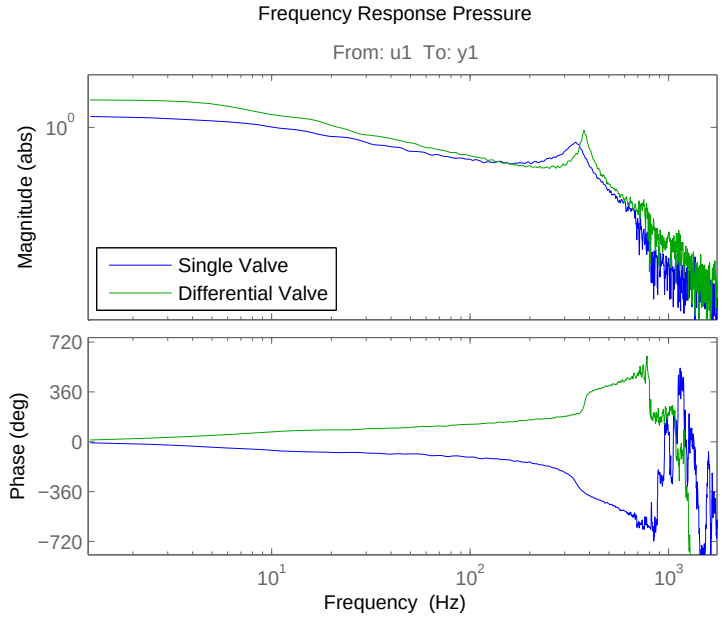

Figure E.7: Frequency Response, Comparison between Differential Valves and Single Valve Configuration

The complexity of the differential configuration brings some difficulty to the system due to the difference between two valves. The difference between two valves causes the system to become highly non-linear and split the working range into two separate part, this configuration didn't bring a very attractive way to improve the performance in this test.

The differential valve-valve configuration has advantages in theory, but considering the complexity and the need of focusing in the theory of pneumatic actuator, the single orifice-valve configuration is chosen in this research. It is recommended to continue the research on the differential valve-valve configuration based on the knowledge developed in this research.

Bibliography

[1] Nelson Air Corp, *Air Bearing Basics,* (2016).

[2] S. H. Chang *et al.*, *An Ultra-Precision $XY\theta_z$ Piezo-Micropositioner Part I: Design and Analysis,* IEEE Transactions on Ultrasonics, Ferroelectrics, and Frequency Control (1999).

[3] S. H. Chang *et al.*, *An Ultra-Precision $XY\theta_z$ Piezo-Micropositioner Part II: Design and Analysis,* IEEE Transactions on Ultrasonics, Ferroelectrics, and Frequency Control (1999).

[4] Dahoon *et al.*, *Development of 4 Degree-of-Freedom ultra-precision Stage with millimeter motion range,* International Conference on Control, Automation and Systems (2012).

[5] Y. Tian *et al.*, *Design and dynamics of a 3-DOF flexure-based parallel mechanism for micro/nano manipulation,* ELSEVIER (2010).

[6] A. Robert L. Williams II, *PLANAR PARALLEL 3-RPR MANIPULATOR,* Ohio University (1999).

[7] P. French, *Reader of the course ET4257 Sensor and Actuators,* TU Delft (2007).

[8] PI Piezo Technology, *Piezo Force and Stiffness,* (2016).

[9] F. Peter Croser, *Pneumatics - Basic Level,* (2016).

[10] A. Bill Black, Mike Lopez, *Basics of Voice Coil Actuators,* (2016).

[11] Festo, *Fluidic Muscle DMSP/MAS,* (2016).

[12] Festo, *Clamping Modules EV,* (2016).

[13] B. L.Sciavicco, *Modellling and Control of Robot Manipulators* (Springer, 1999).

[14] Frank M.White, *Fluid Mechanics* (McGraw-Hill, 2009).

[15] Alexander D.Poularikas, *Analog Filter Approximations* (Springer, 1999).

[16] Festo, *White paper Piezo technology in pneumatic valves,* (2016).

[17] M. Scheuenpflug *et al.*, *Microfluidic Module System with Piezo Driven Microvalve for Synthesis of Radiopharmaceutical Products,* IEEE (2007).

[18] Peter Beater, *Pneumatic Drives* (Springer, 2006).

[19] Murata, *Piezoelectric Sound Components, Application Manual,* (2016).

[20] Karl Johan åAström, Richard M. Murray, *Feedback systems, An introduction for scientists and engineers* (Princeton University Press, 2012).

[21] M. Boerlage *et al.*, *Model-based feedforward for motion systems,* TU Eindhoven .

[22] I. Landau, *The R-S-T digital controller design and applications,* Pergamon (1998).

[23] T.Nijveldt, *Pneumatic Manifold Design,* TU Delft (2015).